



## Durham E-Theses

---

### *Ultrafast processes and excited state dynamics in conjugated polymers*

King, Simon

#### How to cite:

---

King, Simon (2008) *Ultrafast processes and excited state dynamics in conjugated polymers*, Durham theses, Durham University. Available at Durham E-Theses Online: <http://etheses.dur.ac.uk/2192/>

#### Use policy

---

The full-text may be used and/or reproduced, and given to third parties in any format or medium, without prior permission or charge, for personal research or study, educational, or not-for-profit purposes provided that:

- a full bibliographic reference is made to the original source
- a [link](#) is made to the metadata record in Durham E-Theses
- the full-text is not changed in any way

The full-text must not be sold in any format or medium without the formal permission of the copyright holders.

Please consult the [full Durham E-Theses policy](#) for further details.

# **Ultrafast Processes and Excited State Dynamics in Conjugated Polymers**

**By Simon King**

A thesis submitted to the Faculty of Science, The University of Durham, for the  
degree of Doctor of Philosophy

Organic Electroactive Materials Group  
Department Of Physics  
University Of Durham  
January 2008

# Ultrafast Processes and Excited State Dynamics in Conjugated Polymers

Simon King

Submitted For the Degree of PhD, 2008

The photophysics of a number of conjugated polymers used in organic display applications has been studied using ultrafast techniques. An updated method for measuring the intersystem crossing rate was developed. This has been used to measure the intersystem crossing in a number of conjugated polymers and oligomers. It was found that as expected the intersystem crossing in conjugated polymers is generally very low. The intersystem crossing in a molecule that exhibits dual fluorescence depending on the polarity of the environment was investigated. In polar solvents when the molecule forms a twisted interconnected charge transfer state the intersystem crossing rate was found to be ten times that of the planer locally excited state found in non-polar media.

The nature of charge generation in conjugated polymers has also been investigated, it was found that in the prototypical conjugated polymer, polyfluorene, there is no intrinsic charge photogeneration. However, charges can be formed by singlet-singlet annihilation reactions. This is made very efficient in the solid state by the rapid diffusion and migration of excitons. The photophysics of a novel polyfluorene, polyspirobifluorene, was investigated thoroughly; it has been found that the addition of the spiro side group containing electron-donating groups causes a charge transfer state to form between the backbone and the side group. This can act as a reservoir for the emissive singlets, thus giving the polymer a long tail in the fluorescence decay.

Finally, ultrafast pump probe spectroscopy was used to investigate on chain migration of excitons in dilute solutions of a ladder type polymer. The migration to the lowest energy segment of the chain shows up as a shift to the red of the photobleaching signal in the pump probe spectrum. This shows that the low energy states become occupied after the initial excitation, as the high energy states become depopulated by the migration, this process taking about 6.2ps.

The copyright of this thesis rests with the author or the university to which it was submitted. No quotation from it, or information derived from it may be published without the prior written consent of the author or university, and any information derived from it should be acknowledged.

1 2 JUN 2008



## **Acknowledgements**

Throughout the last three years, many people have dedicated their own time and effort towards helping me to both carry out and enjoy the research that is continued in this thesis. The biggest thank you has to go to my supervisor, Professor Andy Monkman for all his help and encouragement throughout my 4 years in the OEM group. I would also like to thank the academics and support staff who have provided me with materials, equipment and many helpful discussions, in particular Hugh Burrows, Martin Bryce, Lars Pålsson and Norman Thompson.

A special mention must go to the members of the OEM group, past and present, who have helped me by providing support, inspiration, biscuits, opportunities for procrastination and even scientific insight. In particular, thanks must go to Dechang, whose knowledge of all things laser was invaluable in getting me off the ground with my ultrafast research; also to Helen who started in the world of scientific research with me 4 years ago and whose constant cups of tea and banter were gratefully appreciated when things went wrong! As well as all my family and friends who have diligently pretended to listen as I told them what exciting experiments I had been up to that day. Finally, special thanks to Mum, Dad, Nicky and Jenny, for all their help and support over the three years.

## **Declaration**

The material in this thesis has not been submitted for examination for any other degree or part thereof, at the University of Durham or any other institution. The material in this thesis is the work of the author except where formally acknowledged by reference.

The copyright of this thesis rests with the author. No quotation from it should be published without his prior consent and information derived from it should be acknowledged.

# Table of Contents

<b>Abstract</b> .....	<b>1</b>
<b>Acknowledgements</b> .....	<b>3</b>
<b>1 Introduction</b> .....	<b>12</b>
1.1 Conjugated Polymers and PLEDs .....	12
1.2 Motivation .....	13
1.3 Previous Studies .....	14
1.4 References .....	15
<b>2 Theoretical Considerations</b> .....	<b>16</b>
2.1 Conjugated Polymers: Structure and Bonding .....	16
2.1.1 Conjugation .....	18
2.2 Optical transitions in Conjugated Polymers .....	20
2.2.1 The Nature of the Excitations in Conjugated Polymers .....	20
2.2.2 Exciton Types .....	21
2.2.3 Polarons .....	22
2.3 Singlet and Triplet Excited States .....	23
2.3.1 Singlet and Triplet Energy .....	24
2.3.2 Intersystem Crossing .....	25
2.4 Electronic Processes in Conjugated Molecules .....	27
2.4.1 Absorption .....	27
2.4.2 Fluorescence .....	29
2.4.3 Non Radiative Decay .....	30
2.4.4 Decay Rates and Quantum Yield .....	30
2.4.5 Higher Excited States .....	31
2.4.6 Phosphorescence .....	32
2.4.7 Induced Absorption .....	32
2.4.8 The Jablonski Diagram .....	33
2.5 Exciton Processes .....	34
2.5.1 Energy Transfer .....	34
2.5.2 Forster Transfer .....	34
2.5.3 Dexter Transfer .....	36
2.5.4 Migration, Diffusion and the DOS .....	37
2.5.5 Conformational Relaxation .....	38
2.6 Interactions Between Excited States .....	39
2.6.1 Singlet-Singlet Annihilation .....	39
2.6.2 Triplet-Triplet Annihilation .....	40
2.6.3 Singlet-Triplet Annihilation .....	40
2.6.4 Charge Trapping .....	41
2.7 References .....	42
<b>3 Experimental Methods</b> .....	<b>45</b>
3.1 Femtosecond Lasers .....	46
3.1.1 Mode-Locking .....	46
3.1.2 The Titanium:Sapphire Laser .....	48
3.1.3 Laser Amplifier .....	50
3.1.4 OPA .....	50
3.2 Development of the Pump-Probe system .....	52
3.2.1 Detection Systems .....	54
3.2.2 Characterisation of the White Light Supercontinuum .....	57

3.3	Quasi-CW Photoinduced Absorption .....	59
3.4	Nanosecond Photoinduced Absorption.....	59
3.5	Variations on the Standard Experiments.....	61
3.5.1	Field Assisted Pump-Probe.....	61
3.5.2	Charge Induced Absorption .....	61
3.6	Phosphorescence Spectra .....	62
3.7	Sample Preparation .....	62
3.8	References.....	63
<b>4</b>	<b>Measurement of Triplet Quantum Yields Of Conjugated Polymers and Oligomers.....</b>	<b>64</b>
4.1	Measurement of the Triplet Quantum Yield by Ground State Recovery ....	65
4.1.1	The Kinetic Scheme For Ground State Recovery.....	67
4.1.2	The Triplet Yield Experiment.....	69
4.2	The Triplet Yield of Polyfluorene and Polyspirobifluorene.....	72
4.2.1	Solid State Triplet Yields.....	76
4.3	The Intersystem Crossing Rate In Conjugated Oligomers And Polymers Containing A Twisted Interconnected Charge Transfer State (TICT).....	78
4.3.1	The Fluorene-Dibenzothiophene- <i>S,S</i> -Dioxide System: Characterisation of a TICT State.....	80
4.3.2	Previous studies of Triplets in TICT forming molecules.....	85
4.3.3	Results: Excited State Absorption .....	86
4.3.4	Ground State Recovery Triplet Yield Measurements.....	88
4.3.5	The CT Forming Polymers .....	89
4.3.6	Phosphorescence and Triplet Decay .....	91
4.3.7	Polyfluorene Oligomers .....	92
4.4	Discussion .....	93
4.4.1	Triplet yield and Intersystem Crossing Rate.....	93
4.4.2	Summary of Results.....	93
4.4.3	The Nature of Intersystem Crossing .....	94
4.4.4	Intersystem Crossing in the TICT state of FSF .....	97
4.4.5	Intersystem Crossing in the Polymeric Analogues of FSF .....	98
4.4.6	The Nature of the Triplet State .....	101
4.5	Conclusion .....	101
4.6	References.....	103
4.7	Publications Arising From This Chapter .....	107
<b>5</b>	<b>Singlet – Singlet and Singlet – Triplet Annihilation in PF2/6.....</b>	<b>108</b>
5.1	High Excitation Dose Phenomena in Conjugated Polymers.....	108
5.2	Annihilation Reactions in Molecular Systems.....	109
5.3	Singlet – Singlet Annihilation and Charge Generation in PF2/6.....	112
5.3.1	Results.....	112
5.4	Singlet-Triplet Annihilation in PF2/6 .....	123
5.4.1	The Delocalisation of the Singlet and Triplet state.....	127
5.4.2	The Orientation of the Singlet and Triplet States .....	128
5.5	Conclusions.....	134
5.6	References.....	135
5.7	Publications Arising From This Chapter .....	139
<b>6</b>	<b>Spiroconjugation Enhanced Intramolecular Charge-Transfer state Formation in a Conjugated Polymer.....</b>	<b>140</b>
6.1	Previous Work - Time Resolved Fluorescence & DFT Calculations .....	143
6.2	Results.....	146

6.2.1	Absorption and Fluorescence.....	146
6.2.2	Ultrafast Excited state Absorption and Ground State Recovery.....	147
6.2.3	Device Measurements: Field Assisted Pump-Probe and Charge Induced Absorption.....	150
6.3	Discussion.....	151
6.3.1	The Kinetic Scheme.....	158
6.3.2	Spiroconjugation.....	161
6.3.3	Significance of the CT State in Device Physics.....	163
6.4	Conclusions.....	164
6.5	References.....	165
6.6	Publications Arising From This Chapter .....	168
<b>7</b>	<b>Directly Probing the Distribution of States in Conjugated Polymers:</b>	
	<b>Intrachain Migration in MeLPPP .....</b>	<b>169</b>
7.1	Principal of the Experiment .....	172
7.2	Results.....	174
7.3	Discussion.....	179
7.4	Conclusion .....	183
7.5	References.....	184
<b>8</b>	<b>General Conclusions.....</b>	<b>186</b>
<b>9</b>	<b>Publication List .....</b>	<b>188</b>



## Table of Figures

Figure 1-1 Some examples of polymer led technology used for lighting and high quality displays. ....	12
Figure 2-1 Schematic of orbital formation and bonding in H <sub>2</sub> . .....	17
Figure 2-2 Formation of sp <sup>3</sup> hybrid orbitals required for the bonding in methane <sup>2</sup> . .....	17
Figure 2-3 The sp <sup>2</sup> hybrid and the formation of σ and π bonds in ethene <sup>2</sup> . .....	18
Figure 2-4 π-bonding in benzene, showing the p-orbitals projecting out of the plane of the molecule and effects of delocalisation and conjugation around the ring <sup>2</sup> . .....	19
Figure 2-5 Polaron transitions are often used in spectroscopy to verify the presence of charges in conjugated polymers. ....	23
Figure 2-6 An illustration of the absorption and fluorescence process demonstrating the need for Franck-Condon overlap and the formation of the vibronic spectra. ....	29
Figure 3-1 Formation of a pulse as the number of modes which become locked increases <sup>6</sup> . .....	48
Figure 3-2 The Kerr lens mode locking process, the pulse is transmitted through the aperture while in cw operation the beam is blocked. The Kerr lens beam shaping is determined by the spatial profile of the laser beam <sup>6</sup> . ....	49
Figure 3-3 The layout of the Coherent Mira 900-F <sup>8</sup> . .....	49
Figure 3-4 The Coherent 9400 OPA; the parametric amplification is performed by two passes through the OPA crystal <sup>9</sup> . .....	52
Figure 3-5 Schematic layout of the pump-probe system with the monochromator and photodiode detection system. The appropriate pump and probe beam can be selected by the flip mirrors as appropriate. ....	53
Figure 3-6 Top, Cross correlations of the different colour components in the white light supercontinuum. Lower: Colour components corresponding to the cross correlation above, the colours of the spectra correspond to the time traces in the top panel. ....	58
Figure 3-7 The empirically derived correction curve for the chirp, with the equation for calculating the required delay adjustment for the different wavelengths derived from figure 3.6. ....	58
Figure 3-8 Quasi CW Photoinduced Absorption Spectrometer. ....	59
Figure 4-1 Solution state absorption (blue) photoluminescence (green), phosphorescence (red), photoinduced triplet absorption (black) for PFO (upper) and PSBF (lower). The dotted lines mark the pump and probe beams for the ultrafast (3.2eV) and nanosecond (3.55eV, 3.06eV) photobleaching as well as the prob beam for the transient triplet absorption (1.58eV). ....	73
Figure 4-2 The ground state recovery for PSBF solution showing: (from top) the ultrafast component of the GSR, the nanosecond component, the combined GSR trace of both components and its associated lineof best fit to equation 4.5, and the transient triplet absorption. ....	74
Figure 4-3 The ultrafast GSR for PFO solution, the solid line is the line of best fit to equation 4.8. The dotted lines give an idea of the error on the calculation of the triplet yield. ....	74
Figure 4-4 Ultrafast ground state recovery for PFO (black) and PSBF (red) films at 10K, the solid lines are line of best fit to equation 4.4 used to calculate the triplet yield. ....	76

Figure 4-5 Comparison between the nanosecond GSR (black) and the transient triplet absorption (red) for PSBF film at 10K. ....	77
Figure 4-6 Compendium of spectra, (from left) absorption, fluorescence and phosphorescence for the FSF oligomer in methylcyclohexane (black) and ethanol (red) solutions. ....	81
Figure 4-7 Normalised emission spectra of the FSF oligomer at different times after excitation, for MCH (left) and Ethanol (right). Data kindly reproduced from the work of Dias et al <sup>48</sup> . ....	83
Figure 4-8 Absorption and emission spectra for PFS30 (L) and PFDBTH30 (R) in toluene solution (black), ethanol solution (red) and the fluorescence in solid state (blue). The formation of the TICT state for PFSF30 in ethanol and the solid state is clearly visible. Data kindly reproduced from the work of Dias et al <sup>48</sup> . ....	85
Figure 4-9 Quasi-cw transient triplet and femtosecond pump-probe spectra for FSF in MCH and Ethanol. ....	87
Figure 4-10 GSR decays for FSF in Ethanol (black) and MCH (red) and for FFF in MCH (green). The solid lines are the fits to the data using equation 4.8. ....	89
Figure 4-11 The ultrafast GSR of the polymers PFSF30 and PFDBTHD30 in toluene (red) and cyclohexanone (black). ....	90
Figure 4-12 A comparison between the excited state absorption measured at 780nm with the ground state recovery measured on the nanosecond timescale. The data shown is the PFSF <sub>30</sub> polymer in cyclohexanone. ....	92
Figure 4-13 variation in the rate of intersystem crossing with oligomer length for fluorene oligomers and polymers in toluene solution. ....	99
Figure 5-1 The structure of PF2/6. ....	111
Figure 5-2 (from left), Absorption, fluorescence, phosphorescence and transient triplet absorption for the polymer Pf2/6. ....	112
Figure 5-3 Room temperature excited state absorption spectra of PF2/6 films at high excitation density (25 $\mu\text{Jcm}^{-2}$ ) (a) and low excitation density (0.35 $\mu\text{Jcm}^{-2}$ ) (b) for different times after excitation. ....	113
Figure 5-4 Decay of PA1, the singlet excited state absorption for high excitation dose (○) (7 $\mu\text{Jcm}^{-2}$ ) and low excitation dose (■) (0.35 $\mu\text{Jcm}^{-2}$ ) at 300K (top) and 10K (lower). ....	114
Figure 5-5 Laser dose dependence of the intensity PA1 and PA2 excited state absorptions for Pf2/6 films at room temperature. The intensity initially and after 100ps are shown. Straight lines of gradient 0.5 and 1 are drawn as a guide to the eye. ....	115
Figure 5-6 Time dependence of the singlet-singlet annihilation parameter, $\gamma$ , at 10k. The curves are calculated from the transient absorption data (■) and a theoretical plot of the expected annihilation parameter from equation 5.6, using the values of R and D given in the text (○). ....	120
Figure 5-7 Double logarithmic plot of the variation of the quenching rate due to SSA with the separation of the excitons. ....	121
Figure 5-8 variation of the separation of singlet excitons at the point where SSA dominates the decay of the singlet excitons (solid), Singlet – Triplet separation when a background of triplet are	

created with cw excitation (dots). Variation with depth into the sample (left) and triplet-triplet annihilation rate (right). .....	124
Figure 5-9 Decay of the singlet exciton excited state absorption PA1 both with ( ) and without (■) a background of triplet population, for cw excitation (100mWcm <sup>-2</sup> ).....	126
Figure 5-10 Absorption and fluorescence of an aligned film of PF2/6 measured with the polarisation parallel (red) and perpendicular (black) to the film orientation. ....	130
Figure 5-11 Polarised phosphorescence spectra measured parallel (red - □) and perpendicular (black - ■) to the chain alignment. ....	130
Figure 6-1 The polymers poly-9,9-diethylhexylfluorene (PF2/6) and polyspirobifluorene (PSBF) ....	140
Figure 6-2 Decays and the decay parameters and PLQYs for PSBF in different solvents, the data is reproduced with the kind permission of S.I.Hintschich. ....	144
Figure 6-3 Results of Density functional theory calculations for an unsubstituted PSBF (a) and an alkoxy substituted PSBF (b &c) similar to the polymer studied. ....	145
Figure 6-4 Absorption and photoluminescence of the polyfluorene derivatives Pf2/6 films (red) and PSBF in solution (green) and PSBF films (black).....	146
Figure 6-5 Compendium of time resolved pump probe spectra, Pf2/6 300K (lower), PSBF 300K (middle) and PSBF toluene solution (top) measured at different delay times after excitation (solid – 10ps, dash – 20ps, dot – 50ps), (pump excitation density ~1μJcm <sup>-2</sup> ). ....	147
Figure 6-6 Pump-probe kinetics for PSBF in solution, compared with the ground state recovery and fluorescence decay. ....	148
Figure 6-7 Dynamics of the excited state features in films of the two polymers, Black – ground state recovery, Red – PA1, Green – PA2, Blue – Fluorescence. ....	149
Figure 6-8 Excitation dose dependence of the intensity of the pump-probe spectral features PA1 initially (●), PA1 after 50ps (○) and PA2 (■). The solid line shows a linear relationship between the pump dose and the intensity of the PA signal. ....	150
Figure 6-9 Top panel: Field assisted pump-probe spectra at various delay times after excitation (Black - 10ps, Red - 20ps, Blue - 30ps). Lower panel: Charge induced absorption spectrum for a PSBF device. ....	151
Figure 6-10 Build up of the field induced pump probe signal at PA1 (o) and PA2, the solid line in the PA2 trace is the fit to a single exponential rise with lifetime rise time 10.5ps.....	154
Figure 6-11 The effect of the temperature on the decay of the singlet induced ansorption signal at PA1. ....	156
Figure 6-12 Arrhenius plot for the energy transfer between charged state and singlet exciton. The values are taken form table 5.10.....	157
Figure 6-13 Reversible two state kinetic model as applied to PSBF. ....	158
Figure 6-14 Amplitudes of the components of fitting the pump - probe decays of PSBF in Toluene solution at the different wavelengths to equation 5.6, Also shown is the amplitude calculated from the fits at t(0); the amplitudes are compared to the pump-probe spectra at t(0), and the charge induced absorption spectrum (scaled appropriately). ....	160

Figure 6-15	The orbital overlap required for spiroconjugation and the effect on the energy levels of the HOMO and LUMO. (a) shows the p-orbitals involved in the interaction, (b) is a Fischer projection of the orbitals where the symmetry is not appropriate for spiroconjugation, (c) shows the correct orbital symmetry for spiroconjugation. (d) shows the effect of the spiroconjugation interaction on the LUMO on one half of the molecule and the HOMO on the other half forming the spiroconjugated frontier orbitals. ....	162
Figure 7-1	Methyl-Ladder-Polyparaphenylene .....	169
Figure 7-2.	(a) An exciton distribution is created high up in the DOS. (b) By dispersive migration the excitons can energy transfer to lower sites until trapped in the tail of the DOS. (c) Alternatively, the sites themselves can relax to lower energy, leaving the rest of the DOS unchanged. ....	173
Figure 7-3	Absorption (■) and Fluorescence (●) spectra for MeLPPP. The red lines are the fits to a series of Gaussians (fluorescence) or the convolution of a Gaussian and an exponential (absorption). The green lines are the individual components. The numbers give an indication of the corresponding oligomer length of various positions in the DOS. ....	174
Figure 7-4	Non-degenerate 3.2eV pump-probe decays for probe energies of 2.72, 2.69 and 2.82eV..	176
Figure 7-5	Pre-exponential factors (Decay Analysed Spectra) for the two decay components (400fs - ●; 4.2ps - ▲; y0 - ■) for the global analysis of non degenerate photobleaching decays at different energies. These are compared with the (inverted) absorption spectrum (dashed) and its first derivative (solid). ....	177
Figure 7-6	Top: Degenerate pump-probe decays at different pump/probe energies, the red lines are examples of the fits, from which the amplitudes in figure 7.7 originate. ....	178
Figure 7-7	Progression of the proportion of states undergoing a rapid decay, with the excitation energy. ....	178
Figure 7-8	Anisotropy decays for non-degenerate pump probe with the pump beam at 3.2eV and the probe beam at 2.73(▲) and 2.78eV (■).....	179
Figure 7-9	Degenerate anisotropy decays for pump and probe at 2.78eV (○) and 2.69eV (■). ....	179

# 1 Introduction

## 1.1 Conjugated Polymers and PLEDs

As we progress into the 21<sup>st</sup> century the demand for sophisticated electronic devices becomes greater every year. The key to commercial success is invariably due to way in which consumers are able to interact with technology; often the display is the key part in this process. The use of organic electronics to improve the quality of displays in consumer electronics is fast becoming a reality, gadgets such as mp3 players and mobile phones employing organic displays are entering the marketplace and have successfully established themselves. While it could be said that the polymer based side of the industry is playing catch up in terms of display quality, polymeric devices hold an important advantage in the potential cost to build. This advantage is seen none more so than in the drive to produce efficient new materials for lighting applications, it is estimated that 25% of the world's electricity is used in lighting for the home and workplace, much of this with inefficient incandescent light bulbs. Through the use of cheap, large area lighting panels based on solution processable conjugated polymers a revolution in lighting can be brought about, the increased efficiency of organic lighting over the incandescent bulb could herald real benefits in terms of the amount of electricity used by the world for lighting.



Figure 1-1 Some examples of polymer led technology used for lighting and high quality displays.

## **1.2 Motivation**

Development of the most efficient materials for polymeric electroluminescent applications is key to the viability of the field of polymer electronics; in order to do this one must understand the electronic processes in the materials that govern light emission. Time resolved spectroscopy allows one to follow the journey of the excitons in the material from their generation to the end of their lifetime; the most important exciton processes for the efficiency of the device are those that do not ultimately lead to the emission of light, the so-called exciton quenching processes. Pump probe spectroscopy, the principal technique used in this thesis, holds a valuable advantage over the more conventional emission spectroscopies such as time resolved luminescence as it allows investigation of the non emitting species as well as those which ultimately lead to light generation. This is of fundamental importance when considering the quenching of excitons as it allows the understanding of the quenching product rather than the overall effect of the process. As typical exciton lifetimes in conjugated macromolecules are below 1ns most of the relevant processes occur on a pico- and femtosecond timescale, thus ultrafast lasers and their associated techniques are ideal for the study of such processes.

The other process of great importance to the field concerns the generation of the emissive excitons themselves. The proportion of the charges injected into the device that result in the emission of light (known as the quantum efficiency of a device) is directly related to the proportion of charges that combine to form the emitting species (excitons). Study of this process is inherently difficult as time resolved electrical measurements are limited to time resolutions far in excess of the lifetime of the exciton so the principal question of whether the exciton is formed directly or via an intermediate state during the device operation is difficult to answer. Femtosecond spectroscopic techniques involving an electric field as well as light can go some way to help understanding these processes of charge trapping and exciton formation.

### 1.3 Previous Studies

The pioneering discovery of electroluminescence from conjugated polymers was made in 1990 by *Burroughes et al*, from the Cambridge group, starting a wave of interest from dozens of groups around the world<sup>1-4</sup>. In the more specific area of pump-probe spectroscopy of conjugated polymers there are fewer groups, some of which have approached the field from a background in ultrafast spectroscopy and some, including our group in Durham, which have made the approach from the side of conjugated polymers. Much of the initial work was carried out by *McBranch et al*<sup>5, 6</sup>, whose research into the pump-probe signatures of the various different types of excitations in a number of pristine conjugated polymers have allowed some general features, which are broadly applicable to most conjugated polymers, to be assigned. Following on from this initial work, the ultrafast spectroscopy group of Lanzani in Milan has studied conjugated polymers extensively, applying some of the more sophisticated techniques such as pump-push-probe, photocurrent cross correlation and field assisted pump-probe spectroscopy<sup>7-9</sup>. These experiments have been used to elucidate the processes which cause excitons to dissociate into charges, and to attempt to understand the charge trapping and exciton formation process. Naturally many other groups have made a valuable contribution to the ultrafast studies of conjugated polymers, including the Cambridge group and many in the USA and much of the work is referenced throughout this thesis.

One of the common criticisms of the early pump-probe work relates to the high excitation densities used. Often the excitation densities required, due to the inherent insensitivity of absorption experiments, compared to, for example fluorescence, are far greater than the excitation densities found in devices. While this is not a problem as such, many of the phenomena observed to dominate at such high excitation density are not so important at the lower excitation densities found in devices or in other experimental techniques. Specifically, the interactions between excitons such as singlet-singlet and singlet-triplet annihilation must be considered for ultrafast experiments whereas in time resolved fluorescence studies they are rarely observed. Efforts have been made in this thesis to avoid such processes where possible, this is achievable because of the superior signal to noise ratio of the pump-probe spectrometer we have developed, which be discussed further in chapter 3.

## **1.4 References**

- <sup>1</sup> R. Friend, D. Bradley, and A. Holmes, *Physics World* **5**, 42 (1992).
- <sup>2</sup> M. A. Baldo, D. F. O'Brien, Y. You, et al., *Nature* **395**, 151 (1998).
- <sup>3</sup> J. H. Burroughes, D. D. C. Bradley, A. R. Brown, et al., *Nature* **347**, 539 (1990).
- <sup>4</sup> Y. Cao, I. D. Parker, G. Yu, et al., *Nature* **397**, 414 (1999).
- <sup>5</sup> B. Kraabel, V. I. Klimov, R. Kohlman, et al., *Physical Review B* **61**, 8501 (2000).
- <sup>6</sup> D. W. McBranch, B. Kraabel, S. Xu, et al., *Synthetic Metals* **101**, 291 (1999).
- <sup>7</sup> T. Virgili, G. Cerullo, L. Luer, et al., *Physical Review Letters* **90**, 247402 (2003).
- <sup>8</sup> G. Lanzani, G. Cerullo, D. Polli, et al., *Physica Status Solidi a-Applied Research* **201**, 1116 (2004).
- <sup>9</sup> C. Gadermaier, G. Cerullo, G. Sansone, et al., *Physical Review Letters* **89**, 117402 (2002).



## 2 Theoretical Considerations

### 2.1 Conjugated Polymers: Structure and Bonding

In a school textbook, organic molecules are considered as covalently bonded molecules joined by the sharing of electrons between each other. In the more sophisticated theory of molecular orbital theory the same idea essentially holds true, each individual atom which makes up a molecule contributes bonding electrons to an orbital which covers the whole molecule<sup>1</sup>.

In a simple diatomic such as molecular hydrogen, H<sub>2</sub>, when the two hydrogen atoms are brought together their individual atomic s-orbitals interact and combine, forming molecular orbitals known as  $\sigma$ -orbitals. The fundamental principle of molecular orbital theory requires conservation of orbitals and overall orbital energy. Thus two  $\sigma$ -orbitals are formed, the  $\sigma$ -orbital which is lower in energy than the original atomic orbitals, and the  $\sigma^*$  which is higher. Once the orbitals are formed one must consider their occupation. Hydrogen atoms have one electron each; the Pauli exclusion principle stipulates that an orbital can hold two electrons of different spin, in order to keep the energy of the system as low as possible the lowest orbitals are filled first. The occupation of the orbitals determines the bonding of the system, because the hydrogen molecule has only two electrons, the  $\sigma$ -orbital, known as the bonding orbital is filled and the  $\sigma^*$ -orbital, the antibonding orbital, remains unfilled. Therefore, the overall energy of the system is lower in the bonded state compared to the atoms being free and hence the molecule is stable. If the overall energy of the bonded system is not lower, i.e. if the antibonding orbital were also filled, the molecule does not form. The example of this would be diatomic Helium, the molecular orbitals are the same as H<sub>2</sub> but the occupation of both the  $\sigma$  and the  $\sigma^*$ -orbital means there is no bonding as there is no energetic advantage. The highest occupied molecular orbital is normally referred to as the HOMO and the lowest unoccupied molecular orbital is the LUMO. The concepts surrounding orbital formation and bonding are shown in figure 2.1.

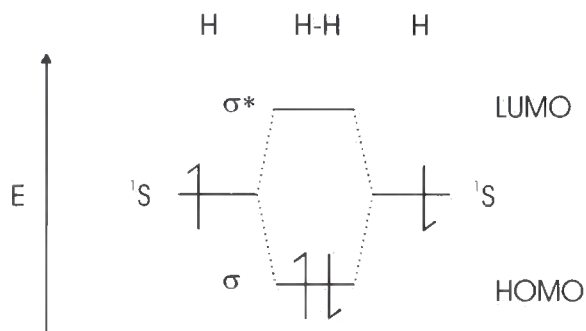


**Figure 2-1 Schematic of orbital formation and bonding in H<sub>2</sub>.**

In larger organic systems, where the atomic orbitals are no longer simple s-orbitals the processes of promotion and hybridisation occur, this is easily demonstrated in the molecule methane, CH<sub>4</sub> which has 4 identical C-H bonds. Firstly, considering the carbon, which in its atomic state has only 2 unpaired electrons, in 2 of the 2p-orbitals. However, forming only two bonds would not fulfil the octet rule; when the outer shell of the atom is complete with 8 electrons it is at the lowest energy. Thus one electron is promoted from the 2s to the remaining 2p to form 4 unpaired electrons in the 2s, 2p<sub>x</sub>, 2p<sub>y</sub> and 2p<sub>z</sub>. The 4 orbitals then become mixed into what are known as hybridized orbitals creating 4 identical sp<sup>3</sup> hybrids (figure 2.2) each containing one valence electron which are able to bond with the hydrogen atoms' s-orbitals creating 4 identical σ-bonds.

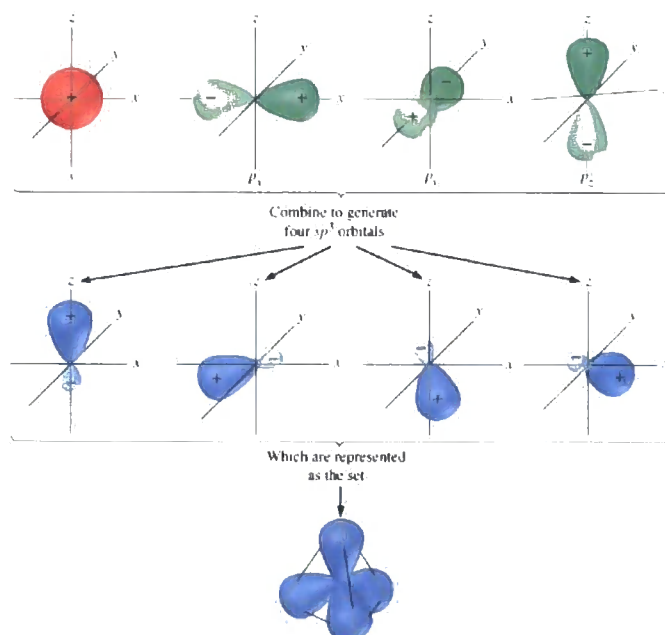


**Figure 2-2 Formation of sp<sup>3</sup> hybrid orbitals required for the bonding in methane<sup>2</sup>.**

Depending on the bonds formed in a molecule different hybrid orbitals are needed, with contributions from different atomic orbitals, of particular interest for conjugated systems is the  $sp^2$  hybrid formed from the  $2s$  and  $2p_x$  and  $2p_y$  orbitals on the carbon atom. In this case the  $2p_z$  is left free thus the atom is only able to form 3  $\sigma$ -bonds. As the  $p_z$  orbital does not take part in these  $\sigma$ -bonds they all remain in the x-y plane, therefore the molecule is flat rather than tetrahedral. The simplest example of  $sp^2$  hybridization would be the molecule ethene. The remaining orbital, the  $p_z$  takes part in the bonding of the molecule in a different way, the two  $p_z$  orbitals on each of the carbon atoms in ethene project out of the molecule so are unable to overlap end to end as in a  $\sigma$ -bond, there can however be a lateral interaction between the orbitals. This interaction is known as a  $\pi$ -bond, the second bond in a so-called double bond. The lateral interaction between orbitals is not as strong as the end on interaction in a  $\sigma$ -bond thus the stabilisation of the filled  $\pi$ -orbital and the energy gap between the  $\pi$  and the  $\pi^*$  is less than the bonding and antibonding orbitals in the  $\sigma$ -framework of the molecule. As a result the HOMO in ethene is the  $\pi$  orbital and the LUMO the  $\pi^*$  orbital. Because the  $\pi$  interaction is through lateral overlap of the orbitals which project out in only one direction there can be no rotation around the bond, the ethene molecule is effectively locked planar by the  $\pi$ -bond.

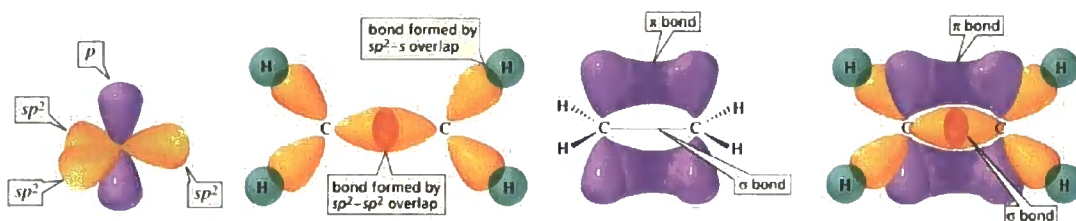
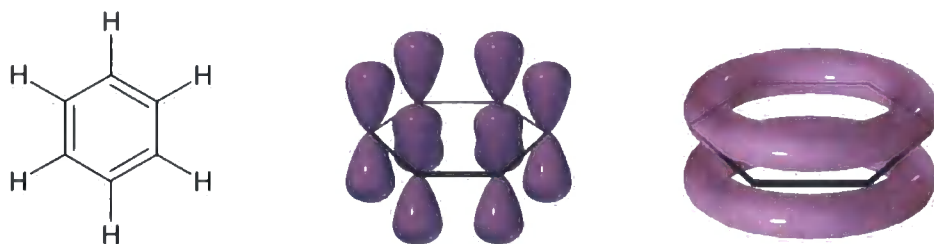


Figure 2-3 The  $sp^2$  hybrid and the formation of  $\sigma$  and  $\pi$  bonds in ethene<sup>2</sup>.

### 2.1.1 Conjugation

The molecule benzene, whose cyclic structure was allegedly discovered by Friedrich Kekulé during an inspirational dream, contains 3 sets of double bonds; in fact the structure is of alternating single and double bonds<sup>3</sup>. The  $\pi$ -orbitals are projected out of the plane of the ring allowing the  $\pi$  electrons to completely delocalise

around the ring. In effect, each  $\pi$  electron is shared by all six carbon atoms. This phenomenon is known as conjugation and it is found in all systems with alternating single and double bonds.



**Figure 2-4  $\pi$ -bonding in benzene, showing the p-orbitals projecting out of the plane of the molecule and effects of delocalisation and conjugation around the ring<sup>2</sup>.**

In conjugated macromolecules like conjugated polymers the  $\pi$ -electron cloud is theoretically delocalised over the whole molecule. There are naturally areas with greater or lesser  $\pi$ -electron density due to ring strains and distortions of the molecule but there is effectively an electron cloud around the molecule and the electrons are generally considered as being relatively free within this cloud. This extended conjugation induces some important electrical and electronic effects in the conjugated polymer. Most importantly for conjugated polymers, the  $\pi$ -electron delocalisation allows the molecule to conduct electric charge, as there is a continuous path of free  $\pi$ -electrons from one end of the molecule to the other. In actual fact the distortions and ring strains prevent pristine conjugated polymers from being fully conducting, thus they are considered as semiconductors<sup>4</sup>. Another important consequence of conjugation is in the positions of the HOMO and LUMO, the energy gap between the  $\pi$  and  $\pi^*$  orbitals is reduced as the energy levels of the molecule become stabilised by more and more electrons taking part in the bonding. This is important because in conjugated macromolecules the energy gap approaches the energy of visible light, thus the molecules become useful in optoelectronic applications<sup>5-8</sup>.

## 2.2 Optical transitions in Conjugated Polymers

### 2.2.1 The Nature of the Excitations in Conjugated Polymers

Initially the observation of the semiconducting nature of the conjugated polymers led scientists to develop theories based on inorganic semiconductor theory, resulting in the development by Su, Schreiffer and Heeger of the SSH Hamiltonian<sup>9-11</sup> for conjugated polymers. In this theory the properties of the material were based on the electron-phonon interactions with little attention paid to the electron-electron correlation. This led to excitations such as polarons, bipolarons and solitons freely carrying charge in a conduction band with a valence band of unexcited electrons below, this is similar to the band description of conventional inorganic semiconductors. However, extensive studies of the optical properties led to a change of thinking, pioneered by *Bassler et al*, the electron-electron interaction is in fact the dominant one and the excitation is like that of small conjugated molecules<sup>12</sup>. This is an excitation of the molecule as a whole, where the electron in the  $\pi^*$  orbital is strongly correlated to the hole in the  $\pi$  orbital, this is similar to the bound electron hole pairs found in inorganic semiconductors and is thus known as an exciton<sup>13</sup>.

The simplest optical transition in conjugated polymers is the  $\pi$ - $\pi^*$  transition which is typically in the visible to near UV wavelengths. An electron can therefore be excited to the LUMO by the absorption of a photon of visible light. The strength of the  $\sigma$ -bond framework and the high energy of the  $\sigma$ - $\sigma^*$  energy gaps means that the  $\pi$  electron can be excited with little effect on the bonding of the molecule. In certain molecules and polymers which contain heteroatoms with a lone pair of electrons which do not necessarily take part in the bonding, (O, N, S etc) extra energy levels are introduced into molecular orbital diagram. It is often the case that one of these additional nonbonding orbitals form the HOMO or LUMO thus the lowest energy optical transition can involve one or other of these orbitals, resulting in an  $n$ - $\pi^*$  or  $\pi$ - $n^*$  transition<sup>14</sup>.

In conjugated polymers there is much disorder compared to smaller conjugated molecules thus it is not generally possible to think of the exciton as an excitation of the whole molecule<sup>15</sup>. It is generally considered as an excitation of a segment of the polymer chain defined by some defect, either chemical or structural; the result of this is that the varying length of the segments or the differing conformations or strains on the polymer segments leads to very inhomogeneously broadened transitions. This wide distribution of states introduces many important effects for the photophysics of conjugated polymers<sup>15-20</sup>.

### 2.2.2 Exciton Types

In semiconductor theory, excitons are generally considered as being analogous to hydrogen atoms; thus, they are divided into three types depending on their Bohr radius, which determines how tightly they are bound and their binding energy<sup>21</sup>. The tightest bound are Frenkel excitons, this is where the Bohr radius is smaller than the internuclear distance. In conjugated molecular systems, this is analogous to the exciton being localised on a single molecule or polymer segment; an intrachain exciton in conjugated polymers, they can also be referred to as a locally excited state (LE). This is the most common type of excitation found in conjugated polymers. A Mott-Wannier exciton has its radius much greater than the intermolecular distance thus the electron and hole would not necessarily be found on the same polymer chain at all, this is often referred to as an interchain exciton. The final type, which is perhaps the most interesting, is the Charge-Transfer exciton, where a distance similar to size of the molecule (or the internuclear distance in semiconductor physics) separates the electron and hole. In molecular systems, these states occur when the excitation of the molecule involves a large movement of electron density from one part of the molecule to another. For example, on excitation the electron could become localised on one part of the molecule or polymer chain rather than being delocalised over a larger area. Consequentially these states are often found in molecules with a large (ground state) inherent dipole moment to drive the movement of the charge, the localisation of the electron away from the hole results in a concomitantly large dipole in the excited state as well. This is often referred to as an intramolecular charge transfer excited state (ICT).

### 2.2.3 Polarons

In molecular systems where uncorrelated charges are found these are known as polarons. Polarons consist of a single charge and its associated polarisation field. In conjugated polymers the field associated with a single charge induces a structural change on part of the chain; a phonon interaction, this combination of an electron and a phonon is a polaron. These free charges are especially important in the conduction of conjugated polymers; they can be induced by chemical doping, charge injection into a device driven by an electric field or by the dissociation of an exciton<sup>22-24</sup>. The dissociation of an exciton results firstly, in the formation of a polaron pair, if the charges remain correlated but not tightly bound this is referred to as a geminate pair. If the charges are no longer correlated they are considered to be analogous to free charges. The free charges are able to travel relatively freely in a polymer film, until they become trapped at a defect or high electron affinity molecule, alternatively two charges may recombine into an exciton. In an electroluminescent device the formation of excitons from charges injected at an electrode forms the basis of the light emission mechanism<sup>24, 25</sup>.

The dissociation of an exciton into charges requires some driving force; the exciton has a binding energy ( $\sim 0.8\text{eV}$ ) which must be overcome. The simplest way is by the application of an electric field to separate the charges; this can either be applied externally<sup>26, 27</sup> or by the local polarisation of the chain by a defect or an electron (or hole) acceptor which draws one of the charges off the chain. Such electron transfer reactions have been observed between conjugated polymers and electron accepting solvents (such as  $\text{CCl}_4$ ); the result is the radical cation of the polymer and the radical anion of the solvent<sup>28</sup>. In terms of chemistry it is a simple redox reaction, the polymer is oxidised and the solvent reduced. The highly reactive radical cation of the polymer is then likely to undergo a chemical reaction causing a permanent defect.

The creation of a polaron or radical ion of the polymer gives rise to a slightly different orbital picture compared to electronic excitation, the unpaired charge results in a singularly occupied molecular orbital (SOMO), the SOMO gives rise to

additional electronic transitions between the HOMO and LUMO and the SOMO which are often used to characterise the polaron<sup>29</sup>.

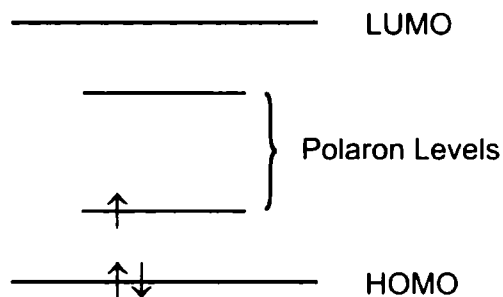


**Figure 2-5** Polaron transitions are often used in spectroscopy to verify the presence of charges in conjugated polymers.

### 2.3 Singlet and Triplet Excited States

As excitons are formed from electrons and holes, the quantum mechanical nature of the particles must be considered, both are spin  $\frac{1}{2}$  fermions thus two spin states are formed when bound; with total spin vector  $\underline{S} = 0$ , spin singlet or triplet  $\underline{S} = 1$  (equation 2.2). Most molecules, including conjugated polymers have a singlet ground state, thus optical transitions can only produce singlet excited states. The spin must be conserved throughout an optically allowed transition and the photon has integer spin so cannot change the spin of an electron to switch between singlet and triplet states. Consequentially radiative decay of purely triplet excited states is forbidden. In conjugated polymer devices this causes problems, the charges are injected with random spins, thus from simple spin statistics one would expect  $\frac{3}{4}$  of the excited states to be triplets. The discussion of the reliability of simple spin statistics is a thesis in itself it is generally found that a large proportion of excitations formed are triplets and therefore the forbidden nature of their radiative decay represents a significant loss channel for conjugated polymer devices. This is just one illustration of the importance of the study of excited states that decay non-radiatively to conjugated polymers for LED applications.

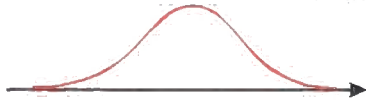
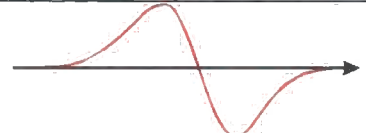
$$\begin{aligned}
 \text{Singlet} &= \frac{1}{\sqrt{2}} [(\uparrow\downarrow) - (\downarrow\uparrow)] \\
 \text{Triplet} &= \begin{cases} (\uparrow\uparrow) \\ \frac{1}{\sqrt{2}} [(\uparrow\downarrow) + (\downarrow\uparrow)] \\ (\downarrow\downarrow) \end{cases}
 \end{aligned}
 \tag{Equation 2-1}$$



### 2.3.1 Singlet and Triplet Energy

Most molecules with a singlet ground state have their lowest excited state energy level as the  $T_1$  triplet state rather than the  $S_1$ . The difference in energy of the triplet state compared to the singlet is known as the singlet triplet splitting. This is a fundamental outcome of some of the founding principles of molecular quantum mechanics, the electron exchange integral. The magnitude of the exchange integral is dependant on two factors, the spatial extent of the wavefunction and the correlation of the charges; the higher the correlation between the two charges the lower the effect of the electrostatic force between them.

The wavefunction of the state is the product of the spin part and the space part of the wavefunction, as the overall wavefunction is antisymmetric, either the space part, or the spin part (but not both) must be antisymmetric. The wavefunctions with an antisymmetric space part have a node in the centre, therefore the probability of finding the charges close together is low. The consequence of this is that the charges are further apart and the electrostatic potential energy of the charges in the antisymmetric space wavefunction is lower. The spin multiplicity of the state becomes important because the triplet states are the symmetric spin states with an antisymmetric space part to their wavefunction. Essentially, in this description the electrons are further apart in the triplet state thus the energies of the triplet states are lower; this is summarised in table 2.1.

	Space Wavefunction	Spin Wavefunction	Electrostatic Energy
Singlet	 Symmetric	$\frac{1}{\sqrt{2}} [(\uparrow\downarrow) - (\downarrow\uparrow)]$ Antisymmetric	High
Triplet	 Antisymmetric	$\frac{1}{\sqrt{2}} [(\uparrow\downarrow) + (\downarrow\uparrow)]$ $(\uparrow\uparrow)$ $(\downarrow\downarrow)$ Symmetric	Low

**Table 2-1** The implications of the wavefunction symmetry on the energy of singlet and triplet states.

The magnitude of the exchange integral is also dependant on the spatial extent of the wavefunction, thus more confined wavefunctions (analogous to a particle in a smaller box) such as those found on small oligomers have a larger exchange integral than highly delocalised wavefunctions (particle in a large box) found in macromolecules and polymers. This is the origin of the reduction in singlet triplet splitting on going from for example 1-fluorene ( $E_{S-T} \sim 1.1\text{eV}$ ) to polyfluorene ( $E_{S-T} \sim 0.75\text{eV}$ )<sup>30, 31</sup>.

### 2.3.2 Intersystem Crossing

Once created, singlet and triplet excitons are not necessarily fixed in their respective spin state. The process of intersystem crossing allows excitations to cross between the two spin manifolds. This falls into two categories,  $S_1-T_1$  intersystem crossing, which allows the formation of triplet excited states from singlets, and  $T_1-S_0$  intersystem crossing, which allows for the radiative decay of the triplet excitons known as phosphorescence. A number of factors govern intersystem crossing rates: the orbital nature of the state, the level of spin orbit coupling, spin vibronic coupling and the overlap of the singlet and triplet states<sup>32-34</sup>.

Firstly, one considers the level of spin orbit coupling; the spin orbit interaction normally provides the necessary perturbation required to flip an electron spin thus transferring the exciton between the manifolds. This perturbation works by allowing a mixing between the singlet and triplet states, naturally the larger the nucleus of the atoms involved the larger the spin orbit interaction. Thus, molecules with heavy atoms have higher intersystem crossing rates. This phenomenon is utilised to great effect in PLEDs, by doping the conjugated polymer with phosphorescent heavy metal complexes the triplets, which would normally decay non-radiatively, can be captured by the complex and utilised for light emission. The precise nature of the mixing between singlets and triplets caused by the spin orbit interaction depends on the symmetry of the molecule and its excited states, as only states of the same symmetry can mix. The perturbation required to change manifold can also be provided by a

phonon, in the form of spin-vibronic mixing, which is the dominant process in the non-radiative decay of the triplet. A number of effects relating to spin orbit coupling and the rate of intersystem crossing are discussed in chapter 4.

The effect of the orbital nature of the states is manifested in El-Sayed's rule which specifies that

$$\langle S_{n-\pi} | H_{SO} | T_{\pi-\pi} \rangle \approx \langle S_{\pi-\pi} | H_{SO} | T_{n-\pi} \rangle \gg \langle S_{\pi-\pi} | H_{SO} | T_{\pi-\pi} \rangle \quad \text{Equation 2-2}$$

There is a higher spin orbit interaction between states of different orbital nature,  $\pi$  or  $n$ . Consequentially there is a high intersystem crossing rate when there is a change in the orbital nature during the transition, therefore molecules with  $n-\pi^*$  and  $\pi-n^*$  singlet excited states are associated with a high intersystem crossing rate. This is the cause of the high triplet yield found in molecules such as benzophenone and thiophene where the excited state involves the lone pair of the heteroatom (non bonding orbital)<sup>34</sup>.

Intersystem crossing between the manifolds is an isoenergetic process, due to the instantaneous nature of the spin flip. Thus (for  $S_1-T_1$ ) there must be an accepting triplet state near in energy to the singlet, this can be a vibronic level of the lowest excited triplet state ( $T_1$ ) or, more commonly, a higher triplet excited state and its associated vibronic levels, which rapidly relaxes to the lowest triplet excited state. This is manifested in the Franck-Condon weighted density of states, which is discussed further in chapter 4.

## 2.4 Electronic Processes in Conjugated Molecules

### 2.4.1 Absorption

An electronic transition in a conjugated molecule can be excited by the absorption of a photon of appropriate energy; in most cases, an exciton is formed. The absorption is considered classically as the interaction of an electromagnetic field with an electric dipole oscillating at the same frequency<sup>35</sup>. The magnitude of the interaction is described by the transition dipole moment which is an integral over the initial and final wavefunctions of the state and the electric dipole moment operator (equation 1.3). It can be considered as the redistribution of charge between the initial and final states that accompanies the excitation. Most electronic transitions are dipolar in nature although in some special cases higher order (e.g. quadrupolar) transitions are possible.

$$\mu_{i-f} = \langle \psi_i | e\vec{r} | \psi_f \rangle \quad \text{Equation 2-3}$$

The dipolar nature of the electronic transition imparts the transition with an orientation, only electromagnetic waves that are oriented in the same direction as the transition dipole moment are able to interact with the state thus only light polarised in the same direction as the transition is absorbed. This can be particularly relevant in conjugated polymers, which are long, and often rigid molecules and so can become oriented resulting in high absorption anisotropy. The willingness of an electronic transition dipole to absorb light is described by its oscillator strength. This takes account of not only the magnitude of the transition dipole moment but also the energy of the transition ( $\nu$ ); it thus connects the quantum mechanical property of the transition dipole moment with the macroscopic world. The oscillator strength is defined as<sup>36</sup>:

$$f_{nm} = \left[ \frac{8\pi^2 m_e c}{3e^2 h^2} \right] \nu_{nm} |\mu_{nm}| \quad \text{Equation 2-4}$$

The oscillator strength is a dimensionless property which can be related to the molar extinction coefficient for a molecule which is essentially a measure of the probability of absorbing a photon of a given wavelength; this extinction coefficient gives rise to the absorption spectrum of a molecule. The proportion of incident light absorbed is related to these properties by the Beer-Lambert law<sup>37</sup>.

$$A(\lambda) = \log\left(\frac{I}{I_0}\right) = \varepsilon(\lambda)cl \quad \text{Equation 2-5}$$

where  $I$  and  $I_0$  are the transmitted and incident light intensities respectively,  $\varepsilon$  is the extinction coefficient,  $c$  the concentration of the molecule and  $l$  the path length.

In addition to electronic transitions, molecules possess a large number of vibrational levels, which can be excited. These are due to vibrations of the bonds in the molecule, these vibrational modes can couple to the electronic transition which gives rise to vibronic replicas of the electronic transition. The different vibronics of the ground state absorption represent excitations from the different vibrational sub levels of the ground state to different vibrational levels of the excited state. As the transition dipole moment describes the change in charge distribution of the molecule on excitation it follows that there are structural changes as well. These often relate to the shortening of bonds as the charge becomes more or less localised between two atoms, for example the atomic separation in a diatomic. A classic example of this is the excitation of benzene, on excitation the charge distribution on the ring changes and this is followed by a relaxation of the structure from the benzoid to the quinoid structure. These structural changes are not instantaneous however, this is described by the Franck-Condon principle which postulates that excitation occurs faster than the vibrations of a molecule and so there can be no change in the position of the nuclei during excitation. Because of this, when the molecular states are drawn on a potential energy diagram radiative transitions are described as vertical transitions because all the energy change is due to the photon and there is no change of structure. Similarly non radiative transitions are horizontal only. If the molecule does not possess a suitable vibrational level to absorb the photon, bond dissociation occurs, i.e. if the excitation is

outside the parabola for the excited state the excited state does not form. As there can be no change of the molecular coordinate during excitation there must be an overlap between the wavefunction in the excited state and the wavefunction in the ground state. Quantum mechanically one can describe the strength of a vibronic transition as the being proportional to the square of the overlap integral between the initial and final vibrational levels, this integral is known as the Franck-Condon Factor. The principal is illustrated in figure 2.6.

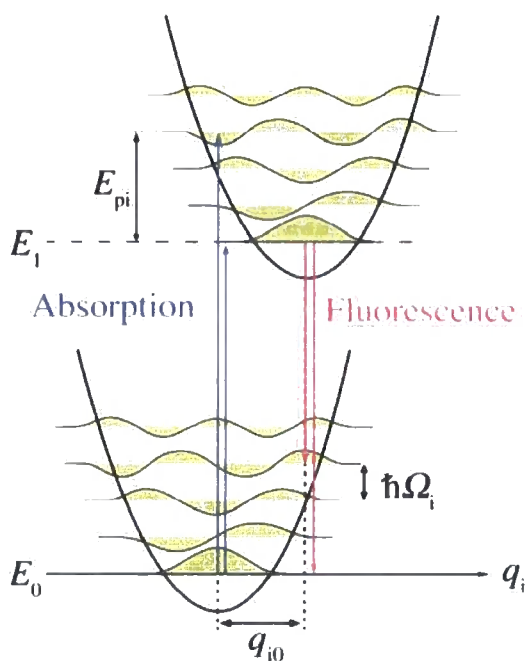


**Figure 2-6 An illustration of the absorption and fluorescence process demonstrating the need for Franck-Condon overlap and the formation of the vibronic spectra.**

## 2.4.2 Fluorescence

Following a vertical transition to an excited state there is normally a rapid relaxation of the molecule to its lowest vibrational level (figure 2.6) and after some time a photon is emitted as the molecule once again returns to its ground state, or a vibrational sub level of the ground state. The rapid relaxation to the lowest vibrational level is known as Kasha's rule, and is the origin of the often observed mirror symmetry between absorption and fluorescence spectra, the vibronic peaks in the absorption and fluorescence spectra are both related to the vibrational sublevels of

the ground state. In addition to the vibrational relaxation there can also be structural relaxation of the excited state, these large-scale conformational changes in the excited state are necessary for the stabilisation of the different charge distribution found in the excited state compared to the ground state. The loss of energy due to such conformational changes is manifested in an energy shift between the high energy absorption of the molecule and the fluorescence, known as the Stokes' shift.

### 2.4.3 Non Radiative Decay

Electronically excited states can also decay non-radiatively to their ground state; this is known as internal conversion and is assisted by vibrational modes in the molecule. All non radiative transitions are described as being 'horizontal' in terms of the potential energy diagram, this means that the transition from one state to another initially requires no change of potential energy of the system. It is a change from an electronically excited state to a vibrationally-excited state, following this horizontal crossing to the lower electronic excited state the energy is lost through vibrational relaxation. Other non radiative processes which result in a loss of singlet excited states can be intersystem crossing to the triplet state (as described previously) or quenching of the emission by energy transfer to another excited state in another molecule.

### 2.4.4 Decay Rates and Quantum Yield

Each process, either radiative or non-radiative is associated with a certain probability as governed by Fermi's Golden Rule.

$$k_{i \rightarrow f} = \frac{2\pi}{\hbar} \langle i | H | f \rangle^2 \rho$$

Equation 2-6

where  $k$  is the rate of the transition between initial state  $i$  and final state  $f$ ,  $\rho$  is the density of states of the final state.

The various decay rates for each process combine to govern the overall decay of the state, thus the observed decay of the fluorescence is a combination of all of these:

$$\frac{dN_s}{dt} = -(k_r + k_{isc} + k_{ic})N_s + G \quad \text{Equation 2-7}$$

where  $k_r$  is the natural decay rate of the singlet states,  $k_{isc}$  is the intersystem crossing rate and  $k_{ic}$  is the rate of internal conversion and  $G(t)$  represents the initial singlet population. One can define the photoluminescence quantum yield as the proportion of all the states that decay radiatively which is a result of the competition of all the decay processes.

$$Q = \frac{k_r}{k_r + \sum k_{nr}} \quad \text{Equation 2-8}$$

#### 2.4.5 Higher Excited States

In addition to excitation to the first excited states  $S_1$  and  $T_1$ , higher energy levels can be accessed, through a number of processes, firstly, should selection rules allow, by direct absorption from the ground state either by one high energy photon or multiphoton absorption. Alternatively, by sequential (induced) absorption, a first excited state is excited by a low energy photon and subsequently the molecule is excited again by a second low energy photon. The higher excited states normally undergo rapid non radiative decay (Kasha's rule) to the first excited state thus no emission is observed. In some cases the absorption of a second photon to a higher excited state gives the molecule sufficient energy to overcome the exciton binding energy and bond dissociation occurs.



## 2.4.6 Phosphorescence

There is no allowed transition between the excited triplet state and the ground state, the change of spin is quantum mechanically forbidden; thus the probability of the radiative triplet decay known as phosphorescence is generally low. The resulting long phosphorescence lifetime (can be in the seconds) means that there is a very high probability of non-radiative triplet decay or quenching, thus the phosphorescence quantum yield is normally very low. As with intersystem crossing, the small amount of radiative decay that is observed is due to the slight mixing of the triplet states with other states of singlet character, mediated by spin orbit coupling; this provides a sufficient perturbation to allow the weak phosphorescence emission. One of the most important sources of triplet quenching comes from the interaction of triplet states with molecular oxygen. Molecular oxygen is paramagnetic, it has a triplet ground state, and thus it can efficiently quench the excited triplet states by energy transfer. This is particularly prevalent in solutions where there can be a large amount of oxygen dissolved in the solvent. In the solid state, triplet quenching is very efficient compared to the radiative decay rate of the triplet. Therefore, it is not normally possible to observe phosphorescence at room temperature, by cooling down to  $\sim 10\text{K}$  the triplet mobility can be reduced to almost nil, thus there is a sufficient reduction in quenching to observe the phosphorescence.

## 2.4.7 Induced Absorption

The absorption of light by an electronic state is not confined to the ground state. Once created, an excited state then has its own characteristic absorption spectrum. This shows the allowed transitions from the state to higher excited states it is best demonstrated by the Jablonski diagram in figure 1.10. The initial excited states (e.g. singlet, triplet or charged states) can be created by any means, either chemical doping (doping induced absorption, DIA); electrical current (charge induced absorption, CIA) or most conventionally, and the focus of this thesis, by absorption of a photon (photoinduced absorption, PIA). In photoinduced absorption the initial excitation light is known as the pump, and the photons absorbed by the higher excited states are known as the probe. Analogous with conventional ground state absorption spectroscopy the proportion of probe photons absorbed is proportional to the number

of molecules in the excited state, the extinction coefficient of the excited state absorption and the distance over which the two beams interact (Equation 2.9). The proportionality between the strength of the absorption and the concentration of molecules in the excited state means that pump-probe spectroscopy is an excellent technique for measuring excited state populations. This is very useful for 'dark' states where fluorescence techniques cannot be used. The resulting pump-probe spectrum shows characteristic features of all the different excited states of the system and time resolved pump-probe techniques can elucidate the dynamics and relationship between the different states.

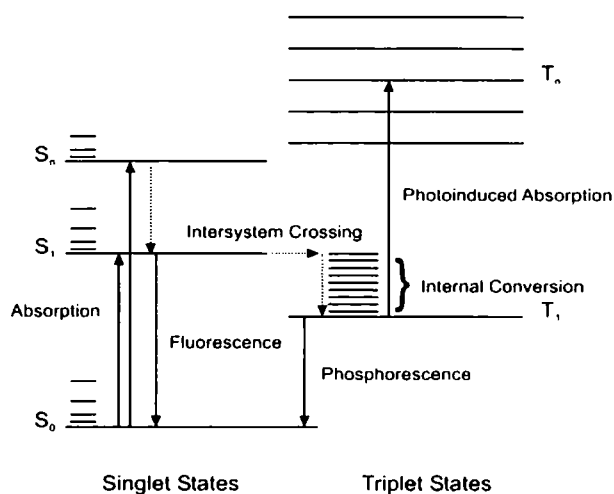
$$-\frac{dT}{T} = \sigma N \frac{l}{A} \quad \text{Equation 2-9}$$

where  $dT$  is the change in transmission when the sample is excited,  $T$  is the sample transmission,  $\sigma$  is the absorption coefficient of the excited state,  $N$  the population concentration of the excited states,  $l$  the length of the interaction of the two beams and  $A$  the area of overlap of the two beams.

In addition to showing the excited state absorption, pump-probe techniques also show the depletion of the ground state. When molecules are in their excited state they can no longer absorb in the ground state, thus the ground state absorption intensity drops and the dynamics of this photobleaching, known as ground state recovery, reflect the decay of all the excited states of a molecule. The ground state partially recovers when each of the excited states has decayed or its energy transferred to a different molecule.

## 2.4.8 The Jablonski Diagram

The Jablonski diagram is a simple way of understanding the relationship between the different excited states, their relative energies and their processes. It can include singlets, triplets, charge transfer states, acceptor molecules and any number of different states and excited state processes. An example is given below in figure 2.10, with a number of the processes discussed above marked.



Equation 2-10 A Jablonski diagram showing some of the most common processes in photophysics for the singlet and triplet states.

## 2.5 Exciton Processes

### 2.5.1 Energy Transfer

Excited states do not necessarily remain static until they decay, there are many dynamical processes that the excited states can take part in. Principally, these can all be considered as energy transfer; either energy transfer to an undesired defect, known as quenching, because the fluorescence quantum yield is reduced; energy transfer to a coloured dopant which is useful for emission tuning; or diffusion and migration of energy between different polymer chromophores. All of these energy transfer processes can be either intermolecular, i.e. between different polymer chains or intramolecular; between different parts of the same chain.

### 2.5.2 Forster Transfer

The simplest type of energy transfer, other than the trivial case of emission and reabsorption, is Forster transfer<sup>35, 38, 39</sup> (also known as resonance energy transfer). The Forster transfer mechanism is one of dipole-dipole coupling, the excited transition dipole of one chromophore couples to another transition dipole in the ground state and the energy is transferred by a resonance interaction. This resonance interaction imparts Forster transfer with a long range of energy transfer resulting in a

$(1/r)^6$ , (where  $r$  is the separation of the donor and acceptor), dependence of the rate of energy transfer. Other controlling factors in the interaction are the energy of the dipoles, as this is a resonance interaction the donor and acceptor dipoles must be of the same energy; both the absorption and fluorescence spectra are broad, thus the rate is proportional to the overlap of the absorption and emission spectra ( $J(\lambda)$ ). The final key term that originated from the resonance nature of the process is the orientation factor  $\kappa^2$  which is the mathematical description of the coupling between the two dipoles, perpendicular dipoles are not coupled at all, thus  $\kappa^2=0$  whereas parallel side by side dipoles are the most strongly coupled  $\kappa^2=4$  and colinear dipoles have  $\kappa^2=2$ . Generally, especially given the amorphous nature of the system one considers the dipoles to be randomly oriented thus  $\kappa^2=2/3$ . The rate of energy transfer is also determined by the refractive index of the medium and the luminescence quantum yield of the donor, the resulting rate of energy transfer is given by equation 2.11.

$$k_T(r) = \frac{Q_D \kappa^2}{\tau_D r^6} \left( \frac{9000 \ln(10)}{128 \pi^4 N n^4} \right) J(\lambda) \quad \text{Equation 2-11}$$

where  $J(\lambda)$  is the integral of the overlap of the absorption spectrum and the area normalised fluorescence spectrum,  $k_T$  is the rate of energy transfer,  $r$  is the separation of the species.  $Q_D$  is the luminescence quantum yield of the donor molecule (in the absence of the acceptor),  $n$  is the refractive index of the medium,  $N$  Avogadro's number,  $\kappa^2$  is the orientation factor described above. From equation 2.12 one can deduce that for two species that do not change; the sixth power in the distance-dependence term is the controlling parameter, thus this type of energy transfer system is often used as a molecular ruler for measuring the distance between two chromophores. The Forster radius, ( $R_0$ ) is the parameter that defines the critical distance for energy transfer, i.e. the distance where the energy transfer competes with the natural decay of the state, the definition is given in equation this is typically a few nanometres, for example for energy transfer between the dye molecules pyrene and coumarine  $R_0 = 3.9\text{nm}$ .

$$R_0^6 = 8.8 \times 10^{-28} \frac{\kappa^2}{n^4} Q_D J \quad \text{Equation 2-12}$$

### 2.5.3 Dexter Transfer

In some cases resonant energy transfer is not the dominant process and for optically forbidden transitions, such as those involving energy transfers to the triplet state, it cannot happen. In these cases energy transfer can still occur by the more generalised mechanism of Dexter transfer<sup>35, 36, 40</sup>. This is a direct electron transfer mechanism where the energy transfer is mediated by electron exchange between the two moieties. As this mechanism requires electrons to move from the donor to the acceptor there must be overlap of the orbitals of the donor with the acceptor. This means that the interaction is only active over a very short range, characterised by the size of the orbital, once again energetic overlap is required, so the spectral overlap integral features, and the characteristic distance which defines the orbital size known as the bohr radius (L) the rate is generalised as,

$$k_{ET} \propto J(\lambda)e^{-2r/L} \quad \text{Equation 2-13}$$

The exponential distance dependence (r) originates from the spatial overlap between the two exponentially decaying wavefunctions of the donor and acceptor, the mathematical implications of this exponential compared to the power law distance dependence of the Förster interaction are clear. When the distance of separation of the donor and acceptor is similar to the spatial extent of the molecules the Dexter rate is faster and thus the energy transfer proceeds via a Dexter mechanism regardless of whether resonant energy transfer is possible or not. At longer distances of course FRET, if allowed, dominates. There are some processes where only the Dexter process can be allowed, the most common is triplet transfer; there can be no resonant triplet transfer because in most systems without high spin orbit coupling, it is spin forbidden. However, the spin conservation rules can be preserved for Dexter transfer by the exchange of two electrons. Additionally, the electron exchange mechanism by which charge is transferred between molecules in devices is the same mechanism that mediates the process of Dexter transfer.

## 2.5.4 Migration, Diffusion and the DOS

Macromolecules such as conjugated polymers tend to have broad electronic transitions, this is primarily due to inhomogeneous broadening<sup>41</sup>. The transitions have a broad distribution of states (DOS) because there is an almost infinite variation of the conformation and configuration of the polymer chains. Even in dilute solution the polymer segments that are excited can be of different lengths and this can be restricted by conformational defects, chemical defects or their local environment. All of these seemingly insignificant factors lead to a very broad distribution of energies for the electronic transitions. It is for this reason that most conjugated polymers show broad featureless absorption spectra. The situation becomes worse in the solid state where the amorphous nature of the material puts the polymer chain into an almost infinite number of possibilities for the conformation, leading to even more inhomogeneous broadening compared to dilute solutions.

The broad nature of the DOS allows for dispersive exciton migration<sup>42-44</sup>. This is where excitons, which are created at high energy by excitation above the absorption edge, are able to rapidly transfer their energy to lower energy sites in the polymer. In a single chain picture, this would be excitons moving from short chain segments, which have a high energy to longer chain, lower energy segments. In solution this is typically a very fast process, taking only a few picoseconds, as the excitons cannot move between the chains so do not move far. In the solid state where there is much more scope for energetic disorder the process can take longer, especially at low temperature. The nature of exciton migration to lower energy sites means that the migration has a time dependent rate, initially the rate is high, because there are many available sites for the exciton to hop to, as the mean energy of the distribution drops there are fewer and fewer available sites for the excitons to migrate to.

After the rapid energetic relaxation of the excitons to the bottom of the DOS by dispersive hopping is over, there follows a non dispersive, slow diffusion of excitations around the film. This is typically a much slower process; the point at

which the slow diffusion of excitations around the bottom of the DOS takes over from the rapid dispersive migration is dependant on the temperature. Generally, in the solid state once the excitons are thermalised below the background energy ( $k_B T$ ) the dispersive migration stops. Consequentially, at very low temperatures, the excitons can become trapped in low energy sites well below  $k_B T$  and there is no longer any diffusion of excitons around the film. This is known as localisation of the excitons; the localisation energy is the energy at which the excitons are trapped into their low energy sites. In solutions where there is generally a much narrower distribution of energies the excitons become rapidly localised into the lowest energy segment of a particular chain. Site selective spectroscopy can be employed to probe the point in energy where diffusive migration can no longer occur; when excitation is made below the localisation energy the excitons cannot energetically relax and very little shift between the absorption and emission energies is observed.

All types of excitation hopping can proceed via either the Forster or Dexter mechanism, depending on which is the more efficient given the situation. One could suggest that the long-range Förster mechanism would be dominant for the migration of singlet excitons in a film due to its inherent efficiency over a large distance. Triplet excitons on the other hand must migrate by the Dexter mechanism, as Forster is forbidden. This necessitates the triplets to move only between neighbouring sites to find the low energy traps thus the migration of triplets is very slow compared to singlets. In addition, they are much more easily localised as their sphere of action for finding a low energy site is comparable to the exciton size rather than the Förster radius.

### **2.5.5 Conformational Relaxation**

Aside from the thermalisation of excitons in the DOS another process contributes to the Stokes' shift, that is the structural relaxation of the exciton itself. In the ground state, the structure of the chromophores is optimised to accommodate the charge distribution in the lowest energy possible energy state<sup>15, 45, 46</sup>. On excitation of a chromophore the charge distribution changes, because there is a difference between

the wavefunction of the excited state compared to the ground state. The structure is no longer optimised for this charge distribution, by the Franck-Condon principle this structural relaxation cannot occur as fast as the absorption of the photon, thus the excited state begins its life in an unoptimised geometry. Following the excitation, the structure, or conformation, of the chromophore relaxes to a lower energy to accommodate better the new charge distribution, with an accompanying shift in the fluorescence. In a molecule with a locally excited (Frenkel) exciton there is generally only a small adjustment of the structure to accommodate the excited state and the energetic relaxation is fast and the Stokes' shift small. However, in molecules with charge transfer excited states, the excited state dipole moment is high thus much larger amplitude motions are often required to stabilise the excited state, this can also be further stabilised by the polarity of the solvent, and is the basis for the Twisted Intramolecular Charge Transfer excited states discussed in chapter 4.

## **2.6 Interactions Between Excited States**

### **2.6.1 Singlet-Singlet Annihilation**

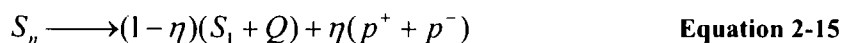
Energy transfer is generally considered to be between an excited donor and an acceptor in the ground state, thus the excitation energy is transferred to the acceptor from the donor. However, in some cases there can be an excitation energy transfer between a donor and acceptor both in the excited state. This is the premise of singlet-singlet annihilation; two excited singlet states interact to form a highly excited singlet state and an unexcited singlet in the reaction<sup>13, 14, 47, 48</sup>:



The condition for this to occur is the same as for energy transfer, except that the spectral overlap must be between the fluorescence of the donor and the excited state absorption of the acceptor and as before the energy transfer could proceed by either mechanism. Following creation of a highly excited singlet state there are two major routes for its deactivation, firstly a non-radiative decay to the  $S_1$  and

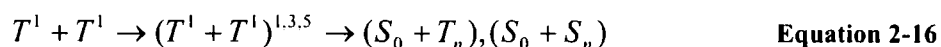


fluorescence, or alternatively as the excess energy provided is normally enough to overcome the exciton binding energy the state may dissociate into a pair of charges.



## 2.6.2 Triplet-Triplet Annihilation

As with singlets, triplet states are able to undergo a similar annihilation reaction, this must be mediated by the Dexter mechanism the result is an intermediate pair of triplets with singlet, triplet or quintuplet character<sup>13, 49, 50</sup>:

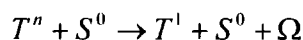


The intermediate pair rapidly decays into either a ground state and an excited triplet or a ground state and an excited singlet, depending on the multiplicity of the intermediate pair. If an excited singlet is formed, once thermalised it decays, and thus the phenomenon of delayed fluorescence is observed as a weak long tail in the singlet emission with the same lifetime as the triplet excited state. As the sphere of interaction of two triplets is very small, delayed fluorescence can be used as a probe of the migration of triplets in the DOS and the dispersive and non dispersive regimes can be easily observed.

## 2.6.3 Singlet-Triplet Annihilation

Excitations of different spin character can also annihilate<sup>13</sup>, if there is sufficient overlap of the singlet emission and the triplet-triplet absorption then singlet-triplet annihilation can occur. This results in an excited triplet state and a singlet ground state which is an allowed transition, as there is no change of spin multiplicity.





Due to the high proportion of triplets found in devices this has been suggested as a significant quenching mechanism for the emissive singlets, experiments to determine the importance of S-S and S-T annihilation are discussed in chapter 6 of this thesis.

## 2.6.4 Charge Trapping

In devices, excitons are not formed by photoexcitation but by charge trapping. This is effectively the binding of two polarons into an exciton, the precise nature of the process is still of some debate, however, the exciton formation is believed to occur over two steps. The theory of Karabunarliev and Bittner suggests that, initially the charges are trapped, and then the exciton becomes self localised, i.e. makes the change from being a loosely bound polaron pair to a strongly bound exciton<sup>24</sup>.

Generally, moieties in the film act as a charge trap for one or other of the charges, to which the other charge becomes attracted and thus the exciton is formed. This is especially relevant when the system contains dopants or the polymer is a copolymer with segments of higher electron affinity, the charge would then be expected to become trapped at these sites preferentially to others.

## 2.7 References

- <sup>1</sup> P. Y. Bruice, *Organic Chemistry* (Prentice Hall, New Jersey, 1995).  
<sup>2</sup> (Prentice Hall Media Portfolio, 2004).
- <sup>3</sup> F. A. Kekule, *Bulletin de la Societe Chimique* **3**, 98 (1865).  
<sup>4</sup> H. S. Nalwa, (Wiley, Chichester ; New York, 1997), p. 4 v.
- <sup>5</sup> J. R. Sheats, H. Antoniadis, M. Hueschen, et al., *Science* **273**, 884 (1996).  
<sup>6</sup> R. Friend, D. Bradley, and A. Holmes, *Physics World* **5**, 42 (1992).
- <sup>7</sup> J. H. Burroughes, D. D. C. Bradley, A. R. Brown, et al., *Nature* **347**, 539  
(1990).  
<sup>8</sup> D. Bloor, *Nature* **349**, 738 (1991).
- <sup>9</sup> W. P. Su, J. R. Schrieffer, and A. J. Heeger, *Physical Review Letters* **42**, 1698  
(1979).  
<sup>10</sup> W. P. Su, J. R. Schrieffer, and A. J. Heeger, *Physical Review B* **22**, 2099  
(1980).
- <sup>11</sup> A. J. Heeger, S. Kivelson, J. R. Schrieffer, et al., *Reviews of Modern Physics*  
**60**, 781 (1988).
- <sup>12</sup> H. Bassler, M. Gailberger, R. F. Mahrt, et al., *Synthetic Metals* **49**, 341 (1992).  
<sup>13</sup> M. Pope and C. E. Swenberg, *Electronic Processes in Organic Crystals and  
Polymers* (Oxford University Press, Oxford, 1999).
- <sup>14</sup> J. B. Birks, *Organic molecular photophysics* (J. Wiley, London, New York.,  
1973).
- <sup>15</sup> K. Mullen and G. Wegner, *Electronic Materials: The Oligomer Approach*  
(Wiley-VCH, Weinheim, 1998).
- <sup>16</sup> H. Meier, U. Stalmach, and H. Kolshorn, *Acta Polymerica* **48**, 379 (1997).  
<sup>17</sup> A. P. Monkman, H. D. Burrows, I. Hamblett, et al., *Journal of Chemical  
Physics* **115**, 9046 (2001).
- <sup>18</sup> J. S. de Melo, *Journal of Chemical Physics* **111**, 5427 (1999).  
<sup>19</sup> J. Rissler, *Chemical Physics Letters* **395**, 92 (2004).
- <sup>20</sup> C. Rothe, K. Brunner, I. Bach, et al., *Journal of Chemical Physics* **122** (2005).  
<sup>21</sup> R. S. Knox, *Theory of Excitons* (Academic Press, New York, 1963).

- 22 T. A. Skotheim, R. L. Elsenbaumer, and J. R. Reynolds, *Handbook of*  
*Conducting Polymers* (M. Dekker, New York, 1998).
- 23 E. Frankevich, H. Ishii, Y. Hamanaka, et al., *Physical Review B* **62**, 2505  
(2000).
- 24 S. Karabunarliev and E. R. Bittner, *Physical Review Letters* **90**, 057402  
(2003).
- 25 Z. Shuai, D. Beljonne, R. J. Silbey, et al., *Physical Review Letters* **84**, 131  
(2000).
- 26 J. Cabanillas-Gonzalez, M. R. Antognazza, T. Virgili, et al., *Physical Review*  
*B* **71**, 155207 (2005).
- 27 R. Kersting, U. Lemmer, M. Deussen, et al., *Physical Review Letters* **73**, 1440  
(1994).
- 28 H. D. Burrows, S. M. King, J. Pina, et al., In preparation (2007).
- 29 D. W. McBranch, B. Kraabel, S. Xu, et al., *Synthetic Metals* **101**, 291 (1999).
- 30 C. Y. Chi, C. Im, and G. Wegner, *Journal of Chemical Physics* **124**, 024907  
(2006).
- 31 D. Wasserberg, S. P. Dudek, S. C. J. Meskers, et al., *Chemical Physics Letters*  
**411**, 273 (2005).
- 32 D. Beljonne, Z. Shuai, G. Pourtois, et al., *Journal of Physical Chemistry A*  
**105**, 3899 (2001).
- 33 S. P. McGlynn, T. Azumi, and M. Kinoshita, *Molecular Spectroscopy of The*  
*Triplet State* (Prentice Hall, Englewood Cliffs, New Jersey, 1969).
- 34 S. K. Lower and M. A. El-Sayed, *Chemical Reviews* **66**, 199 (1965).
- 35 J. R. Lakowicz, *Principals of Fluorescence Spectroscopy* (Kluwer Academic,  
New York, 1999).
- 36 J. B. Birks, *Photophysics of aromatic molecules* (Wiley-Interscience, London,  
New York,, 1970).
- 37 P. W. Atkins, *Physical Chemistry* (Oxford University Press, Oxford, 1998).
- 38 T. H. Forster, in *10th Spiers Memorial Lecture*, 1959), p. 7.
- 39 G. D. Scholes, *Annual Reviews in Physical Chemistry* **54**, 57 (2002).
- 40 D. L. Dexter, *Journal of Chemical Physics* **21**, 836 (1953).
- 41 H. Bassler, *Physica Status Solidi B-Basic Research* **175**, 15 (1993).
- 42 R. Richert and H. Bassler, *Journal of Chemical Physics* **84**, 3567 (1986).

- 43 K. Brunner, A. Tortschanoff, C. Warmuth, et al., *Journal of Physical Chemistry B* **104**, 3781 (2000).
- 44 S. C. J. Meskers, J. Hubner, M. Oestreich, et al., *Journal of Physical Chemistry B* **105**, 9139 (2001).
- 45 F. B. Dias, A. L. Macanita, J. S. de Melo, et al., *Journal of Chemical Physics* **118**, 7119 (2003).
- 46 Z. R. Grabowski and J. Dobkowski, *Pure and Applied Chemistry* **55**, 245 (1983).
- 47 Q. H. Xu, D. Moses, and A. J. Heeger, *Physical Review B* **68**, 174303 (2003).
- 48 S. M. King, D. Dai, and A. P. Monkman, *Physical Review B* **76**, 085204 (2007).
- 49 C. Rothe and A. P. Monkman, *Physical Review B* **68**, 075208 (2003).
- 50 S. King, C. Rothe, and A. Monkman, *The Journal of Chemical Physics* **121**, 10803 (2004).

### 3 Experimental Methods

Measurement of the absorption of a molecule is a trivial process, it is usually done by measuring the transmission of light with and without the sample present<sup>1</sup>. The principal of measurement of the excited state absorption is the same, the transmission of the light through the sample is measured with and without the excited states to be measured present. By the Beer-Lambert law the proportion of the photons absorbed is proportional to the concentration of the molecules in the ground state.

$$A(\lambda) = \log\left(\frac{I}{I_0}\right) = \varepsilon(\lambda)cl \quad \text{Equation 3-1}$$

In the case of photoinduced absorption the presence of the excited states is modulated by modulation of a pump beam which excites the molecules. In a steady state experiment this is trivial, and will be discussed at the end of the chapter. Even time resolutions of ~1ns are possible to measure with relatively simple equipment. However, in the picosecond or femtosecond time regime experiments become more difficult at such times it is no longer possible to use electronics to provide the time resolution, one must use the light itself.

The principal of femtosecond photoinduced absorption is one of pump and probe, the excited states are created by a pump pulse from a laser and the population of the excited states is probed by a second pulse<sup>2</sup>. The time delay between the pulses is varied to give a picture of the time evolution of the states. Ultimately, the time resolution is determined by the correlation of the pump and probe pulses, which is determined by the lengths of the laser pulses themselves. In the photoinduced absorption experiments the signal is measured as the change in probe beam transmission when the sample is excited compared to when it is not. This change in transmission  $dT(\lambda,t)$  must be normalised to account for the spectrum of the probe ( $T(\lambda)$ ), thus the induced absorption signal  $dT(\lambda,t)/T(\lambda)$  is measured. By analogy with the ground state absorption and the Beer-Lambert law, one can arrive at an expression to determine the population of the excited state<sup>3</sup>, equation 3.2.

$$\frac{dT(\lambda, t)}{T(\lambda)} = -\frac{\sigma(\lambda)N(t)l}{A}$$

Equation 3-2

Where,  $\sigma(\lambda)$  is the absorption cross section of the excited state,  $N(t)$  is the excited state population concentration at a given time after excitation,  $l$  the distance over which the beams interact and  $A$  is the area of overlap of pump and probe beams.

### 3.1 Femtosecond Lasers

In general time resolved spectroscopy experiments require pulsed lasers, for femtosecond resolution ultrafast lasers must be used, while development of ultrafast lasers continues relentlessly, the use of mode locked solid state lasers has become the norm for molecular spectroscopy experiments with subpicosecond time resolution<sup>2, 4, 5</sup>.

#### 3.1.1 Mode-Locking

The shortest pulses commercially available are in the femtosecond time regime, this requires a highly sophisticated 'mode locked' laser. This mode locked phenomenon allows the laser to stably pulse at a high repetition rate with pulse durations down to a few tens of femtoseconds. The phenomenon is a function of the laser cavity, all laser cavities form a Fabry-Pérot interferometer, thus gain can be supported by multiple longitudinal modes in the cavity. A cw laser (such as the Ar<sup>+</sup>) can independently lase on either all of the modes, or one can be selected by adjusting the laser gain at different wavelengths, providing a narrow emission band. In a cw laser the modes of different frequency bear no phase relationship to each other, thus interference results in a continuous, random phase output. If for example, many modes are all in phase with one another at a given point in space and time then they will interfere constructively giving an increase in the intensity of the laser. Conversely at other points in space at the same time the modes will interfere destructively giving no output. Of course, for a given point in space the same thing will happen in time, there will be intensity changes as the waves constructively and destructively interfere. One can represent the modes of a laser by a fourier series, the

greater the number of frequencies in the series that interfere constructively at the given point in space and time the temporally narrower the intensity maximum is, this is illustrated in figure 3.1. The trick of a mode locked laser is to ensure that a broad spectrum of modes interfere constructively at a point in time thus, by phase locking a large number of longitudinal cavity modes of the laser, so called ‘mode locking’, a pulse of light is produced. The minimum temporal duration of the pulse is determined through the Heisenberg uncertainty relation by the spectral width of the mode locked pulse. This gives the form of equation 3.3, where  $\Delta\omega_0$  is the bandwidth of the pulse; pulses which strictly obey this relationship are said to be transform limited<sup>2, 4</sup>.

$$\tau_p = \frac{2\sqrt{2}}{\pi\Delta\omega_0} \ln 2 \quad \text{Equation 3-3}$$

Locking the phase of the modes is easiest done by controlling the lasing temporally, if all modes start lasing at the same time, they are naturally phase locked at this zero time. This can be done trivially by pumping the laser with another mode locked pulse, or actively controlling the laser’s gain with an electronically controlled modulator in the cavity, a Q-switch. Unfortunately, active control cannot be used to generate pulses in the femtosecond or picosecond regime as the gain cannot be modulated electronically at such speeds, so passive mode locking must be used.

Initially, ultrafast mode locking was generally achieved in picosecond dye lasers using a saturable absorber, that is a molecule or crystal whose transmission is near unity for high light intensities but low for low light intensities. When a pulse passes through the saturable absorber the low intensity at the front and tail of the pulse are absorbed much more than the high intensity at the peak of the pulse. Such a system in combination with a gain medium which tends to have a higher gain for low intensities leads to an optimum pulse shape thus the stable pulse shape is maintained. Once stable mode locking can be maintained like this, starting the process is trivial. An instability in the cavity leads to an intensity fluctuation, which is rapidly accentuated by the relationship between the saturable absorber and the gain medium. The laser then rapidly becomes stable as the competition between the saturable absorber and the gain saturation causes the optimum pulse shape to form.



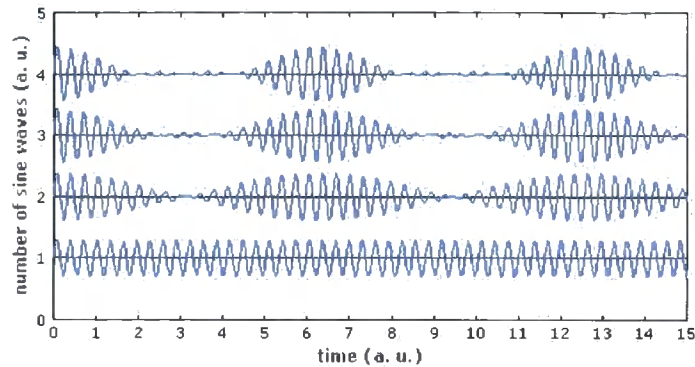


**Figure 3-1 Formation of a pulse as the number of modes which become locked increases<sup>6</sup>.**

### **3.1.2 The Titanium:Sapphire Laser**

A revolution in ultrafast spectroscopy was brought about in the mid 1990s by the development of the Ti:sapphire laser<sup>7</sup>. The rod of Ti:Al<sub>2</sub>O<sub>3</sub> which acts as the gain medium, is stable, non toxic and has a broad absorption in the visible, enabling it to be pumped by a variety of high power gas lasers, or more recently, diode pumped solid state lasers. The range over which the material lases is broad, from ~700nm – 1000nm with the peak gain at about 800nm. Additionally, the Ti:sapphire laser exhibits the phenomenon of self mode locking. This phenomenon is brought about by the optical Kerr effect, the non-linear change of the refractive index with intensity. This phenomenon in combination with a simple slit is equivalent to the saturable absorber in the picosecond dye laser. At the high instantaneous intensities in pulsed operation, the light through the crystal is focussed due to the effect of the Gaussian spatial profile of the beam and the optical Kerr effect causing the wings of the beam to see a different refractive index to the centre. The focussed beam is therefore able to pass through the slit, its intensity unaffected (figure 3.2). At low intensities, the light is focussed less and does not pass through the slit unattenuated; thus the saturable absorber condition is formed by the combination of the lasing crystal itself and a slit. This process is known as ‘Kerr lens mode locking’.

The tuneability of the Ti:sapphire is achieved by controlling the gain at different wavelengths, this is normally done using a birefringent filter. By exploiting the varying polarisation rotation of different wavelength of light in a birefringent

crystal and a polariser, the cavity loss can be effectively minimised for a narrow band of wavelengths. The repetition rate of the laser is simply the time it takes for the pulse to make one round trip in the cavity:  $2c/L$ , where  $L$  is the length of the cavity.

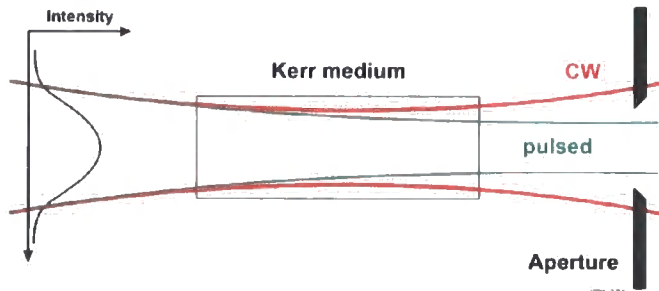


Figure 3-2 The Kerr lens mode locking process, the pulse is transmitted through the aperture while in cw operation the beam is blocked. The Kerr lens beam shaping is determined by the spatial profile of the laser beam<sup>6</sup>.

The femtosecond oscillator used in this study is a Coherent Mira 900-F Ti:Sapphire laser. The layout of the cavity is shown in figure 3.4 below. The laser is pumped by a Coherent Verdi V-5 frequency doubled Nd:YVO<sub>4</sub> laser providing upto 5W output at 532nm. Naturally the cavity contains more than just the simple elements described above. In addition to the Ti:sapphire crystal and slit there is also a bow tie modulator to provide the initial intensity perturbation to kick start the mode locking; a birefringent filter (BRF) to tune the wavelength; and a prism compressor (P1,P2) to compress to pulse to maintain the transform limited duration.

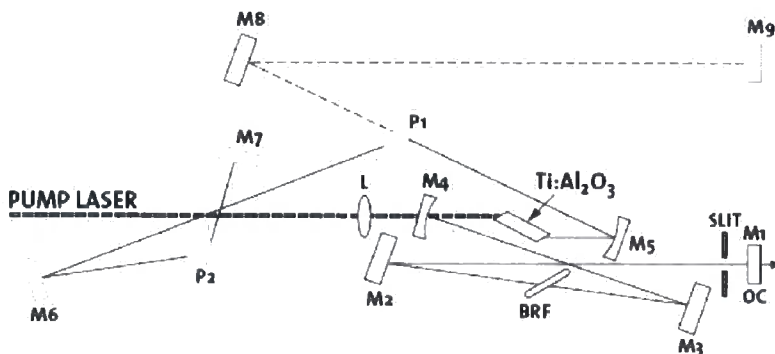


Figure 3-3 The layout of the Coherent Mira 900-F<sup>8</sup>.

### 3.1.3 Laser Amplifier

The Femtosecond oscillator generates 160fs, 780nm pulses at a repetition rate of 80MHz. Unfortunately, the pulse energy is only a few nanojoules per pulse which is insufficient for the pump probe experiment. Therefore, the pulse energy must be amplified and the repetition rate reduced, this is done with a laser amplifier; in our system, a Coherent RegA 9000 regenerative amplifier is used. The regenerative amplification technique works by trapping a seed laser pulse from the fs oscillator inside a second excited Ti:Sapphire laser cavity; the seed pulse can then travel many times through the excited crystal of Ti:Sapphire. After each pass of the seed pulse through the gain medium there is amplification, until the excitation energy in the gain medium is depleted and the pulse energy saturates, at which point the now high energy pulse is let out of the cavity. In the RegA 9000 the injection and ejection of the pulse in the cavity is controlled by a Pockels cell and an acousto-optic modulator respectively and the Ti:Sapphire crystal is continuously pumped by a 10W Coherent Verdi V-10. The amplified pulses have pulse energy of about 5 $\mu$ J at a repetition rate of 100kHz.

When the system was first built, only a single pump laser was used to pump the oscillator and amplifier, the beam from the 10W Coherent Verdi V-10 was split to provide power for both the amplifier and the oscillator. This proved unsatisfactory, as there was insufficient pump power for both the oscillator and amplifier to run stably. To correct this, an additional 5W pump laser was purchased for the oscillator allowing independent pumping of the two lasers, which has since proved to be far more stable, and as a result, more time can be spent on experiments rather than on laser alignment.

### 3.1.4 OPA

Pulses from the laser amplifier, while at an appropriate pulse energy for experiments are not at a useful wavelength, 780nm is in the near infra red, away from the optical absorptions of the conjugated polymers under study. Non-linear optical processes must be used to generate suitable wavelengths for pump and probe; these

are generated inside an optical parametric amplifier (OPA). Firstly, a portion (75%) of the 780nm pulse is frequency doubled using second harmonic generation inside a BBO crystal to generate a pump beam at 390nm, which is suitable for most experiments on conjugated polymers. The remaining portion is tightly focussed into a sapphire plate to generate a white light supercontinuum. This is a laser beam of broadband white light, which is generated in the sapphire plate by a combination of multiple non-linear processes, including self phase modulation, which occur at the very high excitation densities found in the short pulse. The white light beam is chirped, that is, its colour components are delayed in time with respect to one another. The chirp is due to the refractive index dispersion of the sapphire plate and other transmissive optical elements changing the group velocity of the different colour components of the light pulse. The blue end of the spectrum of the pulse is delayed with respect to the red end. This white light supercontinuum can be used on its own as the probe beam. By using a monochromator a narrow wavelength band can be selected and the different excited state absorptions probed.

In addition to the supercontinuum and 390nm pump beam the OPA utilises the process of optical parametric amplification, this involves the mixing of the supercontinuum with the 390nm beam inside a second BBO crystal. The effect is to amplify a portion of the supercontinuum and generate a narrow wavelength tunable beam in the visible (signal beam). The remaining energy of the UV beam once the signal beam is generated is in the infrared and this is known as the idler beam. The wavelength tunability is achieved by exploiting the chirp of the white light, only a narrow wavelength band can be made to overlap spatially and temporally with the UV beam inside the crystal. Thus, once the appropriate crystal angle is selected to achieve the appropriate phase matching condition a narrow wavelength band is amplified. The signal and idler beams are used as probe beams or in certain circumstances as the pump beam. Table 3.1 shows all the different beams available and their most common uses.

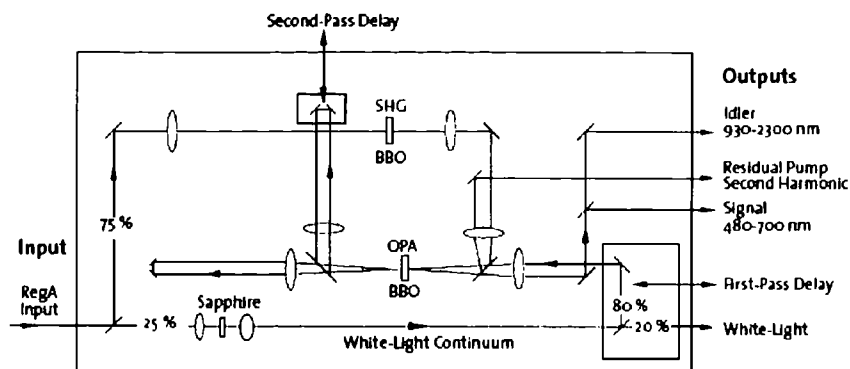


**Figure 3-4** The Coherent 9400 OPA; the parametric amplification is performed by two passes through the OPA crystal<sup>9</sup>.

	Wavelength / energy	Common Usage
Fundamental	780nm / 1.6 eV	Probe
Second Harmonic	390nm / 3.2eV	Pump / Probe
Signal Beam	Tuneable 440nm - 720nm	Pump / Probe
Idler	Tuneable 900nm-2300nm	Probe
Supercontinuum	460nm – 1000nm	Probe

**Table 3.2** The different outputs from the OPA and their uses in the photo induced absorption experiment.

### **3.2 Development of the Pump-Probe system**

The pump probe system built for the work in this thesis is based on a typical pump-probe layout. A schematic of the layout is shown in figure 3.5. The time delay between the pump and probe pulses is achieved by a retro-reflector mounted on a linear translation stage, by varying the path length of the pump pulse it is possible to vary the time interval between pump and probe at the sample. The pump and probe beams are then brought together in a narrow angle geometry (20°) at the sample. This

is typically done without focussing the beams, ensuring the excitation density remains low at the sample, however, when higher excitation densities are needed, for example, in low absorbing samples focussing may be used. It is important to keep the probe beam smaller on the sample than the pump beam in order to ensure that the whole area that is being probed has been excited by the pump. The various options for pump and probe beams from the OPA are coupled into the required beam paths by a number of flip mirrors allowing the different experiments to be carried out easily. Degenerate pump-probe experiments i.e. where pump and probe are at the same wavelength, are performed by using a beam splitter to split off a small portion (<5%) of the pump beam before the translation stage to serve as the probe beam. In order to perform polarisation dependant pump probe studies with the system a Berek compensator is setup as a variable wavelength  $\lambda/2$  waveplate is used to rotate the orientation of the pump or probe beam so that decays can be recorded with the beams parallel or perpendicular as appropriate. The photo in figure 3.6 shows a number of the

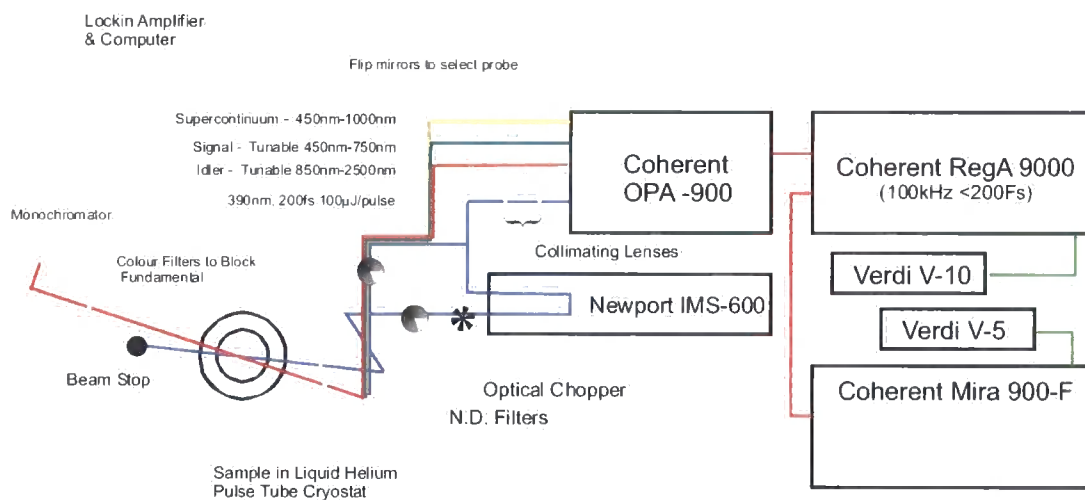


**Figure 3-5 Schematic layout of the pump-probe system with the monochromator and photodiode detection system. The appropriate pump and probe beam can be selected by the flip mirrors depending on the experiment.**

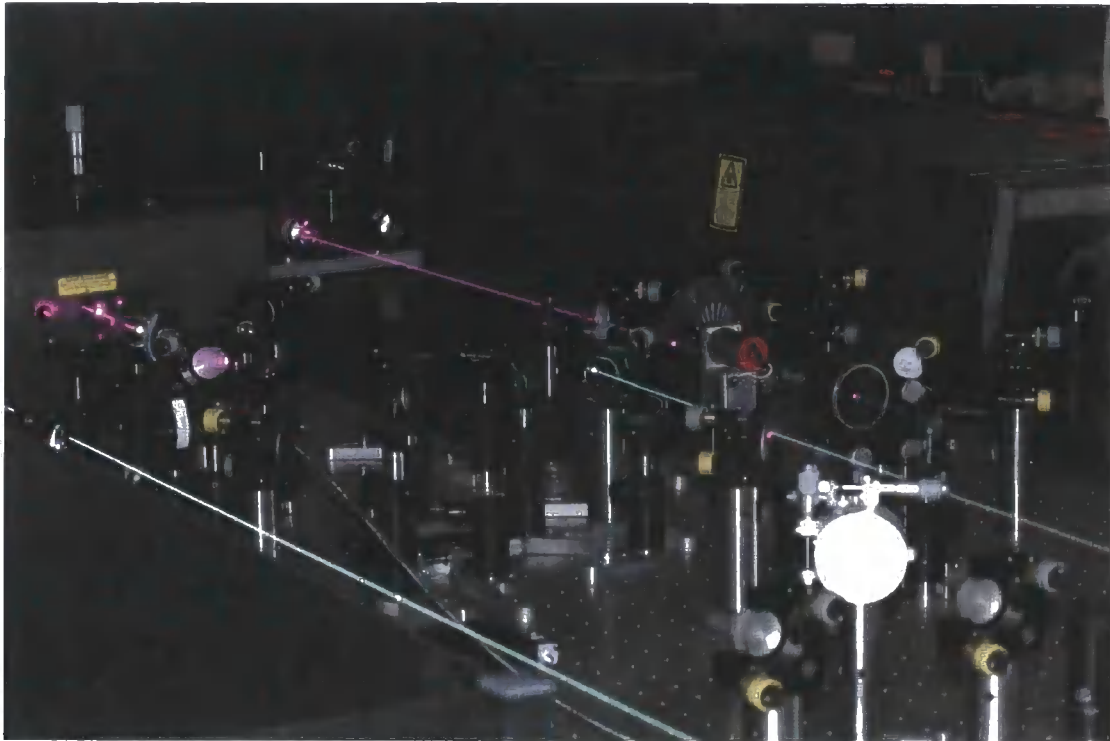


**Figure 3-6** Photograph of part of the experimental setup, clearly visible are the 390nm pump beam, the white light supercontinuum probe beam, as well as the retro-reflector mounted on the delay stage for controlling the time delay and the chopper.

### 3.2.1 Detection Systems

Throughout the development of the experiment, two different detection systems have been used. Initially the probe beam, typically the white light supercontinuum, was split into two beams, one which travelled through the excited part of the sample (the probe) and one through the unexcited part (the reference). The probe and reference were then focussed into a pair of fibre coupled diode array spectrometers, the two spectra were then used to calculate the induced absorption spectra following equation 3.4.

$$\frac{dT(\lambda)}{T(\lambda)} = \frac{I_{probe}(\lambda) - I_{ref}(\lambda)}{I_{ref}(\lambda)} \quad \text{Equation 3-4}$$

This system works well for large (>1%) induced absorption signals, however, when the signal is small the problems are three fold, firstly the slight difference in the

response of the detectors means that the spectra must be corrected by a calibration file, this is relatively trivial. The second problem arises from the poor dynamic range of the spectrometer / ADC means that measurement of a signal change of  $<0.1\%$  will never be possible. Finally, the biggest problem arises from the stability of the white light spectrum. The white light supercontinuum intensity fluctuates by about 2% especially at the blue edge; the large part of this is in the pointing stability of the beam, the effect of which is accentuated by the comparatively long path lengths of our set up and the difficulty in coupling the light into the fibre spectrometer. These comparatively large changes in the intensity of the light swamp the photoinduced absorption signals at low signal intensity.

As an alternative to the diode array spectrometer, we have moved to lock-in detection for small signal intensities. After probing the sample, the probe beam is focussed through a monochromator and onto a photodiode. The pump beam is mechanically chopped prior to the sample and a lock-in amplifier is used to detect changes in the probe beam intensity at the frequency of the chopper. For a single wavelength measurement the monochromator position is fixed and the delay stage adjusted to measure the decay of the pump-probe signal. To measure spectra for a given time delay the delay stage position can be fixed and the monochromator scanned to measure the spectrum. Measurement of spectra in this way requires the background, normally due to some of the sample fluorescence or scattered pump light reaching the detector, to be subtracted manually, this is done by recording a spectrum prior to time zero (the time at which pump and probe arrive at the sample together) and subtracting it from the other spectra. Although this technique is more time consuming the improvements over the diode array spectrometer are significant. Not only does the lockin remove the effect of all instabilities of the probe beam so that  $dT/T$  signals of down to  $10^{-6}$  can be resolved but also the effect of the chirp on the white light can be easily removed. With the slits closed ( $\sim 1\text{mm}$ ) on the monochromator the spectral resolution is approximately 5nm, for weak signals the slits can be opened further but spectral resolution is lost.

As the white light is chirped, the colour components do not arrive at the sample at the same time, they are spread over approximately 3ps, the effective time zero for each colour is different. Thus, the time resolution of the diode array



spectrometer method is significantly compromised. The scanning monochromator method of spectrum acquisition however, allows this effect to be removed by making small adjustments to the delay stage to compensate for the chirp as the wavelength of the monochromator is adjusted. Once the chirp of the white light is well characterised this works remarkably well and spectra can be acquired with a time resolution of better than 500fs.

Samples can be measured either in solution in a quartz cuvette or as thin films held in a Cryomech Pulse-Tube helium cryostat. This allows the temperature of the film to be controlled down to approximately 5K. In order to prevent photooxidation all thin film samples, even at room temperature, are held in a dynamic vacuum of  $\sim 10^{-5}$  mbar.



**Figure 3-7 Sample in cryostat, the residual pump light and the transmitted probe beam are visible, a pair of mirrors is used to align the probe beam before being filtered and focussed on the slit of the monochromator.**

Custom written Labview programs that generally run two different experiments control the system, either the wavelength is fixed at the monochromator and the delay stage scanned to measure the decay of a feature in the spectrum. The alternative is to measure a whole spectrum for a few different positions of the delay

stage, to see spectral changes with time; it is also possible to measure a large number of spectra each separated by only a short time, to create a 3-dimensional picture of the evolution of the states with time and wavelength. Unfortunately, although looking impressive in presentations, this is very time consuming and really of little analytical value.

### 3.2.2 Characterisation of the White Light Supercontinuum

The white light supercontinuum is a broad spectrum, which is comprised of two main components, the broadening of the fundamental and a high energy shoulder, these combine to give the spectrum in figure 3.8, the intensity varies a lot with wavelength and the light contains a significant portion of the residual fundamental.

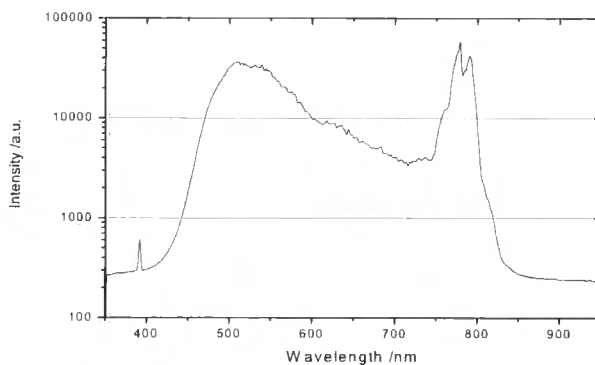


**Figure 3-8 Spectrum of the white light supercontinuum used as probe beam, an 800nm high pass filter has been used to reduce the intensity of the fundamental.**

As previously discussed the white light supercontinuum is chirped, the different colour components are delayed in time with respect to one another this is caused by the group velocity dispersion of the wavepacket in the transmissive optics. In order to compensate for this the chirp must be characterised this has been done using non-linear optics. Building a single pass collinear OPA just before the sample allows the measurement of the time wavelength relationship of the components as figures 3.9 and 3.10 show. This can be used to calculate a correction curve to adjust the delay stage as the monochromator is scanned. In addition the width of the cross correlation between the pump and probe gives an accurate measure of the time

resolution of the system, throughout the wavelength range this gives a time resolution 240ps for the system.

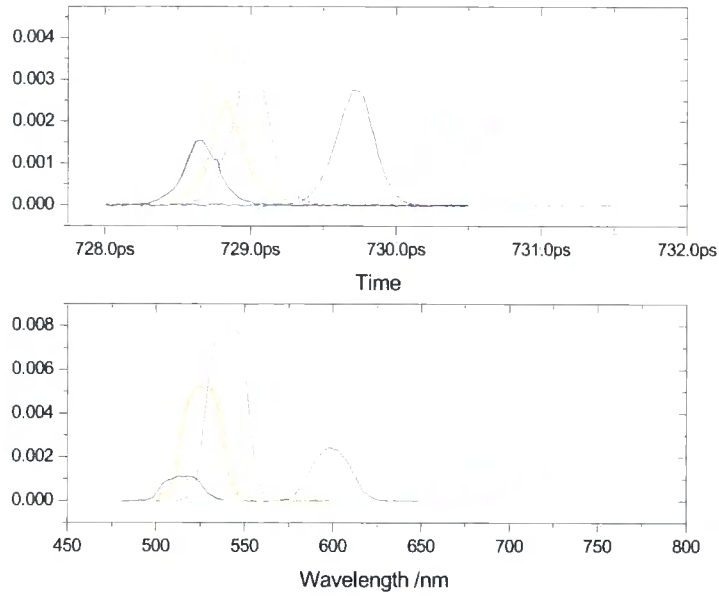


**Figure 3-9 Top, Cross correlations of the different colour components in the white light supercontinuum. Lower: Colour components corresponding to the cross correlation above, the colours of the spectra correspond to the time traces in the top panel.**

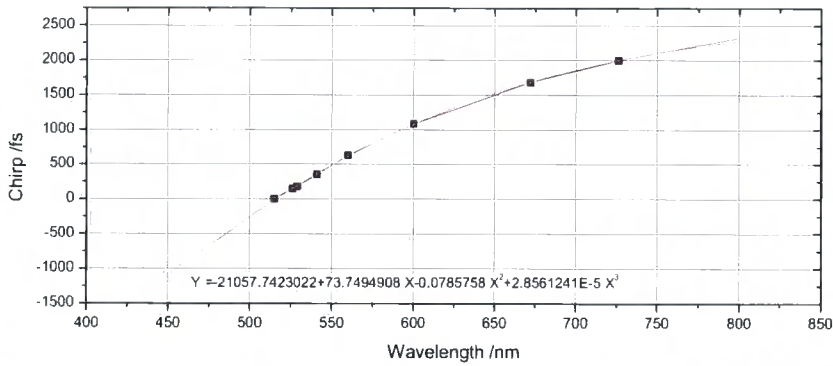


**Figure 3-10 The empirically derived correction curve for the chirp, with the equation for calculating the required delay adjustment for the different wavelengths derived from figure 3.9.**

### 3.3 Quasi-CW Photoinduced Absorption

The photoinduced absorption spectra of long lived states such as Triplet states can be measured in a steady state experiment, by the so called quasi-cw technique<sup>10</sup>. This involves using a chopped excitation beam as the pump and a tungsten lamp as the probe, small a lock-in amplifier measures variations in the probe transmission. For our system, the excitation beam is a 405nm diode laser which is electronically modulated by the internal oscillator of the lock-in amplifier<sup>11</sup>. This is an exceptionally stable experiment and time averaged changes in probe transmission of  $dT/T < 10^{-6}$  can be measured. The experimental setup is shown below in figure 3.11.

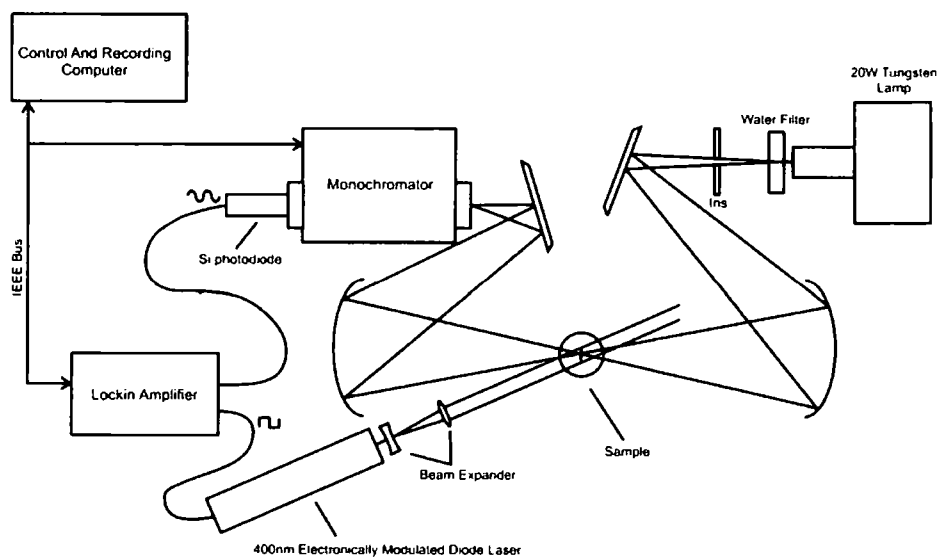
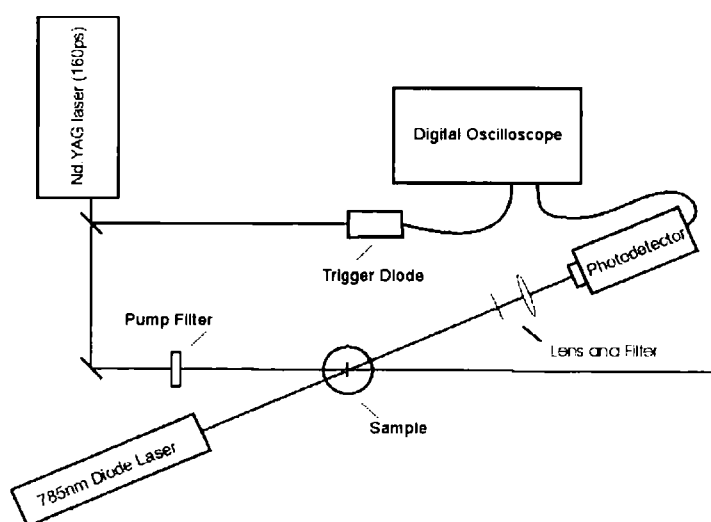


Figure 3-11 Quasi CW Photoinduced Absorption Spectrometer

### 3.4 Nanosecond Photoinduced Absorption

While the quasi-cw experiment gives the spectra of long lived photoinduced absorption signals kinetics can be difficult to obtain. Frequency resolved quasi-cw PA experiments can go some way towards the kinetics of very long live species in the ms time regime. However, the method requires a model to be created and fitted, which can become difficult when the decay of the species is not governed by simple exponentials.

Previously in our group we have developed a method of measuring PA kinetics on the ns-s scale based on a system of pump and probe<sup>11</sup>. However, unlike the femtosecond system we use a continuous wave probe beam with a pulsed pump. The sample is excited by the 3<sup>rd</sup> harmonic of a 160ps Nd:YAG laser (EKSPLA) and the probe beam is a thermally stabilised continuous wave diode laser (Laser 2000, Roithner Lasertechnik etc.) chosen to be at the peak of the photoinduced absorption spectrum of the species to be investigated. The two beams overlap on the sample and the transmission of the probe beam is measured by a silicon p-i-n photodiode directly coupled to a 2GHz transimpedance amplifier (Femto GmbH). A 1GHz oscilloscope (Agilent technologies) records the changes in transmission of the probe beam. The system allows time resolution of better than 1ns, measured by the instrument response to the laser pulse. The experiment is performed in an almost collinear geometry, with the angle between pump and probe approximately 10°. The use of a diode laser rather than the more conventional tungsten lamp as probe beam removes the need for light collection optics, which would collect the prompt fluorescence of the sample, saturating the detector during the first few nanoseconds of the decay, rendering measurement of the initial photoinduced changes in absorption impossible. Additionally, after passing through the excited sample a band pass filter (typically 10nm FWHM) is used prior to focussing the probe beam, with a short focal length lens, onto the detector to ensure that minimal sample fluorescence is detected by the photodiode. The experimental setup is shown in figure 3.12.



**Figure 3-12 Apparatus for measuring the nanosecond photoinduced absorption kinetics.**

## **3.5 Variations on the Standard Experiments**

### **3.5.1 Field Assisted Pump-Probe**

In addition to the standard pump probe measurements field assisted pump probe spectroscopy has been employed to help to understand the relationship between singlet states and charged species in chapter 6. This technique shows the effect of an electric field on the photoinduced absorption spectrum<sup>3, 12, 13</sup>. By applying, a modulated electric field to the polymer in a conventional device structure during the pump probe experiment and using lockin detection at the frequency of modulation of the electric field the difference between the photoinduced absorption spectrum with the electric field on and off is measured. When the spectra are displayed in terms of absorbance, a negative signal represents a reduction in the photoinduced absorption when the field is applied and a positive signal is an increase in the photoinduced absorption on application of the field. For stimulated emission signals in the pump-probe spectra the reverse is observed. In the same way as for the standard photoinduced absorption the signal is proportional to the population of the excited states, thus the spectra shows the change in the excited state populations when the field is applied. The experiments are carried out on the polymer in a standard PLED structure and a  $1.5 \times 10^6 \text{ Vcm}^{-1}$  field is applied in reverse bias so that no current is injected into the device and only the effect of the electric field, rather than the field and any injected carriers is observed.

### **3.5.2 Charge Induced Absorption**

Quasi-cw photoinduced absorption is a widely used technique to show the absorption of long-lived excited states in conjugated polymers. A variation of this technique is also used in this thesis, again in chapter 6, charge induced absorption<sup>14-16</sup>. In this experiment the absorption of a polymer LED in forward bias, with a modulated current flowing is measured. The probe beam is a tungsten lamp focussed on the active area of the diode and reflected off the back electrode of the device through a monochromator onto a Si-photodiode. A lockin amplifier referenced to the frequency

of the current modulation resolves the signal. This experiment is only carried out at room temperature so the signal is dominated by the charges and charged states formed in the device. Care must be taken to use relatively slow chop rates, below the RC time of the device, otherwise the device cannot switch on and off as fast as the modulation rate and the signal measured diminishes.

### **3.6 Phosphorescence Spectra**

While measurement of fluorescence emission is relatively trivial, the long lifetime and low population of triplet excitons makes measurement of phosphorescence difficult. Using a time gated, intensified, CCD camera in combination with a pulsed laser allows the collection of spectra to be delayed after excitation, thus the long lifetime phosphorescence spectrum can be measured after the intense fluorescence emission has decayed. By using a long integration time, one can measure the weak phosphorescence spectra of pristine conjugated polymers. This technique has been developed and described extensively by previous members of our research group.<sup>11, 17</sup>

### **3.7 Sample Preparation**

The work in this thesis contains data on both solutions of polymers and oligomers and thin films. Solutions are prepared in a variety of solvents as appropriate, for pump-probe experiments concentrations of OD  $\sim 1$  are used, which leads to typical concentrations of  $10^{-5}$  by weight the solutions are then held in a 1mm quartz cuvette. If the signals are particularly weak then a longer path length can be used but this reduced the time resolution of the system significantly. Thin films were typically prepared by spin casting from a solution of 10mg/ml in toluene; a spin speed of 2500rpm was used resulting in a typical sample thickness of 85nm. Thin films were prepared in a clean room environment after which they are stored in the dark to prevent sample degradation. Long term storage of all materials investigated is in a nitrogen filled glovebox.

### 3.8 References

- <sup>1</sup> J. R. Lakowicz, *Principals of Fluorescence Spectroscopy* (Kluwer Academic, New York, 1999).
- <sup>2</sup> C. Rulliere, *Femtosecond Laser Pulses, Principals and Experiments* (Springer, New York, 2004).
- <sup>3</sup> G. Lanzani, G. Cerullo, D. Polli, et al., *Physica Status Solidi a-Applied Research* **201**, 1116 (2004).
- <sup>4</sup> W. T. Silfvast, *Laser Fundamentals* (Cambridge University Press, Cambridge, 1996).
- <sup>5</sup> W. Demtroder, *Laser Spectroscopy: Basic Concepts and Instrumentation* (Springer, Berlin, 2003).
- <sup>6</sup> R. Paschotta, in [www.rp-photonics.com](http://www.rp-photonics.com), (2007).
- <sup>7</sup> D. E. Spence, P. N. Kean, and W. Sibbett, *Optics Letters* **16**, 42 (1991).
- <sup>8</sup> Coherent Inc, *Coherent Mira 900-F: User Guide*, (2005).
- <sup>9</sup> Coherent Inc, *Coherent OPA-9000: User Guide*, (2005).
- <sup>10</sup> P. O'Connor and J. Tauc, *Physical Review B* **25**, 2748 (1982).
- <sup>11</sup> S. King, C. Rothe, and A. Monkman, *The Journal of Chemical Physics* **121**, 10803 (2004).
- <sup>12</sup> T. Virgili, G. Cerullo, L. Luer, et al., *Physical Review Letters* **90**, 247402 (2003).
- <sup>13</sup> S. M. King, S. I. Hintschich, D. Dai, et al., *Journal of Physical Chemistry C* **111**, 18759 (2007).
- <sup>14</sup> Y. Y. Deng and H. Sirringhaus, *Physical Review B* **72**, 45207 (2005).
- <sup>15</sup> M. Wohlgenannt, E. J. W. List, C. Zenz, et al., *Synthetic Metals* **116**, 353 (2001).
- <sup>16</sup> S. M. King, S. I. Hintschich, C. Rothe, et al., *Journal of Physical Chemistry B* **In Press**.
- <sup>17</sup> C. Rothe and A. P. Monkman, *Physical Review B* **65**, 73201 (2002).



## 4 Measurement of Triplet Quantum Yields Of Conjugated Polymers and Oligomers

The relationship between singlets and triplets in conjugated polymers is of fundamental importance to polymer light emitting devices. The formation of triplets after electrical excitation represents a major loss of efficiency, while the precise ratio of singlets to triplets formed in devices is hotly debated it is generally accepted triplets are produced in a significant proportion possibly up to the statistically expected 75%<sup>1-6</sup>. The subsequent non-radiative decay of the triplets represents a major loss of efficiency and their propensity to interact with one another in bimolecular annihilation reactions can result in the formation of highly excited singlets or charge pairs, which hold potential for causing chemical damage to conjugated polymers<sup>7-9</sup>. The advent of triplet emitting devices involving phosphorescent emitters represents a way to capture the non-emissive triplet states for light emission thus their study is currently a pertinent one<sup>10-12</sup>.

In an attempt to improve the efficiency of polymer devices a number of different polymers are emerging as candidates for efficient light emission. There are two general methods of developing new polymers, firstly a conventional polymer backbone such as polyfluorene or poly-phenylenevinylene are often functionalised by the addition of side groups with specific properties for charge transport or injection<sup>13, 14</sup>. Alternatively, copolymers have been made with different moieties with similar properties for enhancing the device efficiency or tuning the colour<sup>15-19</sup>.

Understanding the excitations lost to triplets in these new materials is therefore important for the successful development of new materials. This singlet triplet ratio has been measured in many different ways thus far. Experimentally, most techniques use transient absorption to measure the proportion of triplets generated upon electrical excitation and fluorescence to measure the number of singlets generated. One of the most successful methods is to use optical excitation as a ruler to quantify the number of triplets generated electrically<sup>6, 20</sup>. Quantitative use of the triplet transient absorption is difficult because the extinction coefficient of the triplet

absorption is necessary which in turn requires knowledge of the number of triplets generated optically: the triplet quantum yield.

#### **4.1 Measurement of the Triplet Quantum Yield by Ground State Recovery**

The very low phosphorescence quantum yield and high non radiative decay rate of triplets in most conjugated polymers makes emission studies to determine the triplet QY impossible<sup>21, 22</sup>. Thus far, two methods have emerged for the measurement, photoacoustic calorimetry and singlet-oxygen energy transfer<sup>23, 24</sup>. The former relies on the thermal energy given out by non radiative decays; thermal (acoustic) waves are collected by a transducer following intense photoexcitation<sup>25</sup>. The non-radiative energy is divided into three categories, intersystem crossing from the singlet to the triplet, internal conversion from the singlet to the ground state and intersystem crossing from the triplet to the ground state. From knowledge of the singlet energy, the triplet energy and the photoluminescence quantum yield, the triplet quantum yield and the non-radiative decay can be resolved from the data. The current alternative of singlet oxygen energy transfer is reliant on the quenching of polymer triplet states by paramagnetic molecular oxygen dissolved in the same solvent as the polymer. The phosphorescence of the oxygen is then compared to a known standard and the triplet quantum yield obtained. Neither method is particularly robust and both are difficult to perform; for the PAC there are many parameters required in the fitting of the data and the relative nature of the measurement for the both methods introduces additional sources of error. The methods are often not even consistent with each other, high relative errors are often found and in some cases absolute errors of up to 25% have been recorded<sup>26</sup>. The most important conclusion that can be gained from this previous work is firstly that it is not a trivial measurement especially when the triplet quantum yield is low and secondly that in most conjugated polymers the triplet quantum yield is very low<sup>27</sup>. Additionally and most importantly for measurements on polymer devices neither method can be used in the solid state or at low temperature, if the triplet yield is to be used in calculations relating to device efficiency these are both of paramount importance.

To solve the problem of measuring the triplet quantum yield we have developed a method first used by *Von Jena et al* in the 1970s, the technique is based around the recovery of the ground state absorption after photo excitation<sup>28-30</sup>. Given that the ground state recovery shows the decay of all the states created in the polymer, in principal two regimes are observed in the recovery, a fast recovery due to the decay of singlet states and a slow recovery from the decay of the triplets. Conjugated polymers are ideally suited to this technique: the highly spin forbidden nature of the triplet decay means that the triplet lifetime is long and hence the triplet component of the ground state recovery can be easily distinguished from the singlet. Furthermore, in dilute solutions and at low excitation density it is generally accepted that the only excitations formed in significant number are the singlet and triplet excitons. In solid state, the picture becomes more complicated as exciton-exciton annihilation reactions have been shown to provide enough energy to overcome the exciton binding energy and cause dissociation into charges<sup>31-33</sup>. However, as the process is generally diffusion controlled such problems can be minimised by using low excitation density and low temperature to reduce the chance of two excitons interacting<sup>34</sup>. Additionally, the charges formed in solid state can be easily detected in the transient absorption spectrum (chapter 5) and their lifetime determined so that the effect of charges could be easily distinguished from the triplet signal in the ground state recovery.

In an ultrafast time resolved experiment, the fast and slow recoveries of the singlets and triplets are represented in a peak and plateau, the peak from the absorption of both the singlets and the triplets and the plateau from the absorption of just the long-lived triplet states. In previous experiments, achieving sufficient time resolution to perform a proper time resolved measurement was difficult and this is potentially why the technique did not become widely used. Either a lockin amplifier was used to determine the difference between the peak and the plateau, or complex deconvolution was used, neither is ideal as accurate determination of the peak of the signal is key to the calculation<sup>28, 29</sup>. The method developed here uses both femtosecond and nanosecond pump-probe experiments to resolve the recovery of the ground state over up to 12 orders of magnitude in time<sup>30</sup>. Thus, the recovery due to both the singlets and triplets can be accurately determined. An example of the decay of the photobleaching (ground state recovery - GSR) is shown further on in figure 4.2. The one caveat to the experiment must be that for the calculation of the triplet yield to

remain simple, there must be no overlap between the photobleaching at the wavelength of the probe and either the fluorescence or any of the photoinduced absorptions of the various excited states, the spectra shown in this chapter for the various molecules under study show that this is satisfied.

### 4.1.1 The Kinetic Scheme For Ground State Recovery

The ground state recovery (the decay of the photobleaching) is made up of all the various decay channels of the states, considering the singlet population,  $N_s$ :

$$\frac{dN_s}{dt} = G(t) - N_s k_s \quad \text{Equation 4-1}$$

And the triplet population,  $N_T$ , independently:

$$\frac{dN_T}{dt} = N_s k_{isc} - N_T k_T \quad \text{Equation 4-2}$$

where,  $G(t)$  is the time dependant generation of the singlets by the laser pulse,  $k_s$  is the decay rate of the singlet,  $k_{isc}$  is the intersystem crossing rate and  $k_{nr}$  is the rate of non radiative decay of the singlets.

Now considering that the only excited states are singlet and triplet, we consider the total number of excited states,  $N$

$$\frac{dN}{dt} = -N_s k_s - N_T k_T \quad \text{Equation 4-3}$$

And

$$N = N_0 + N_s + N_T \quad \text{Equation 4-4}$$

The solution to the above coupled differential equations with a  $\delta$ - pulse excitation at  $t = 0$  is as follows:

$$N_S(t) = Ge^{-k_s t}$$

$$N_T(t) = G(e^{-k_T t} - e^{-k_s t}) \left( \frac{k_{isc}}{k_s - k_T} \right) \quad \text{Equation 4-5}$$

$$N_0(t) = N - N_S(t) - N_T(t) = N - G \left[ e^{-k_s t} + (e^{-k_T t} - e^{-k_s t}) \left( \frac{k_{isc}}{k_s - k_T} \right) \right]$$

Thus introducing the definition of the triplet yield  $\phi = k_{isc} / k_I$  the change in ground state population is given by:

$$N(t) = N_S + N_T = G \left[ (1 - \phi) e^{-k_s t} + \phi e^{-k_T t} \right] \quad \text{Equation 4-6}$$

The experimental decay of the photobleaching is thus fitted to a two exponential decay of the following form,

$$N = Ae^{-k_s t} + Be^{-k_T t} \quad \text{Equation 4-7}$$

Hence the triplet yield  $\phi_T$  is the ratio of the pre-exponential factors:

$$\phi_T = \frac{B}{A + B} \quad \text{Equation 4-8}$$

From the triplet yield and the fluorescence lifetime, the rate of intersystem crossing can be calculated;

$$k_{isc} = \frac{\phi_T}{\tau_f} \quad \text{Equation 4-9}$$

If the triplet lifetime is much longer than the lifetime of the singlet and data is recorded over a few multiples of the singlet lifetimes, one can approximate the solution of the system to:

$$N_0 = Ae^{-(k_s t)} + B \quad \text{Equation 4-10}$$

Thus, a plateau is observed after all the singlets decayed and before the triplets have decayed; the ratio of this plateau compared to the total photobleaching signal determines the triplet yield.

### 4.1.2 The Triplet Yield Experiment

The ultrafast measurement of the recovery of the ground state after photobleaching is performed with the femtosecond pump-probe system with the pump and probe at the same wavelength, near the absorption edge of the material studied. The second harmonic of the Ti:Sapphire laser at 390nm is a convenient wavelength to use for many conjugated polymers and oligomers, especially polyfluorene derived materials<sup>16, 35</sup>. The linear translation stage used allows a time window of upto ~3.5ns of the decay to be measured. This system is adequate for molecules with singlet decay times of ~1ns and below as the singlet has decayed sufficiently for the plateau of the triplets to be easily resolved. For materials with a longer singlet lifetime, especially if the triplet yield is low, the recovery must be followed further; this is done using the nanosecond photoinduced absorption system outlined in section 3.4 and our previous publications<sup>36, 37</sup>. In this case, the pump beam is a frequency triplet Nd:YAG laser (355nm) and the probe beam a 405nm laser diode. There is sufficient time overlap of the two systems that there is a region of overlap in the data and they can be put together to show the whole ground state recovery of both the singlet and triplet states. Not only does this allow a good estimate of the triplet yield to be made, but also it provides additional verification that there are only two species in the ground state recovery, the singlet and triplet excitons. Care must be taken when combining the data from two experiments in this way that the experiments are done under as similar experimental conditions as possible. The most important factor, which must be controlled, is the excitation dose. At high excitation density, accelerated bimolecular decay of the singlet and triplet can occur which will alter the decay of the singlet and hence the triplet yield.

The experiment can be performed in dilute solutions, at room temperature or on thin films held in the helium cryostat. In order to reduce the effect of sample degradation, which could cause an accelerated decay of the singlet or additional long lived states in the polymer. The film samples were held in a dynamic vacuum of  $<10^{-5}$  mbar and the experiments were repeated to ensure there was no change in either the absolute signal intensity of the peak photobleaching or the shape of the decay, between successive experiments.

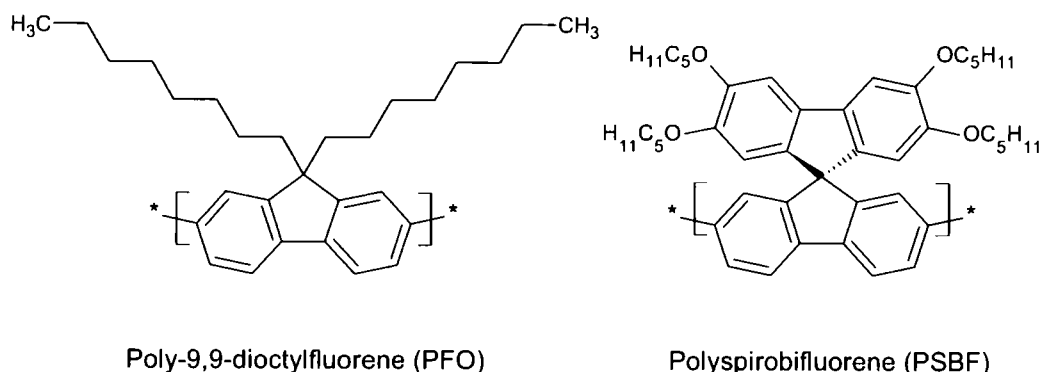
In the solid state, the excited state dynamics are always more complicated, once the trivial case of sample degradation has been avoided, the presence of accelerated singlet and triplet decays must be taken into account. For high excitation density, in the solid state, bimolecular annihilation of both singlet and triplet excitons begins to dominate the decays of both the singlets and triplets the phenomenon of singlet annihilation is dealt with in detail in chapter 5 and triplet-triplet annihilation has been extensively investigated in the literature<sup>9</sup>. The effect of singlet-singlet annihilation is to accelerate the decay of the singlet excitons and create long-lived charged states, both phenomena that would cause a problem with the calculation of the triplet yield and intersystem crossing rate. The accelerated decay of the singlets results in a lower triplet yield, as is expected from a simple competition between two competing decay rates. In addition, the long-lived charged states that are formed as a product of singlet annihilation would create an artefact in the data and change the premise of the experiment that only singlet and triplet excitons are formed by photo excitation of a pristine polymer. This can of course be taken into account, the lifetime of the charged states can easily be measured by pump-probe spectroscopy and an additional component added into the decay to take account for this. Thus the ratios of singlets, triplets, and charged species could be calculated. However, this method would not only complicate the fitting of the data, increasing the errors on the triplet yield, but more importantly the triplet yield measured would not be the intrinsic triplet yield of the pristine polymer. It is therefore more useful to measure the triplet yield in solid state without the effect of the singlet annihilation. This is done by performing the experiment at low temperature, where the singlet mobility is low, and at pump fluence below the threshold for singlet annihilation to dominate the decay<sup>34</sup>, typically the experiment is performed at 5K with a pump fluence of ( $\sim 300 \text{ nJ cm}^{-2}$ ). The use of such low pump fluences presents no problem for the femtosecond pump-probe system, the lockin detection allows signals as low as  $dT/T \sim 10^{-6}$  to be resolved with adequate signal to noise ratio for fitting. However, the nanosecond system which relies on repetitive averaging has a detection threshold of only  $dT/T \sim 10^{-4}$ . This coupled with the high noise level in the early time (crucial for overlapping the data from the two experiments) means that it is only possible to measure the nanosecond ground state recovery at pump fluences approximately 1 order of magnitude greater than the femtosecond experiment. It would therefore be unwise to put the data from the two experiments together in this case. Fortunately the singlet lifetime is generally

short in the solid state (typically  $<300\text{ps}$ ) so there is generally adequate time window in the fs pump probe system to estimate the triplet yield from the plateau in the ground state recovery after the singlets have decayed.



## 4.2 The Triplet Yield of Polyfluorene and Polyspirobifluorene

The polymers poly-9,9-dioctylfluorene (PFO) and polyspirobifluorene are two prototypical conjugated polymers for blue emitting polymer LED devices<sup>13, 38</sup>. The structures of the derivatives used are shown below. PFO represents one of the most commonly studied derivatives of polyfluorene and its photophysics is well characterised and understood, the triplet yield has been measured previously by photoacoustic calorimetry and singlet oxygen measurements<sup>26</sup>. Even though the previous measurements are often associated with large errors for this polymer the values are consistent giving a triplet yield of  $\phi_T = 0.031$ , it is thus included in this part of the study as a check that the ground state recovery method is in agreement with previous reports. The polymer polyspirobifluorene (PSBF) is a more sophisticated derivative of the polyfluorene backbone; the aliphatic side chains of PFO are replaced by an additional fluorene unit coupled in a spiro configuration at the -9 carbon of the two fluorene units. The unique photophysics of this polymer is studied in detail in chapter 6.



The motivation for studying the triplet yield in this particular polymer (PSBF) relates to its excellent performance in PLED devices. The polymer devices have been extensively characterised, with particular attention paid to the ratio of singlet to triplet formation following charge trapping; in order to perform this calculation the triplet yield was required<sup>6</sup>.

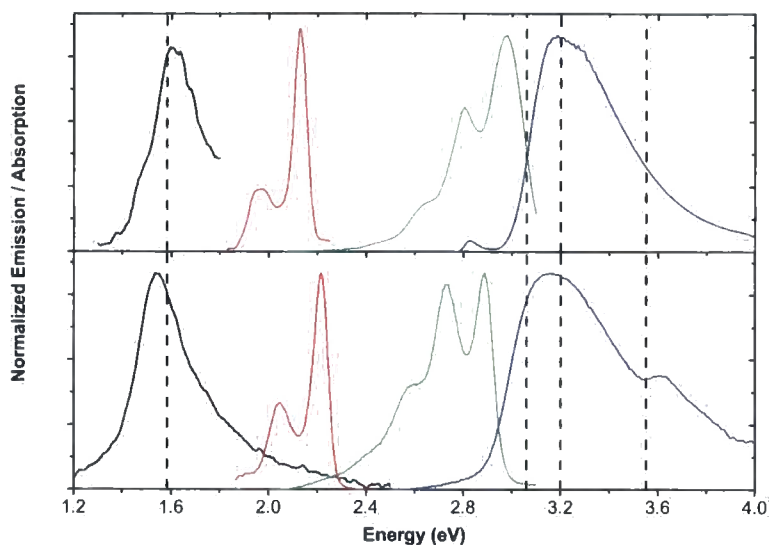


**Figure 4-1** Solution state absorption (blue) photoluminescence (green), phosphorescence (red), photoinduced triplet absorption (black) for PFO (upper) and PSBF (lower). The dotted lines mark the pump and probe beams for the ultrafast (3.2eV) and nanosecond (3.55eV, 3.06eV) photobleaching as well as the probe beam for the transient triplet absorption (1.58eV).

The absorption, fluorescence, phosphorescence and quasi-cw transient triplet absorption of the polymer are shown in figure 4.1 for PSBF and PFO in dilute ( $10^{-5}$  w/w) toluene solutions. These are very similar to other reported spectra for polyfluorene homopolymers; of particular interest is the transient absorption at 1.6eV, which has been previously unambiguously assigned to the triplet exciton<sup>36, 39</sup>. The energies used for the measurement of the ground state recovery in the femtosecond pump-probe experiment (3.2eV), the nanosecond experiment (pump 3.55eV, probe 3.06eV) and to measure the decay of the transient triplet absorption (pump 3.55eV probe 1.6eV) are shown on the graph. The pump and probe energies are all near to the peak of the appropriate absorption spectra apart from the pump beam for the nanosecond experiment that is unfortunately fixed at 3.55eV; this is close to the second peak of the ground state absorption rather than being in the main band. However, no difference in the fluorescence is observed for excitation throughout the absorption spectrum of PSBF so this should present no problem<sup>40</sup>. The ground state recovery decays are shown for the two polymers in figure 4.2 and 4.3 in a double logarithmic presentation. For the PSBF the femtosecond component and the nanosecond component are shown separately alongside the combined decay; this

demonstrates the excellent agreement of the two methods. The two decays overlap well, with the same shape observed; the double logarithmic presentation also serves to illustrate the need for time resolution of at least  $\sim 10\text{ps}$  to measure the maximum of the photobleaching that is so crucial to the calculation of the triplet yield.

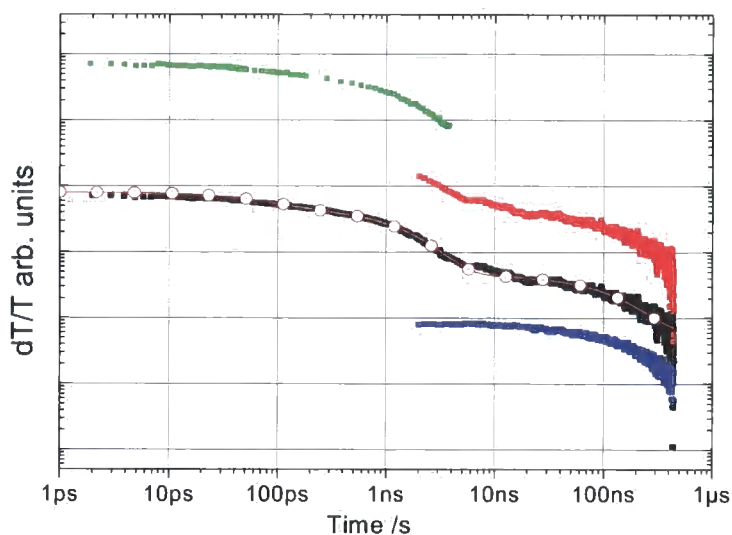


**Figure 4-2** The ground state recovery for PSBF solution showing: (from top) the ultrafast component of the GSR, the nanosecond component, the combined GSR trace of both components and its associated line of best fit to equation 4.5, and the transient triplet absorption.

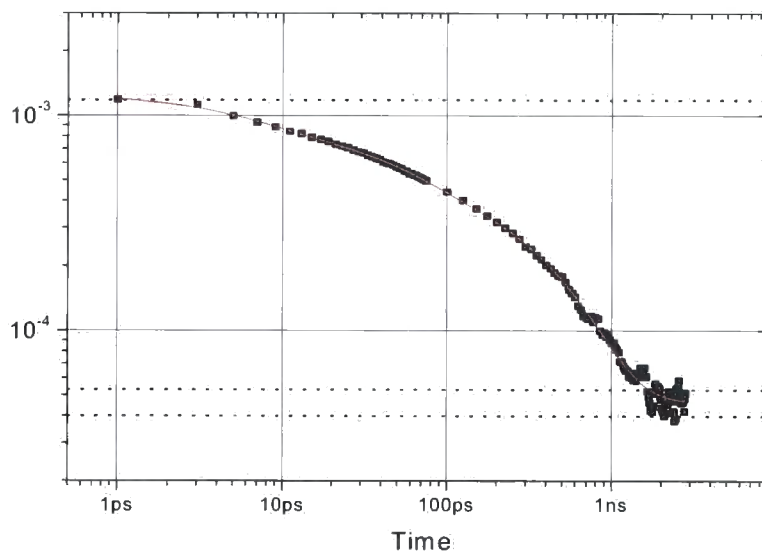


**Figure 4-3** The ultrafast GSR for PFO solution, the solid line is the line of best fit to equation 4.8. The dotted lines give an idea of the error on the calculation of the triplet yield.

The decay of the triplets in a single exponential decay of 180ns is in excellent agreement with the long components of the ground state recovery, this is important verification that the only long lived excitations are triplet excitons. For PFO, in figure 4.3, within the timescale of the ultrafast experiment the plateau of the constant population of triplets is clear because the measured singlet lifetime is only 403ps and it is not necessary to piece the data from the two experiments together. This in fact means that it is easier to calculate the triplet yield of PFO from just the femtosecond data using equation 4.8. The (red) lines through the data are the fitted exponential decays for the photobleaching used in the calculation of the triplet yield using equations 4.5 & 4.6 for PSBF and PFO respectively. In PSBF neither the fast decay of the ground state recovery nor the fluorescence follow strict single exponential decays, with lifetimes upto 2.3ns observed. This is considered further in chapter 6 therefore the data has been fitted with a 3 exponential model, and all the fast (<2.3ns) components attributed to singlet excited states.

For the data shown above, using equations 4.5 and 4.6 the triplet yield for PSBF is calculated to be  $\phi_T = 0.05 \pm 0.005$  and for PFO,  $\phi_T = 0.036 \pm 0.005$ . The triplet yield for PFO agrees reasonably well with the previously reported value of  $\phi_T = 0.031$  although it is slightly higher than this value. The authors of the previous paper note that there are often inconsistencies between their photoluminescence quantum yield, their triplet yield and their yield of non radiative decay which add up to greater than 1, therefore one can expect significant sources of error from the PAC experiment used.

The triplet yield itself is an important value for the calculation of the singlet triplet generation ratio in conjugated polymer devices, however, it should really be thought of as a deactivation process for the singlet excited states. Therefore, it is useful to calculate the intersystem crossing rate from the triplet yield and the singlet decay rate, this relationship was previously described in equation 4.7. The intersystem crossing rate for PSBF,  $k_{isc} = 5.5 \times 10^7 \text{ s}^{-1}$  and for PFO  $k_{isc} = 8.6 \times 10^7 \text{ s}^{-1}$ . In the context of aromatic molecules which do not contain any heteroatoms which can increase the intersystem crossing rate by the intramolecular heavy atom effect or a change of orbital character of the state, these values for the intersystem crossing rate are fairly standard. Reported values of the intersystem crossing rate for such aromatics are over

a large range<sup>41,42</sup>, for example for naphthalene  $k_{isc} = 1.6 \times 10^6 \text{ s}^{-1}$  whereas anthracene has  $k_{isc} = 1.1 \times 10^8 \text{ s}^{-1}$ . The fact that this factor of  $\sim 70$  difference is observed for two similar molecules serves to demonstrate the complex nature of intersystem crossing in aromatic molecules.

### 4.2.1 Solid State Triplet Yields

In the solid state, similar measurements of the triplet yield have been made at low temperature and low excitation density, as described in the introduction to this chapter the data cannot be combined into a single ground state recovery decay trace, the fs and ns components of the decay are shown separately in figures 4.4 and 4.5.

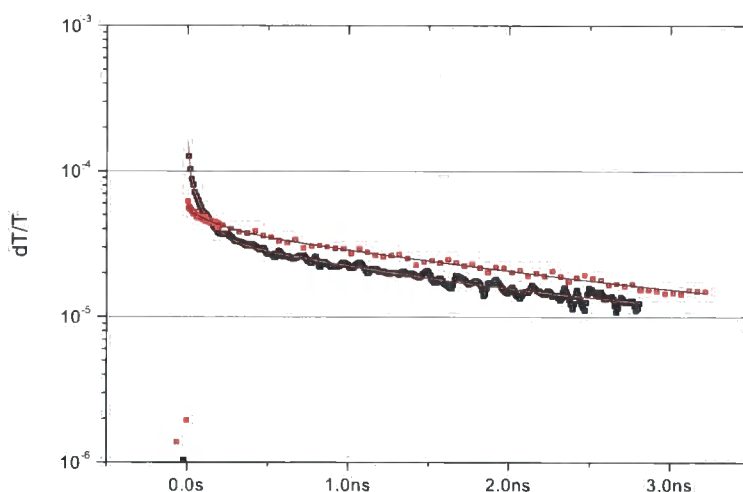


**Figure 4-4** Ultrafast ground state recovery for PFO (black) and PSBF (red) films at 10K, the solid lines are line of best fit to equation 4.4 used to calculate the triplet yield.

In order to understand the best way to analyse the data one must build up a picture of the excited states in solid state. The ground state recovery for both polymers contains fast components due to quenching of the excited state, most likely by defects in the film, this results in the decay being more than just a simple one or two exponential fit. In actual fact the polymer PSBF has very complex excited state behaviour especially in the solid state; this is dealt with in more detail in chapter 6.

Considering this one can once again consider that all of the fast  $<5\text{ns}$  components originate from singlet excited states and the slow decay is due to triplet excitons.

Confirmation that all the slow components of the ground state recovery are from the triplet exciton is once again provide by the good correlation of the transient triplet absorption decay with the nanosecond GSR. Even though at the pump dose used in this nanosecond experiment ( $\sim 10\text{uJcm}^{-2}$ ) the triplet exciton clearly has a non exponential decay, most likely due to triplet-triplet annihilation, there are no additional components in the nanosecond GSR which do not originate from either the triplet exciton or the singlet excited state decay. Indeed the only deviation of the GSR from the triplet PA is from the tail of the singlets in the 1-2ns region.

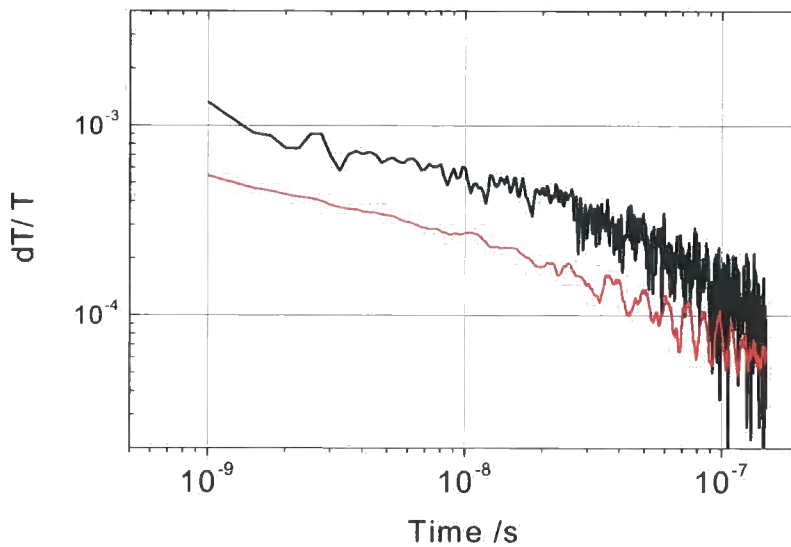


**Figure 4-5 Comparison between the nanosecond GSR (black) and the transient triplet absorption (red) for PSBF film at 10K.**

The difficulty in combining the data from the nanosecond and femtosecond GSR experiments combined with the long lifetime of some components of the singlet decay makes the use of equation 4.8 to calculate the triplet yield difficult. In both the femtosecond GSR and the luminescence decay, components of  $\sim 2.0\text{ns}$  are measured, small changes in the lifetime of this 2.0ns component will make a large difference to the offset due to the triplets. This is particularly problematic because the maximum time delay of the pump probe system in this configuration is  $\sim 3.5\text{ns}$  so the longest component remains poorly defined and as a result, the errors on the triplet yield are

higher than in solution. By this method of fitting and equation 4.8, the calculation of the triplet yield can be made, giving  $\phi_T = 0.12 \pm 0.02$  for PSBF; and  $\phi_T = 0.033 \pm 0.01$  for PFO; the corresponding intersystem crossing rates are  $k_{isc} = 8.0 \times 10^8 \text{ s}^{-1}$  and  $k_{isc} = 10.0 \times 10^8 \text{ s}^{-1}$  respectively.

### **4.3 The Intersystem Crossing Rate In Conjugated Oligomers And Polymers Containing A Twisted Interconnected Charge Transfer State (TICT)**

As the field of polymer electronics becomes more advanced, materials scientists are searching for more and more ways to enhance the efficiency and optimise the emission energy of conjugated polymer materials. One method of doing this is to tailor different materials to do different jobs through the functionalisation of a standard polymer with different moieties with specific properties. This can be done by side chain modification, end capping or most pertinently, by copolymerisation<sup>17, 19, 43, 44</sup>. While the introduction of different cooligomers into a system can be used to improve the charge mobility, injection or recombination efficiency of a device, often the electronic properties and photophysics are also affected in an undesirable way.

Systems with improved electron injection or transport are often based around copolymerisation with moieties of high electron affinity. This results in strong dipoles along the chain between the high electron affinity units and the 'normal' backbone cooligomers; consequentially, in some cases, the exciton does not remain tightly bound and a charge transfer state is formed between the units of different electron affinity. When the state is excited, the electron becomes more localised at the high electron affinity unit and the hole remains on the backbone. The resulting intramolecular charge transfer (ICT) excited state is often characterised by a broad emission which can be used to build efficient white emitting polymer LEDs<sup>18</sup>. An additional bonus of such charge transfer states is that the high electron affinity groups are expected to act as strong traps for the electrons in devices, the improvement of

charge trapping results in a concomitant increase in device efficiency. In charge transfer states there is great potential for increased mixing between singlet and triplet states due to the much lower energy gap between the singlet and triplet compared to locally excited states<sup>42</sup>. In addition the localisation of the electron and hole on separate parts of the molecule that causes the formation of such ICT states often causes high levels of conformational relaxation, these structural changes can be associated with an increase in intersystem crossing rate<sup>45</sup>. Thus, given the importance of the relationship between singlets and triplets for device physics it is pertinent to study the effects of such ICT states on triplet formation.

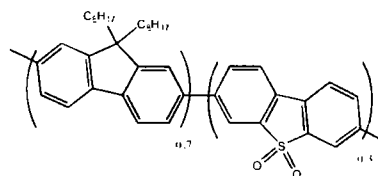
One such copolymer system is the class of copolymers of fluorene and dibenzothiophene-*S,S*-dioxide. These polymers show improved charge balance and hence quantum efficiency in devices over polyfluorene homopolymers due to the improved electron injection and transport obtained from the inclusion of the high electron affinity dibenzothiophene-*S,S*-dioxide unit. Studies on copolymers of different ratio show that the optimum charge balance can be achieved with inclusion of ~30% of the co-oligomer. The disadvantage of this is that the saturated blue emission is lost and the PLEDs emit a broad greenish-white colour, which is attributed to the formation of the ICT state mentioned above<sup>18, 46, 47</sup>.



### 4.3.1 The Fluorene-Dibenzothiophene-*S,S*-Dioxide System: Characterisation of a TICT State



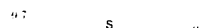
**FSF**



**PFS<sub>30</sub>**



**FFF**



**PFDBTH<sub>30</sub>**

To understand the photophysics that results in the ICT emission it is often necessary to take a step back from the polymer to consider a shorter oligomeric analogue of the system. With this in mind much of the characterisation of the system has been done on a fluorene – dibenzothiophene-*S,S*-dioxide – fluorene trimer (FSF). This has been used to characterise the nature of the ICT excited state and understand more of the processes leading to its formation, the work has then been extended to the polymers, where broadly the same properties are observed. Other members of the research group including project students have carried out much of the initial photophysical characterisation of the excited state in these molecules. It must however, be included here in order to understand the consequences for the formation of triplets and intersystem crossing in such ICT states considered in this chapter<sup>47, 48</sup>.

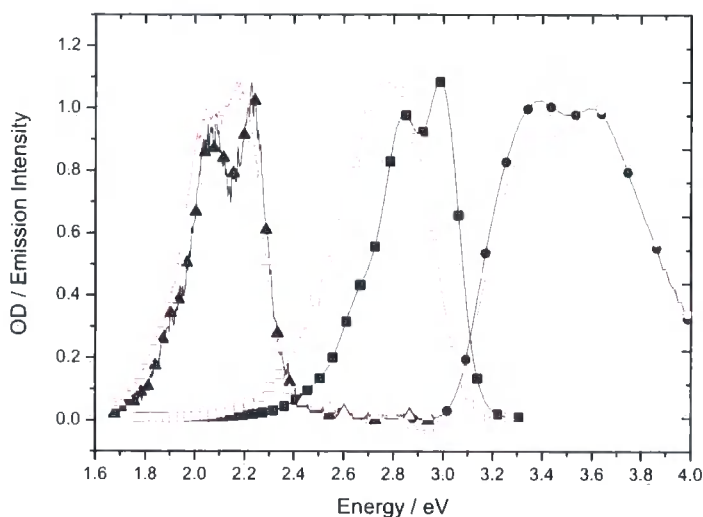
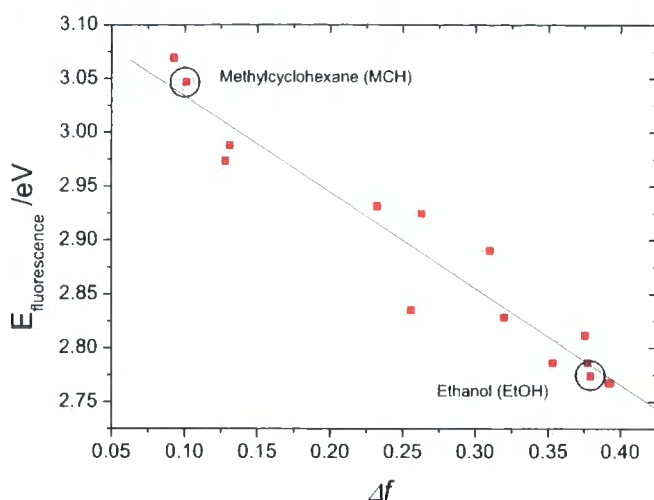


**Figure 4-6 Compendium of spectra, (from left) absorption, fluorescence and phosphorescence for the FSF oligomer in methycyclohexane (black) and ethanol (red) solutions.**

Fluorescence and absorption spectra recorded in different solvents for the molecule FSF and the polymers PFS30 PFDBTH30 are shown in figure 4.6. Considering the oligomer alone the changes to the emission spectrum on changing the polarity from the unpolar methycyclohexane (MCH) to the highly polar ethanol, is clear. The broadening of the fluorescence without a change in the absorption spectrum immediately suggests that there is a change in the stabilisation of the state due to the solvent. If the broad emission were from the formation of a radically different excited state through for example, the formation of a dimer or aggregate state, one would expect to see a change in the ground state absorption spectrum, which does not occur. In order to quantify the change of emission with solvent polarity with a range of different solvents, the emission energy is plotted against the solvent polarisability parameter,  $\Delta f$  (Lippert-Mataga polarisation parameter) in figure 4.9. Such a plot shows a good linear relationship between the solvent polarisability parameter and the emission energy, with a decrease in the emission energy as the solvent becomes more polar. This means that the dipole in the excited state is greater than that in the ground state, i.e. the charges are more separated in the excited state compared with the ground state<sup>49, 50</sup>.



**Equation 4-11** Lippert plot for the FSF oligomer, showing a reduction in the energy of the fluorescence peak with increasing polarisability ( $\Delta f$ ) of the solvent. The two solvents used in the study (MCH and Ethanol) are marked. Data kindly reproduced from the work of Dias et al<sup>48</sup>.

Similar spectral changes and the observation of solvent controlled dual fluorescence have been observed previously, in small molecules such as 4-diaminobenzonitrile (DMABN). The observed phenomena are explained by the presence of two excited states, a locally excited exciton (LE) which is highly correlated and an intramolecular charge transfer state (ICT) which is less tightly bound consequently the LE state shows a structured emission and the ICT a broad fluorescence band. The effect of the polar solvent cage around the molecule is to stabilise the dipole of the ICT state so that it is lower in energy than the LE and the ICT is thus formed in the polar solvent. The theory was initially proposed by Lippert et al<sup>51</sup>, but has since been developed into two competing ideas, the twisted intermolecular charge transfer and planar interconnected charge transfer state (TICT and PICT)<sup>49, 52-54</sup>. In the TICT system there is a twist in the molecule of up to 90° between the two parts of the molecule where the electron and hole reside, this further stabilises the charge separation resulting in a long fluorescence lifetime and lower energy of the state.

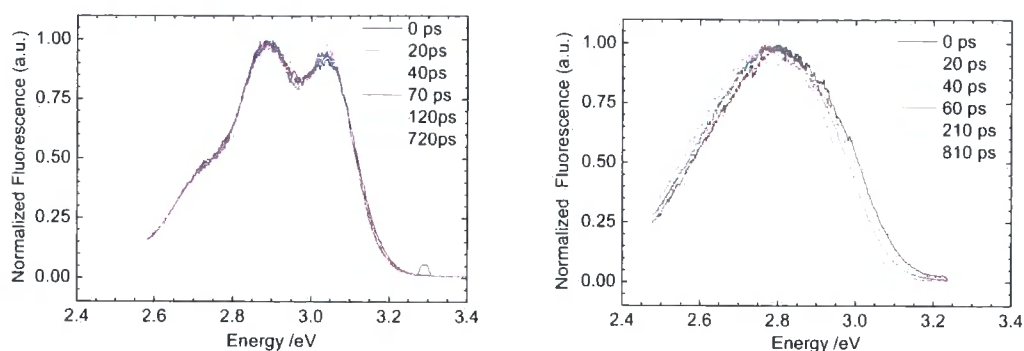


**Figure 4-7 Normalised emission spectra of the FSF oligomer at different times after excitation, for MCH (left) and Ethanol (right). Data kindly reproduced from the work of Dias et al<sup>48</sup>.**

For the FSF system, the adoption of the TICT model is supported by studying the time resolved emission in different solvents. Figure 4.7 shows the emission of the FSF molecule in the two solvents at different times, immediately clear is that there is no evolution of the shape of the emission spectra over time for either solvent. Importantly there is no build up of the ICT emission in the ethanol solution as the LE state decays; this proves that the ICT state is formed by a rapid intramolecular electron transfer which would be expected to take place in  $\ll 1$ ps. There is however, further stabilisation of the emission energy in the ethanol solution extending throughout the lifetime of the state. By measuring temperature dependent decays at wavelengths on the low and high energy side of the fluorescence one quantifies the rate of the spectral relaxation of the CT state. The amplitudes and lifetimes for such decays are shown in table 4.1, these data show two lifetimes,  $\tau_1$  from the actual radiative decay of the state, and  $\tau_2$  which characterises the relaxation of the state. As the temperature is reduced the relaxation rate of the CT state is reduced, the obvious conclusion that can be drawn is that the relaxation rate increases due to the increase of the solvent viscosity at low temperature. Thus, there must be a large structural change associated with the relaxation of the ICT state; as a result we have adopted the TICT model over and above its planar analogue for the system. The ICT state is stabilised by a twist in the molecule, the rate of which is controlled by the solvent viscosity.

		$\lambda$ /nm	$\tau_1$ ( $A_1$ ) /ns	$\tau_2$ ( $A_2$ ) /ns	$\tau_3$ ( $A_3$ ) /ns
MCH	300K	410	1.03 (1)	-	-
		460	1.03 (1)	-	-
EtOH	300K	410	1.81 (0.2)	0.043 (0.32)	0.01 (0.48)
		550	1.81 (1)	0.034 (-0.36)	-
EtOH	160K	410	1.62 (0.42)	0.38 (0.3)	-
		550	1.05 (1.0)	0.40 (-0.2)	-

**Table 4-1 Lifetimes and amplitudes of the components in the decay of the fluorescence of the FSF oligomer measured in the two different solvents. The effect on temperature on the relaxation time ( $\tau_2$ ) of the TICT state is clear. Data kindly reproduced from the work of Dias et al<sup>48</sup>.**

In the PFS30 polymer system which is analogous to the FSF oligomer similar behaviour is observed<sup>48</sup>. In polar solvents such as cyclohexanone and chlorobenzene, the polymer displays the characteristic low energy broad emission of the stabilised ICT state, whereas in non-polar toluene or MCH the emission is that of the LE state, very similar to a polyfluorene homopolymer (figure 4.8). The PFDBTH30 polymer is structurally very similar to PFS30, except without the oxygen substitutions on the central sulphur atom. This reduces the electron affinity of the dibenzothiophene unit sufficiently to prevent the formation of the CT state, thus the polymer has similar excited state behaviour to a polyfluorene homopolymer in all solvents. In the solid state and in electroluminescent devices, the PFSF30 polymer displays predominantly ICT excited state behaviour, caused by the polar nature of molecules surrounding the excited molecule essentially acting like the polar environment of a polar solvent. Conversely, PFDBTH30 displays LE state behaviour in the solid state.

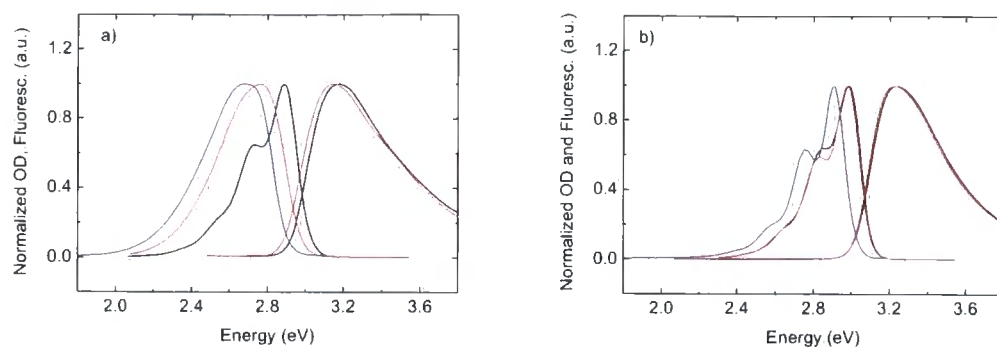


**Figure 4-8 Absorption and emission spectra for PFS30 (L) and PFDBTH30 (R) in toluene solution (black), ethanol solution (red) and the fluorescence in solid state (blue). The formation of the TICT state for PFS30 in ethanol and the solid state is clearly visible. Data kindly reproduced from the work of Dias et al<sup>48</sup>.**

### 4.3.2 Previous studies of Triplets in TICT forming molecules

Many TICT state forming molecules are well characterised in terms of their fluorescent properties, the rate of formation of the ICT state and the factors controlling their dual fluorescence. However, few previous studies have been made into the triplet states in such molecules. In addition, neither the singlet nor the triplet photoinduced absorption of TICT forming molecules has been investigated thoroughly in the literature. In one flash photolysis study of the molecule DMABN two long lived features are observed which are attributed to the existence of triplet states of the LE and CT states<sup>55</sup>. However, in other studies no evidence has been found for the existence of the triplet CT state<sup>56</sup>. The commonly held position in the literature is that the lowest triplet state is the LE triplet, which is in agreement with the notion that the S-T splitting in charge transfer states is generally lower than that of strongly correlated exciton states such as those found in conjugated polymer homopolymers<sup>53, 57</sup>. In previous studies of the rate of intersystem crossing in TICT state forming molecules authors have predicted that the rate should increase in the TICT state compared with the LE state<sup>48, 56</sup>. This prediction has been made by drawing comparison with intermolecular charge transfer exciplexes which can relax via a charge recombination mechanism yielding either the singlet ground state or the triplet excited state. This phenomenon has been observed in both small molecule and polymer blend based intermolecular CT states<sup>58, 59</sup>; however, an increase in the

intersystem crossing rate has not thus far been reported in intramolecular TICT state forming molecules<sup>56, 60</sup>.

### 4.3.3 Results: Excited State Absorption

Excited state absorption spectra for the molecule FSF in ethanol and MCH are shown in figure 4.10, both the quasi-cw spectra that show the long-lived states and the ultrafast pump-probe spectrum measured at a delay of 1.0ps (chirp corrected) are shown. The fs pump-probe spectra show similar phenomena to the fluorescence, in MCH solution the single feature observed peaks at 1.71eV, the absorption decays with an ~800ps lifetime, similar to the 1.0ns of the LE fluorescence previously measured by time correlated single photon counting<sup>47</sup>. Also, the similarity between the position and shape of this 1.71eV feature and the previously reported spectrum for the S<sub>1</sub>-S<sub>n</sub> transition of a fluorene trimer confirms that the feature is the excited state absorption of the LE singlet state<sup>61</sup>. On changing to ethanol solution there is a blue-shift of the peak to 1.87eV and the lifetime is extended to 1.7ns, a good comparison with the ICT fluorescence lifetime of 1.8ns. The energy change of 160meV is of similar magnitude to the 230meV relaxation in the energy of the fluorescence on going from the LE to ICT state. Broad, high energy excited state absorption features such as this in conjugated polymers usually characterise charged states, either intra-chain CT states, inter-chain states or individually charged species<sup>62-64</sup>. The solvatochromic shift in the excited state absorption is in the opposite sense to the fluorescence, the excited state absorption moves to higher energy whereas the fluorescence is stabilised to low energy. This is a strong indicator of the change of character from a more tightly bound exciton state to one of charge transfer character in a polar solvent.

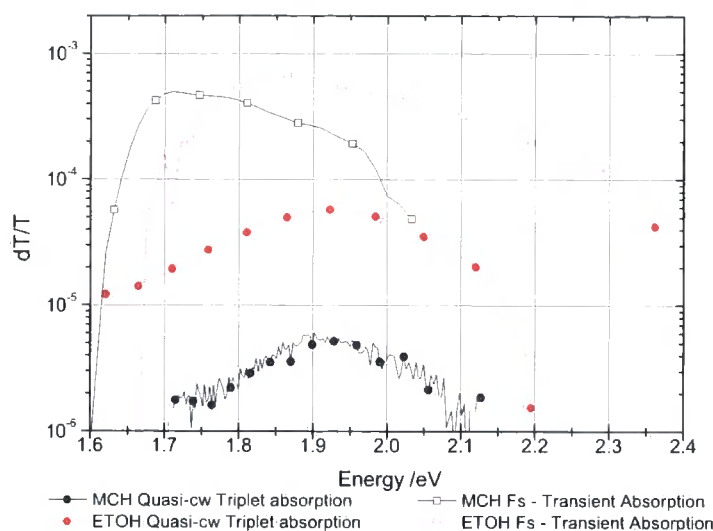


**Figure 4-9 Quasi-cw transient triplet and femtosecond pump-probe spectra for FSF in MCH and Ethanol**

The quasi-cw photoinduced absorption spectra in the two different solvents are almost identical in peak position and width. When measured with the nanosecond photoinduced absorption decay system the feature has a long lifetime, which is quenched by oxygen, therefore it can easily be attributed to the excited state absorption of the triplet state ( $T_1$ - $T_n$ ). In addition, the peak position is very similar to that reported previously in the literature for the triplet excited state absorption of the fluorene trimer<sup>61</sup>. There is a large difference in the amplitude of the absorption between the two solvents, the ethanol solution shows triplet excited state absorption intensity  $\sim 11$  times greater than the MCH solution; this is an initial indicator that either there are more triplet states present in the polar solvent or the oscillator strength of the state is increased. The absence of any solvatochromic shift in the triplet absorption suggests that the final triplet is of LE character rather than ICT, as one would expect a charge separated triplet ICT state to have a strong solvatochromic shift like the singlet ICT state. The similarity of the spectra therefore suggests the observed triplet states are the same thus confirming the increase in triplet state population rather than a change of oscillator strength.



#### 4.3.4 Ground State Recovery Triplet Yield Measurements

Ground state recovery decays in figure 4.11 for the FSF oligomer show that there is a significant difference in the kinetics for the two media. In the MCH solution almost all of the excited states decay in the 4ns time window of the experiment leaving few long-lived triplet excited states. In the polar environment of the ethanol solution, there is a large offset in the GSR at long times from the triplet excited states. The lifetimes of the fluorescence measured previously with TCSPC are 1.0ns and 1.8ns for the MCH solution and ethanol respectively<sup>47</sup>. The ground state recovery kinetics are fitted with biexponential decays incorporating the lifetimes of the fluorescence as well as an offset for the triplets which do not significantly decay within the time window of the experiment. An additional fast component is present in the ground state recovery over and above the singlet lifetime; this is attributed to the non-radiative decay processes of the states and is the second exponential in the fit (equation 4.8). From the ratio of the offset due to the triplets and the maximum absorption the yield of intersystem crossing is calculated, for the FSF oligomer in MCH and ethanol  $\Phi_T = 0.007 \pm 0.005$  and  $\Phi_T = 0.10 \pm 0.02$  respectively. As a check, one can calculate the proportion of the states which recover with the fluorescence lifetime and compare this with the fluorescence quantum yield of the oligomers<sup>47</sup>. There is excellent agreement in both cases, for MCH  $0.83 \pm 0.05$  of the states decay with 1.0ns lifetime and the photoluminescence quantum yield is  $0.82 \pm 0.05$ ; for ethanol  $0.69 \pm 0.05$  of the states decay with the fluorescence lifetime of 1.8ns compared to a PLQY of  $0.66 \pm 0.05$ . The low triplet yield of the FSF oligomer in MCH compares well with the triplet yield measured by GSR for a fluorene only trimer (FFF), which is also shown in figure 4.11, where  $\Phi_T = 0.004 \pm 0.005$ .

The increase in the triplet yield of FSF observed in the ground state recovery is similar to that observed in the magnitude of the quasi-cw transient triplet absorption spectra, an increase of 11 times is observed in the spectra compared to an increase of ~14 times in the GSR measurement. Although the spectral changes do agree with the GSR measurements, the quasi-cw measurement can be regarded as being less accurate. Even though care was taken to ensure that the spectra were measured with solutions of the same OD at the pump wavelength and that the overlap of the beams

was not changed. The need to degas the solutions to see the transient triplet absorption and the changeover between the samples makes the measurement less quantitative than the GSR measurement. As the GSR calculates the triplet yield as the ratio of the peak to plateau, any effect of changes in the overall signal magnitude are removed and a comparison between different samples is simple.

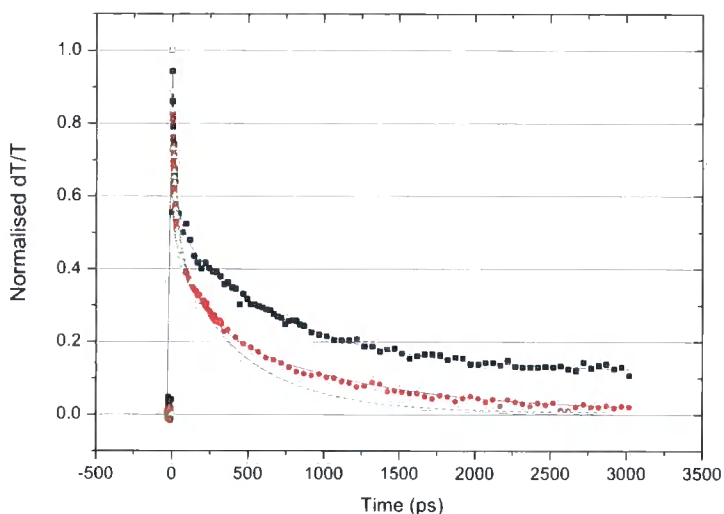


**Figure 4-10** GSR decays for FSF in Ethanol (black) and MCH (red) and for FFF in MCH (green). The solid lines are the fits to the data using equation 4.8.

The triplet yield for longer 5-member oligomers of the same system, FFSFF and FFFFF, has also been measured; the results are presented in table 4.2 along with all the triplet yields measured in this chapter. There is once again a significant increase in the triplet yield on going from the LE exciton in non-polar toluene to the ICT state in ethanol. The triplet yield of the LE state in FFSFF is similar to the non-TICT forming FFFFF analogue,  $\Phi_T=0.006$  and  $\Phi_T=0.005$  respectively, compared to  $\Phi_T=0.025$  for the ICT state in FFSFF. The increase in triplet yield is smaller than with the trimers, only 4 times the number of triplets are formed in the TICT state compared to the LE.

### 4.3.5 The CT Forming Polymers

The GSR data for the polymers PFSF<sub>30</sub> and PFDBTH<sub>30</sub> in table 4.1 shows the triplet yields for the two polymers. In the polymer PFDBTH<sub>30</sub> where there is never a charge transfer state formed, there is little difference in the ground state recovery in either the polar or unpolar solvent. Using the same fitting procedure as for the

oligomers one estimates a triplet yield (toluene) of  $\Phi_T = 0.07 \pm 0.02$ . For the polymer PFS<sub>30</sub> in the non-polar toluene a triplet yield of  $\Phi_T = 0.07 \pm 0.02$  is measured, the favourable comparison between the two materials in non-polar solvents provides assurance that the LE states of the two polymers are similar. In contrast to PFDBTH<sub>30</sub> in the polar solvents chloroform and cyclohexanone, PFS<sub>30</sub> shows significant increase in the triplet yield up to  $\Phi_T = 0.14 \pm 0.02$  in cyclohexanone.

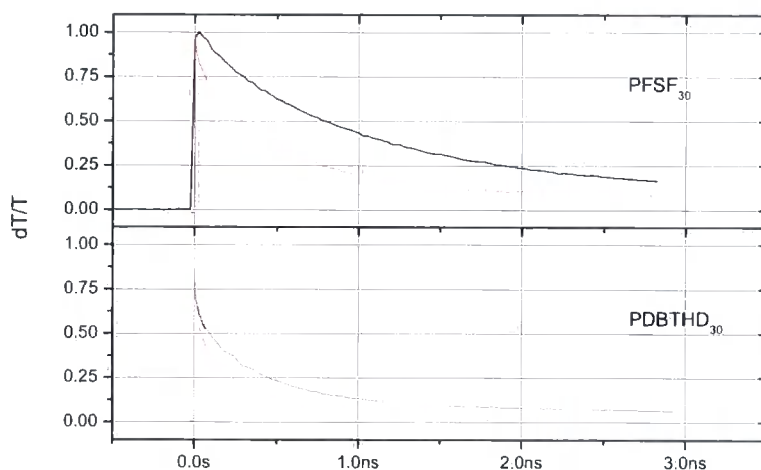


**Figure 4-11** The ultrafast GSR of the polymers PFSF<sub>30</sub> and PDBTHD<sub>30</sub> in toluene (red) and cyclohexanone (black).

In the solid state, thin films of the polymers PFS<sub>30</sub> and PFDBTH<sub>30</sub> show similar behaviour, the PFS<sub>30</sub> has a higher triplet yield than the PFDBTH<sub>30</sub>. The ICT state in PFS<sub>30</sub> is stabilised by the interactions between neighbouring chains which, due to their polar nature act as a polar environment for the excited state, allowing the stabilisation of the TICT state, which results in a larger triplet yield. Conversely, in the polymer PFBTH<sub>30</sub> where the excited state is always of LE character, the triplet yield remains low, similar to a film of the prototypical polyfluorene PFO. The situation does of course become more complicated in the solid state as one must account for the accelerated decay rate for the singlets attributed to the diffusion controlled bimolecular annihilation of the excitons<sup>34, 65</sup>. As before, effort has been made to minimize this effect by performing the experiment at low temperature (10K) and very low excitation density ( $<1 \mu\text{Jcm}^{-2}$ ). In the solid state it is common for the

excited state lifetime to be not simply a single exponential decay, often many components are observed due to quenching, interchain effects and other solid-state interactions, therefore fitting of the ground state recovery is not always easy in the solid state. In order to improve the accuracy of the fitting, global analysis of the data at the wavelength of the ground state recovery and the singlet excited state absorption has been used to ensure the singlet state decay is fully incorporated into the ground state recovery decay. In this technique, both decays are fitted with the same lifetimes, improving the quality of the fitting. This leads to a triplet yield of  $\Phi_T = 0.03 \pm 0.01$  for the non ICT forming PFDBTH<sub>30</sub> and  $\Phi_T = 0.13 \pm 0.02$  for the CT state forming PFS<sub>30</sub>. The PFO film has  $\Phi_T = 0.03 \pm 0.01$  which is very similar to the LE state triplet yield in PFDBTH<sub>30</sub>.

#### 4.3.6 Phosphorescence and Triplet Decay

In order to verify that the method of measuring the triplet yield by GSR is valid, one must prove that there are no long lived excited states other than the triplet state. This is done in the same way as in the earlier work on polyfluorene and polyspirobifluorene, by verifying that the decay of the transient triplet absorption and the ground state recovery are the same in the nanosecond – millisecond time. This is shown for the polymer PFSF<sub>30</sub> in figure 4.12; the decays are very similar for all time regimes. In the early time, there is a rapid decay at 780nm, the wavelength of the excited state absorption and at 405nm, the wavelength of the GSR. At 780nm the probe beam is probing both the singlet excited state absorption and the triplet excited state absorption, which have similar spectral positions. Initially there is a fast decay from the decay of the singlet feature and a slow decay from the decay of the triplet excited state absorption. In the GSR at low pulse energy two decays are observed also, one from the singlet decay and one from the triplet. It is important to note that when the pulse energy is increased to very high levels ( $>100 \mu\text{Jcm}^{-2}$ ) does an additional long lived state appear in the GSR. However, the lowest pulse energy used ( $25 \mu\text{Jcm}^{-2}$ ) in this nanosecond transient absorption system is far in excess of the typical pulse energies used in the ultrafast pump-probe system ( $\sim 1 \mu\text{Jcm}^{-2}$ ).

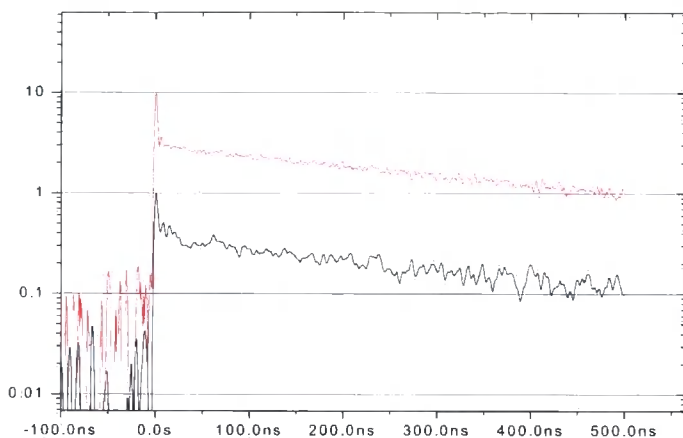


**Figure 4-12** A comparison between the excited state absorption measured at 780nm with the ground state recovery measured on the nanosecond timescale. The data shown is the PFSF<sub>30</sub> polymer in cyclohexanone.

### 4.3.7 Polyfluorene Oligomers

In the previous paragraphs, the triplet yields of the FSF oligomers have always been compared to the triplet yield of polyfluorene oligomers of the same number of repeat units. This is because the triplet yield appears to increase with the oligomer length; in order to gain further insight into this phenomenon polyfluorene polymers of 10 and 20 repeat units were also measured. The results in the summary table 4.2 show a clear increase in the triplet yield as the length of the oligomers increases, from  $\Phi_T = 0.004 \pm 0.005$  for the trimer FFF, to  $\Phi_T = 0.036 \pm 0.005$  for long chain PFO.

## 4.4 Discussion

### 4.4.1 Triplet yield and Intersystem Crossing Rate

The increase in the intersystem crossing yield on going from the LE singlet to the TICT singlet state is clear from the data in table 4.2 and described above. This increase in the triplet yield would be unsurprising if it were accompanied by a concomitant increase in the singlet lifetime, for a constant rate of formation of triplets there would be for example, a doubling of the triplet yield for a doubling of the singlet lifetime. In order to quantify the effects that contribute to a high intersystem crossing, one must calculate the intersystem crossing rate thus removing any effect of the change in singlet lifetime. This is particularly important when comparing the intersystem crossing in the TICT state with that of the LE, as there is an approximate doubling of the lifetime of the excited state when forming the TICT state. The intersystem crossing rate is given earlier and is repeated below in equation 4.10. In many cases particularly with the polymers in solid state; the decay of the singlet is not a single exponential therefore the lifetime used to calculate the rate if intersystem crossing is the weighted average of the lifetimes calculated from the preexponential factors in the decay.

$$k_{isc} = \frac{\Phi_T}{\tau_f}$$

Equation 4-12

### 4.4.2 Summary of Results

	Solvent	Emission	$\tau_f$ /ns (a)	$\Phi_T$	$K_{isc} /10^6s^{-1}$
FSF	MCH	415nm/3.00eV	1.0	0.007	8.5
FSF	EtOH	448nm/2.77eV	1.8	0.1	83
FFF	Toluene	400nm/3.10eV	0.66	0.004	5.3
FFSFF	Toluene	430nm/2.88eV	0.6	0.006	9.0
FFSFF	EtOH	453nm/2.74eV	1.0	0.025	25
FFFFF	Toluene	407nm/3.05eV	0.55	0.005	13
PFDBTH <sub>30</sub>	Toluene	415nm/3.00eV	0.35	0.065	185
PFDBTH <sub>30</sub>	C-	415nm/3.00eV	0.38	0.060	158

	hexanone				
<b>PFS<sub>30</sub></b>	Toluene	430nm/2.88eV	0.55	0.072	130
<b>PFS<sub>30</sub></b>	Chloroform	450nm/2.76eV	0.85	0.11	129
<b>PFS<sub>30</sub></b>	C-hexanone	465nm/2.67eV	1.1	0.14	127
<b>PFDBTH<sub>30</sub></b>	Film	431nm/2.88eV	0.26 (b)	0.03	113
<b>PFS<sub>30</sub></b>	Film	469nm/2.64eV	0.67 (b)	0.13	195
<b>PFO (long)</b>	Toluene	413nm/3.00eV	0.42	0.036	85
<b>PFO</b>	Film	420nm/2.95eV	0.32 (b)	0.033	100
<b>PF2/6 (20mer)</b>	Toluene	413nm/3.00eV	0.41	0.013	31
<b>PSBF</b>	Toluene	430nm/2.88eV	1.1 (b)	0.05	55
<b>PSBF</b>	Film	435nm/2.85eV	0.66 (b)	0.12	80

**Table 4-2 Triplet yields, singlet lifetimes and intersystem crossing rates for all the different polyfluorene copolymers and oligomers measured.**

- (a) Fluorescence lifetimes taken from single photon counting<sup>47, 48, 66</sup> and the calculated rates of intersystem crossing.
- (b) Decay lifetimes calculated from the weighted average of the singlet decay components in the pump probe data, and the intersystem crossing rates calculated from these.

#### 4.4.3 The Nature of Intersystem Crossing

In molecular excited states, intersystem crossing is merely a special case of a radiationless transition<sup>42, 67</sup>. It is a radiationless transition which includes a change of spin multiplicity of the excited state, essentially a change of angular momentum of one of the charges. This leads to two requirements for intersystem crossing; the first is a perturbation of the state that allows the change of angular momentum. This causes a mixing of some singlet states with the triplet which facilitates the normally spin forbidden triplet state formation. In most cases, the perturbation originates from the spin orbit interaction between the  $\pi$ -electrons and the nuclei of the molecule. In some special cases, the perturbation can also come from spin-vibronic and vibrational mixing. The second requirement for intersystem crossing is drawn from its non radiative nature, there must be an accepting triplet present, either electronic or a vibrational sub level of an electronic transition, close to the donating singlet to allow the isoenergetic crossing to the triplet manifold to take place. This is expressed as the

Franck-Condon weighted density of states (FCWD) which is an overlap integral between the accepting triplet's density of states and the Franck-Condon vibrational overlap between the states of the singlet and the triplet. A small vibrational overlap between the donor singlet and the accepting triplet results in a low rate of intersystem crossing. The two requirements for intersystem crossing can be expressed as the rate of the transition by considering Fermi's golden rule<sup>41, 42, 68</sup>:

$$k_{i \rightarrow f} = \frac{2\pi}{\hbar} \langle i | H | f \rangle^2 \rho \quad \text{Equation 4-13}$$

The initial and final states ( $i, f$ ) are the donating singlet and accepting triplet, ( $^1\Psi^0, ^3\Psi^0$  respectively), and the final density of states ( $\rho$ ) is the Franck-Condon Weighted Density of States [FCWD]. The Hamiltonian for the interaction which mixes the singlet and a triplet state, is that of the spin orbit interaction:

$$H_{SO} = \alpha_{fs}^2 \sum_{\mu}^N \sum_i^n \frac{Z_{\mu}}{r_{i\mu}^3} \vec{L}_i \vec{S}_i \quad \text{Equation 4-14}$$

where  $\alpha_{fs}$  is the fine structure constant,  $Z_{\mu}$  is the charge on a nucleus,  $\mu$ , and  $L$  and  $S$  are the orbital and spin angular momenta, respectively. This gives the spin orbit interaction for an electron  $i$  moving in the field of a nucleus  $\mu$ . The resulting rate of the intersystem crossing is:

$$k_{isc} = \frac{2\pi}{\hbar} \langle ^1\Psi^0 | H_{SO} | ^3\Psi^0 \rangle^2 [FCWD] \quad \text{Equation 4-15}$$

In order to consider the effect of the spin orbit interaction in more detail one should perform the integral, however, this requires complex modelling of the excited states and their interaction and is a project in itself. It is possible to use general knowledge about the wavefunctions of the singlet and triplet excited states to draw some general conclusions, which will help to understand the intersystem crossing from the TICT and LE singlet states. Firstly, one can consider that in the planar polyacenes the triplet state is generally oriented out of the plane of the molecule, this



is also true in the polyfluorenes (chapter 5) conversely; the singlet state is along the backbone of the molecule<sup>69-75</sup>. The effect of this is that for a planar molecule the mixing between singlet and triplet is very difficult. Generally, the mixing of two  $\pi$ - $\pi$  states is only allowed by the out of plane components of the spin orbit operator ( $H_{SO}$ ) because both  $H_{SO}$  and the  $\pi$  states are symmetric to in plane rotation<sup>41, 42</sup>. In a planar molecule this mixing will be very low as there is little overlap between the out of plane components of  $H_{SO}$  and the predominantly in-plane singlets. Consequentially the molecule has a very low intersystem crossing rate. If non-bonding electrons were involved in the excited state, the in plane components of  $H_{SO}$  are able to mix  $\pi\pi$ - $n\pi$  and consequentially the (3-centre) spin orbit integral is greater, with a concomitant increase in the intersystem crossing rate. For transitions with a large  $S_1$ - $T_1$  gap there is the possibility of intersystem crossing to higher triplet ( $T_n$ ) levels, the differing symmetry of these states could allow a larger mixing between the singlet and triplet states and a higher intersystem crossing rate<sup>42</sup>.

The FCWD factor, which describes the extent of the vibrational overlap required for the non-radiative transition, is very important as it is directly affected by the density of the vibrational transitions in the molecule, which are a product of the structure of the molecule. The overlap integral between the vibrational states increases at low energies, increasing FCWD factor, so as the donating singlet becomes closer in energy to the electronic triplet state the intersystem crossing becomes more efficient. This is effectively the often observed energy gap law for radiationless transitions applied to intersystem crossing<sup>41</sup>. In addition to this if the singlet-triplet energy gap is large then there could be higher electronic triplet states between the  $S_1$  and the  $T_1$  which could contribute to intersystem crossing through the FCWD factor, by reducing the energy gap. In some planar polyacenes such as anthracene, triplet states intermediate to the  $S_1$ - $T_1$  gap, have been observed and some calculations on conjugated polymers and oligomers show that intersystem crossing proceeds via higher triplet states. If this is the case then one would expect that there is rapid relaxation of the triplet state to its lowest state ( $T_1$ ), so the observed phosphorescence originates only from the lowest triplet state, in line with Kasha's rule. Unfortunately, this means that whether the intersystem crossing is to a higher triplet state or to  $T_1$  is very difficult to determine.

#### 4.4.4 Intersystem Crossing in the TICT state of FSF

The oligomer FSF shows an almost 10 fold increase in the intersystem crossing rate in the TICT excited state compared to the LE state, on going to the longer oligomer the FFSFF the effect is diminished to approximately 3 times. In the polymer, PFSF<sub>30</sub> there is no increase in the intersystem crossing rate and the increase in the triplet yield seems to be only due to the change in the singlet lifetime. The increase in the intersystem crossing rate in twisted excited states has been postulated previously, calculations on short thiophene oligomers suggest that twisted ter- and bithiophenes have a higher intersystem crossing rate than the more planar longer oligomers<sup>45, 76, 77</sup>. Furthermore ultrafast studies on the intersystem crossing in terthiophene have shown that there is a reduction of the intersystem crossing to the triplet state as the molecule relaxes to a more planar conformation with time<sup>78, 79</sup>. There are two main conclusions that come from this previous work, firstly that in the thiophenes twisted excited states have a higher intersystem crossing rate, and secondly that the longer thiophene oligomers are less twisted and therefore have a concomitantly lower intersystem crossing rate. The data presented here on the intersystem crossing in the FSF and FFSFF oligomers mirror these conclusions, when the TICT state is switched on and the molecule has a twisted excited state there is a higher intersystem-crossing rate.

Rationalising the increase in the intersystem crossing rate in the twisted excited state can be easily done by remembering the reason for the low intersystem crossing in planar polyacenes. In a twisted molecule there is clearly more potential for the mixing of the singlet and triplet states by the out of plane components of the spin orbit interaction because the singlet itself has an out of plane component, i.e. the totally planar symmetry of the molecule is broken. This is the reason attributed to the higher level of intersystem crossing in the twisted excited states of the short thiophenes and is easily applied for the FSF system studied here. It is therefore possible to switch the intersystem crossing on by inducing a twist in the molecule, which is inherent in the formation of the TICT singlet state from the planar LE singlet state. To the best of our knowledge, this is the first observation of a dynamically

controllable intersystem crossing rate. In the longer FFSFF oligomer the increase in the intersystem crossing rate on the formation of the TICT state is reduced, this is consistent with larger molecule having a less twisted conformation in the TICT state compared to the smaller molecule. The reduction in the twist of the TICT state formed in the polar solvents on going to the longer oligomers is supported by the fluorescence lifetimes. It is expected that the more twisted the excited state is the lower the coupling to the ground state, and therefore there would be a longer fluorescence lifetime. This hypothesis is confirmed by the 1.8ns TICT state lifetime in the FSF compared with the 1.0ns lifetime of the TICT in FFSFF.

The conclusion that the higher intersystem crossing in the TICT state is due to the twisted nature of the state is not only in agreement with the aforementioned calculations on thiophene systems, but also in agreement with the general trend in aromatic systems. Nijegordorov and Downey have made measurements of the intersystem crossing rates for a large number of small aromatic molecules, revealing a trend towards higher intersystem crossing in molecules with a flexible or twisted conformation compared to planar, rigid molecules<sup>80</sup>.

#### **4.4.5 Intersystem Crossing in the Polymeric Analogues of FSF**

On going to the polymer analogues of the FSF system there is no increase in the intersystem crossing rate between the TICT state and the LE excited state. In the non-TICT forming polymer PFDBTH30, the intersystem crossing rate is generally slightly higher than in the TICT forming PFSF30. This can be explained by the potential interaction of the nonbonding electrons of the sulphur lone pair with the excited state. As there can be some non bonding character mixed into the excited state there can be higher intersystem crossing as is found in the thiophenes, benzophenone and other molecules with  $n-\pi^*$  excited states. This phenomenon is described by the previously mentioned El-Sayed's rule<sup>68</sup>. In order to understand the lack of a change of intersystem crossing rate on the formation of the TICT state in the polymers one first notes the higher intersystem crossing rate in the polymers generally compared to the oligomers. To rationalise this fully it is best to consider generally the change in

intersystem crossing rate with oligomer length, which is best done by comparing the intersystem crossing rates in the fluorene oligomers and polymers.

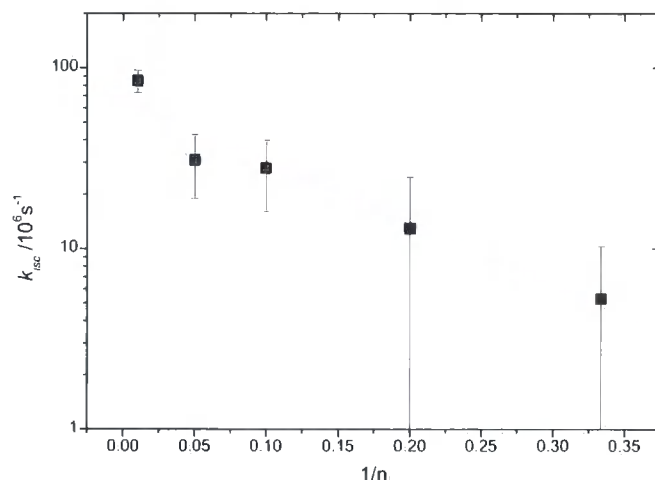


**Figure 4-13 variation in the rate of intersystem crossing with oligomer length for fluorene oligomers and polymers in toluene solution.**

In the fluorene only oligomers and polymers there is a clear increase in the intersystem crossing rate as the length of the oligomers is increased, a plot of the intersystem crossing rate with inverse oligomers length is shown in figure 4.13 above. The relationship approximates to an exponential decay of the intersystem crossing rate with inverse chain length, leading to a saturation value of  $k_{isc} = 12 \times 10^6 s^{-1}$  for the infinite chain. To understand the reason for this increase in the intersystem crossing rate with chain length, one can apply a similar argument to the increased intersystem crossing in TICT states; the twisted nature of the polymers structure. Polyfluorene polymers are subject to a large degree of conformational disorder, this is well studied and is one origin of the high degree of inhomogeneous broadening of the absorption and emission spectra. The conformational disorder is generally in the form of twists between the neighbouring units, which occur over a few repeat units.. In longer oligomers the probability of there being a twist in the molecule is greatly increased as the molecule contains many more repeat units and therefore when considered as a whole is more disordered.<sup>35</sup> X-ray diffraction studies indicate a torsion angle of  $135^\circ$  between neighbouring fluorene units in high molecular weight polyfluorene<sup>81</sup>. In addition to this, there are some reports in the literature of a planarization of the chain segment that the excited state occupies. In short oligomers, one might expect this to

be more efficient as the excited state occupies the whole molecule and is therefore able to planarise the entire molecule. In a long polymer where the excited state only occupies a segment of the chain, not only would the planarization be slower, but also there is far greater chance of twists remaining between excited states, in the much more sterically hindered polymer compared to the predominantly planar small oligomers. Therefore, the variety of different torsion angles between the neighbouring chromophores on a polymer chain<sup>35, 82</sup> could lead to many possibilities for different degrees of mixing of singlet and triplet states and an increase in the intersystem crossing rate over the predominantly planar conformation of the smaller (non TICT forming) oligomers. In addition to the conformational disorder increasing the intersystem crossing rate, there is also energetic disorder originating from the differing conjugation lengths of the polymer this energetic disorder can have a dramatic effect on the intersystem crossing. For example in a system where the  $S_1-T_1$  FCWD factor is small, an increase in the width of the distribution of states will have a significant increase in the overlap integral between the singlet and the accepting triplet and hence the intersystem crossing rate. In the solid state where the conformation of the molecules are dominated by interchain interactions the system becomes more complex and even more disordered.

One must also consider the position of higher triplet states; generally as the chain length increases the triplets become more closely packed in energy terms with a trend to decreased singlet triplet splitting<sup>83, 84</sup>. Thus, there may be more possibilities for energetically favourable accepting triplet states close to the singlet energy in the polymers compared to oligomers. The collective result of all these effects is that there is a significant increase in the intersystem crossing rates of polyfluorene oligomers with chain length.

Returning to the PFSF30 copolymers, not only are all the effects which increase the intersystem crossing rate in a homopolymer active, they are in fact more prevalent, as the presence of the co-oligomer in the system acts to increase further the energetic disorder of the polymer, accentuating the effects seen in homopolymers. This is evidenced by the greater intersystem crossing rate shown by both the copolymers compared to PFO, or the PF2/6 20mer which is approximately the same

number of repeat units as the copolymers. Thus one can suggest that the increase in the intersystem crossing rate, which would be expected from the formation of a twisted excited state is insignificant, compared to the generally high intersystem crossing rate in the polymer due to the conformational and energetic disorder already present in the polymer. It is also very likely that the increased steric hindrance in a large polymer is actually reducing the amount of twisting in the TICT singlet state compared to the smaller molecules, as was seen with the FFSFF compared to the FSF, this will reduce the effect of the formation of the TICT state on the intersystem crossing.

#### **4.4.6 The Nature of the Triplet State**

The nature of the accepting triplet state is of interest to the mechanism of intersystem crossing, one would expect that, due to the lower singlet triplet splitting in CT states compared to LE states, in every case the lowest triplet state to be the LE state. Indeed, all the evidence (phosphorescence, transient triplet absorption) points to this being the case. There are therefore two possibilities; either the accepting triplet could be of LE character, with the intersystem crossing directly between the LE or CT singlet and the LE triplet. Or, there could be intersystem crossing from the ICT singlet to an ICT triplet in the polar media followed by relaxation to the LE triplet. The difference between these two mechanisms is very difficult to distinguish, as the energetic relaxation of the triplet to the lower LE triplet is expected to be rapid. While it is clear that in the oligomers the presence of an ICT state does sensitise the triplet states by increasing the intersystem crossing rate, whether this is through a triplet ICT state intermediate or directly to the LE triplet is impossible to determine.

#### **4.5 Conclusion**

In conclusion, the method of measuring the intersystem crossing yield and rate by ground state recovery has been developed and the results verified by comparison with previous measurements. The rates of intersystem crossing of a number of conjugated polymers and oligomers have been calculated and from these, a number of



broad trends can be distinguished. Firstly, the intersystem crossing in conjugated systems that do not contain heavy atoms or an  $n-\pi^*$  state is inefficient. In addition, TICT excited states have generally higher intersystem crossing rates compared to their corresponding LE states; this is due to the twisted nature of the excited state allowing greater mixing between the singlet and triplet states and therefore the change of spin which facilitates triplet formation is more probable. In longer oligomers and polymers, the effect of the twisted nature of the ICT singlet state on the intersystem crossing rate is reduced because of a reduction in the twist in the larger molecules. The third conclusion from this chapter is that the intersystem crossing rate in polyfluorene oligomers increases as the chain length increases, due to the increased energetic and conformational disorder in polymers compared to short oligomers. This contributes by two mechanisms, the twists between sections of the chain increase the intersystem crossing rate, and the larger triplet manifold greatly improves the probability of finding a triplet state isoenergetic to the singlet to facilitate the intersystem crossing.

## 4.6 References

- <sup>1</sup> C. Yang, Z. V. Vardeny, A. Kohler, et al., *Physical Review B* **70**, 241202 (2004).
- <sup>2</sup> A. Kohler and J. Wilson, *Organic Electronics* **4**, 179 (2003).
- <sup>3</sup> M. Wohlgenannt, X. M. Jiang, and Z. V. Vardeny, *Physica B-Condensed Matter* **338**, 318 (2003).
- <sup>4</sup> J. Y. Zhang, S. D. Kan, Y. G. Ma, et al., *Chinese Journal of Polymer Science* **19**, 591 (2001).
- <sup>5</sup> Z. Shuai, A. Ye, D. Beljonne, et al., *Synthetic Metals* **121**, 1637 (2001).
- <sup>6</sup> C. Rothe, S. M. King, and A. P. Monkman, *Physical Review Letters* **97** (2006).
- <sup>7</sup> V. Dyakonov, G. Rosler, M. Schwoerer, et al., *Physical Review B* **56**, 3852 (1997).
- <sup>8</sup> D. Hertel, H. Bassler, R. Guentner, et al., *Journal of Chemical Physics* **115**, 10007 (2001).
- <sup>9</sup> C. Rothe and A. P. Monkman, *Physical Review B* **68**, 075208 (2003).
- <sup>10</sup> M. A. Baldo, S. Lamansky, P. E. Burrows, et al., *Applied Physics Letters* **75**, 4 (1999).
- <sup>11</sup> X. Gong, J. C. Ostrowski, D. Moses, et al., *Advanced Functional Materials* **13**, 439 (2003).
- <sup>12</sup> P. A. Lane, L. C. Palilis, D. F. O'Brien, et al., *Physical Review B* **63**, 235206 (2001).
- <sup>13</sup> D. Neher, *Macromolecular Rapid Communications* **22**, 1366 (2001).
- <sup>14</sup> T. Miteva, A. Meisel, W. Knoll, et al., *Advanced Materials* **13**, 565 (2001).
- <sup>15</sup> M. Kreyenschmidt, G. Klaerner, T. Fuhrer, et al., *Macromolecules* **31**, 1099 (1998).
- <sup>16</sup> J. Cornil, I. Gueli, A. Dkhissi, et al., *Journal of Chemical Physics* **118**, 6615 (2003).
- <sup>17</sup> B. Liu, W. L. Yu, Y. H. Lai, et al., *Macromolecules* **33**, 8945 (2000).
- <sup>18</sup> I. F. Perepichka, S. M. King, M. R. Bryce, et al., *Advanced Materials* **submitted** (2007).



- 19 A. Charas, J. Morgado, J. M. G. Martinho, et al., *Chemical Communications*,  
1216 (2001).
- 20 T. M. Hong and H. F. Meng, *Physical Review B* **63**, 075206 (2001).
- 21 Y. V. Romanovskii, A. Gerhard, B. Schweitzer, et al., *Physical Review Letters*  
**84**, 1027 (2000).
- 22 D. Hertel, S. Setayesh, H. G. Nothofer, et al., *Advanced Materials* **13**, 65  
(2001).
- 23 J. S. de Melo, L. M. Silva, L. G. Arnaut, et al., *Journal of Chemical Physics*  
**111**, 5427 (1999).
- 24 J. S. de Melo, F. Elisei, C. Gartner, et al., *Journal of Physical Chemistry A*  
**104**, 6907 (2000).
- 25 L. G. Arnaut, R. A. Caldwell, J. E. Elbert, et al., *Review of Scientific*  
*Instruments* **63**, 5381 (1992).
- 26 H. D. Burrows, J. S. de Melo, C. Serpa, et al., *Journal of Chemical Physics*  
**115**, 9601 (2001).
- 27 H. D. Burrows, J. S. de Melo, C. Serpa, et al., *Chemical Physics* **285**, 3 (2002).
- 28 H. E. Lessing, A. Von Jena, and M. Reichert, *Chemical Physics Letters* **42**,  
218 (1976).
- 29 H. E. Lessing, D. Richardt, and A. Von Jena, *Journal of Molecular Structure*  
**84**, 281 (1982).
- 30 S. M. King, C. Rothe, D. Dai, et al., *Journal of Chemical Physics* **124**, 234903  
(2006).
- 31 I. B. Martini, A. D. Smith, and B. J. Schwartz, *Physical Review B* **69** (2004).
- 32 C. Gadermaier, G. Cerullo, G. Sansone, et al., *Physical Review Letters* **89**,  
117402 (2002).
- 33 C. Silva, A. S. Dhoot, D. M. Russell, et al., *Physical Review B* **64**12 (2001).
- 34 S. M. King, D. Dai, and A. P. Monkman, *Physical Review B* **76**, 085204  
(2007).
- 35 F. B. Dias, A. L. Macanita, J. S. de Melo, et al., *Journal of Chemical Physics*  
**118**, 7119 (2003).
- 36 S. King, C. Rothe, and A. Monkman, *The Journal of Chemical Physics* **121**,  
10803 (2004).
- 37 C. Rothe, S. King, and A. P. Monkman, *Physical Review B* **73** (2006).

- 38 D. Vak, C. Chun, C. L. Lee, et al., *Journal of Materials Chemistry* **14**, 1342  
(2004).
- 39 A. Pogantsch, F. P. Wenzl, U. Scherf, et al., *Journal of Chemical Physics* **119**,  
6904 (2003).
- 40 S. Hintschich, S. M. King, S. J. Clarke, et al., in preparation (2006).
- 41 J. B. Birks, *Organic molecular photophysics* (J. Wiley, London, New York,,  
1973).
- 42 S. P. McGlynn, T. Azumi, and M. Kinoshita, *Molecular Spectroscopy of The  
Triplet State* (Prentice Hall, Englewood Cliffs, New Jersey, 1969).
- 43 A. van Dijken, J. Bastiaansen, N. M. M. Kiggen, et al., *Journal of the  
American Chemical Society* **126**, 7718 (2004).
- 44 G. Barbarella, L. Favaretto, G. Sotgiu, et al., *Journal of the American  
Chemical Society* **122**, 11971 (2000).
- 45 D. Beljonne, Z. Shuai, G. Pourtois, et al., *Journal of Physical Chemistry A*  
**105**, 3899 (2001).
- 46 I. I. Perepichka, I. F. Perepichka, M. R. Bryce, et al., *Chemical  
Communications*, 3397 (2005).
- 47 F. B. Dias, S. Pollock, G. Hedley, et al., *Journal of Physical Chemistry B* **110**,  
19329 (2006).
- 48 F. B. Dias, S. M. King, R. J. Matherson, et al., *Journal of Physical Chemistry  
B*, (In press) (2007).
- 49 Z. R. Grabowski, K. Rotkiewicz, and W. Rettig, *Chemical Reviews* **103**, 3899  
(2003).
- 50 J. Herbich and A. Kapturkiewicz, *Journal of the American Chemical Society*  
**120**, 1014 (1998).
- 51 G. Wermuth, W. Rettig, and E. Lippert, *Berichte Der Bunsen-Gesellschaft-  
Physical Chemistry Chemical Physics* **85**, 64 (1981).
- 52 T. Yoshihara, S. I. Druzhinin, and K. A. Zachariasse, *Journal of the American  
Chemical Society* **126**, 8535 (2004).
- 53 Z. R. Grabowski and J. Dobkowski, *Pure and Applied Chemistry* **55**, 245  
(1983).
- 54 K. A. Zachariasse, M. Grobys, and E. Tauer, *Chemical Physics Letters* **274**,  
372 (1997).

- 55 N. Chattopadhyay, C. Serpa, L. G. Arnaut, et al., *Helvetica Chimica Acta* **85**,  
19 (2002).
- 56 G. Kohler, G. Grabner, and K. Rotkiewicz, *Chemical Physics* **173**, 275 (1993).
- 57 A. P. Monkman, H. D. Burrows, L. J. Hartwell, et al., *Physical Review Letters*  
**86**, 1358 (2001).
- 58 T. A. Ford, I. Avilov, D. Beljonne, et al., *Physical Review B* **71** (2005).
- 59 M. Gordon and W. R. Ware, *The Exciplex* (Academic Press, New York,  
1975).
- 60 A. R. Horrocks, T. Medinger, and Wilkinso.F, *Photochemistry and*  
*Photobiology* **6**, 21 (1967).
- 61 J. Cabanillas-Gonzalez, M. R. Antognazza, T. Virgili, et al., *Physical Review*  
*B* **71**, 155207 (2005).
- 62 S. J. Pomfret, E. Rebut, L. Abell, et al., *Synthetic Metals* **84**, 729 (1997).
- 63 B. Kraabel, V. I. Klimov, R. Kohlman, et al., *Physical Review B* **61**, 8501  
(2000).
- 64 G. Lanzani, G. Cerullo, D. Polli, et al., *Physica Status Solidi a-Applied*  
*Research* **201**, 1116 (2004).
- 65 B. Kraabel and D. W. McBranch, *Chemical Physics Letters* **330**, 403 (2000).
- 66 C. Y. Chi, C. Im, and G. Wegner, *Journal of Chemical Physics* **124**, 024907  
(2006).
- 67 J. B. Birks, *Photophysics of aromatic molecules* (Wiley-Interscience, London,  
New York,, 1970).
- 68 S. K. Lower and M. A. El-Sayed, *Chemical Reviews* **66**, 199 (1965).
- 69 S. M. King, H. L. Vaughan, and A. P. Monkman, *Chemical Physics Letters*  
**440**, 98 (2007).
- 70 A. Dkhissi, D. Beljonne, R. Lazzaroni, et al., *International Journal of Quantum*  
*Chemistry* **91**, 517 (2003).
- 71 L. O. Palsson, H. L. Vaughan, and A. P. Monkman, *Journal of Chemical*  
*Physics* **125**, 164701 (2006).
- 72 F. Dorr and H. Gropper, *Angewandte Chemie-International Edition* **74**, 354  
(1962).
- 73 J. S. Wilson, R. J. Wilson, R. H. Friend, et al., *Physical Review B* **67**, 125206  
(2003).

- 74 J. J. Dekkers, G. P. Hoornweg, K. J. Terpstra, et al., *Chemical Physics* **34**, 253  
(1978).
- 75 J. J. Dekkers, G. P. Hoornweg, W. P. Cofino, et al., *Chemical Physics Letters*  
**67**, 24 (1979).
- 76 R. S. Becker, J. S. deMelo, A. L. Macanita, et al., *Journal of Physical*  
*Chemistry* **100**, 18683 (1996).
- 77 F. D. Lewis and X. B. Zuo, *Journal of the American Chemical Society* **125**,  
8806 (2003).
- 78 J. P. Yang, W. Paa, and S. Rentsch, *Chemical Physics Letters* **320**, 665 (2000).
- 79 W. Paa, J. P. Yang, and S. Rentsch, *Applied Physics B-Lasers and Optics* **71**,  
443 (2000).
- 80 N. I. Nijegorodov and W. S. Downey, *Journal of Physical Chemistry* **98**, 5639  
(1994).
- 81 M. Knaapila, V. M. Garamus, F. B. Dias, et al., *Macromolecules* **39**, 6505  
(2006).
- 82 K. Brunner, A. Tortschanoff, C. Warmuth, et al., *Journal of Physical*  
*Chemistry B* **104**, 3781 (2000).
- 83 D. A. dos Santos, D. Beljonne, J. Cornil, et al., *Chemical Physics* **227**, 1  
(1998).
- 84 D. Wasserberg, S. P. Dudek, S. C. J. Meskers, et al., *Chemical Physics Letters*  
**411**, 273 (2005).

#### **4.7 Publications Arising From This Chapter**

S.M. King, C. Rothe, D. Dai, and A.P. Monkman, *Femtosecond ground state recovery: Measuring the intersystem crossing yield of polypirobifluorene*. *Journal of Chemical Physics*, 2006. **124** (23) 234903.

S.M. King, R. Matheson, F.B. Dias, and A.P. Monkman, *Enhanced Triplet Formation by Intramolecular TICT Excited States in Conjugated Oligomers and Polymers*. *Journal of Physical Chemistry B*, 2008 (In Press).

## **5 Singlet – Singlet and Singlet – Triplet Annihilation in PF2/6**

### **5.1 High Excitation Dose Phenomena in Conjugated Polymers**

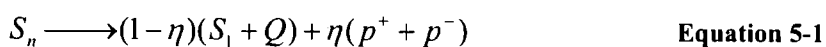
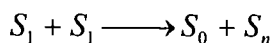
The processes that excited states take part in generally fall into two categories, the intrinsic processes such as absorption and spontaneous emission and the processes, which involve interaction with another state, such as energy transfer, quenching or excimer formation<sup>1-5</sup>. Of the latter, one important class of processes are those which occur between two excited states, these are the so-called annihilation reactions; annihilation reactions are possible between all types of excited states, singlet – singlet, singlet – triplet and triplet – triplet. As all the interactions require two excited states to form and interact, it follows that the annihilation reactions will be more prevalent at high excitation density. In the basic photophysics experiments such as absorption and fluorescence the excitation density is generally very low so the effect of high excitation density phenomena is rarely seen. However, in less sensitive experimental techniques such as transient absorption, the excitation density can be such that these non-linear, extrinsic, phenomena dominate the photophysics of the material. In addition, processes which dominate the photophysics of the conjugated polymers at high excitation density are becoming relevant to the OLED community, with the current drive towards high brightness devices for lighting applications and the potential for organic lasers processes which affect the emission efficiency or laser gain at high excitation density are clearly of interest<sup>6-8</sup>.

Previously, many ultrafast experiments on conjugated polymers have been carried out<sup>9-11</sup>; in most cases the decay lifetimes of the singlet states were not consistent with those found in low excitation density experiments such as time resolved fluorescence<sup>11, 12</sup>. In many cases, very high excitation densities with photon fluences two orders of magnitude higher than in this study have been used. Almost universally, strong excitation quenching and generation of other excited states, in particular charges, has been observed. The lack of low excitation density data has led to many conclusions about the generation of charges in conjugated polymers to be

drawn. Some reports have said that charge generation is an intrinsic process in the solid state, some suggest exciton annihilation and some prefer a theory of sequential excitation of the singlet by the pump laser to a state above the singlet dissociation energy<sup>13-17</sup>. In many cases, intensity dependant phenomena dominate the decay even at the very lowest excitation densities available. In this chapter the processes surrounding charge generation and exciton annihilation in a prototypical polymer, PF2/6, have been studied. By using our high repetition rate, low pulse energy, pump-probe system, the excellent signal to noise ratio has made it possible to study the crossover region between the high excitation density phenomena and the intrinsic processes thus clarifying the mechanism of charge generation in polyfluorene.

## 5.2 Annihilation Reactions in Molecular Systems

The annihilation reactions mentioned above and in the introduction can represent a major loss of efficiency in conjugated polymers<sup>18, 19</sup>. For the case of singlet-singlet annihilation (SSA), excitation energy is transferred from one excited singlet state to another, in this way the singlet becomes excited to a higher excited state<sup>20, 21</sup>. Following this, the highly excited singlet state relaxes rapidly back to the  $S_1$  level<sup>22</sup>, thus the annihilation of two singlet states, results in the formation of one singlet in the  $S_1$  excited state and a singlet ground state ( $S_0$ ). This is a loss of half of the original singlets. Alternatively, as the highly excited singlet created by the annihilation reaction has sufficient energy to overcome the  $\sim 0.4\text{eV}$  exciton binding energy, there is the potential for exciton dissociation, thus generating a pair of charges<sup>21, 23</sup>. The scheme is generally expressed as follows.



where  $S_0$  is the singlet ground state,  $S_1$  is the excited singlet state,  $S_n$  are higher excited singlet states which rapidly thermalize to the  $S_1$  with the release of heat ( $Q$ ),  $p^+$  and  $p^-$  are a pair of charges which are generated with a proportion  $\eta$ .

Annihilation reactions are not a phenomenon unique to conjugated polymers; they have been studied previously in many molecular crystal systems. Fluorescence spectroscopy has been used to show a reduction in the PLQY of crystals of anthracene and tetracene at high excitation density<sup>21</sup>. The reduction of the PLQY showed a quadratic dependence on the excitation density, which is consistent with a bimolecular quenching process such as SSA. In addition, as this is simply an energy transfer reaction, the Förster radius for such an interaction can be calculated by Förster's equation (equation 2.11). When calculating the overlap of the donor fluorescence and the acceptor absorption in Förster's equation one must remember that the acceptor is the excited singlet state, thus it is the excited state absorption that is used rather than the ground state absorption. This can be measured by pump-probe, or flash photolysis spectroscopy. In a system with low excited state mobility the Förster radius can be well correlated with the distance over which the interaction occurs. This is usually calculated from the progression of the quenching rate with excitation density, the correlation is good in many molecular crystal systems and origin of the fluorescence quenching at high excitation density is confirmed as SSA by Förster transfer.

In similar systems of molecular crystals the interaction of singlet states with triplet states has been observed<sup>21</sup>. Singlet-triplet annihilation (STA) has generally been studied in the same way as SSA. However, the low intersystem crossing rate in simple aromatic systems means that the triplet population is lower, thus higher excitation densities are required for the process to become a significant contributor to the decay of the singlets. At low temperatures, the long lifetime of the triplet states can be exploited, allowing a large triplet population to build up during continuous excitation, which can then be used to test the theories of STA.

In conjugated polymers SSA has been studied as a quenching mechanism for the singlets, the main conclusion being that at the high excitation density that the experiments were carried out SSA is a significant quencher for the singlet states and it may contribute to the production of charges<sup>9, 23</sup>. In addition, in more complicated conjugated polymer based systems such as highly ordered stacks of oligo-phenylenevynalenes the singlet annihilation is more efficient due to the ease of energy transfer between the oligomers<sup>19</sup>.

Singlet-Triplet annihilation in conjugated polymers has only been studied in very few papers<sup>24, 25</sup>. These have generally dealt with the annihilation between singlets and triplets of different polymers in a blended system or in polymers with a high triplet yield; the general conclusion is that STA only occurs at very high excitation density due to the very small Forster radius of the energy transfer process from the singlet to the excited triplet.

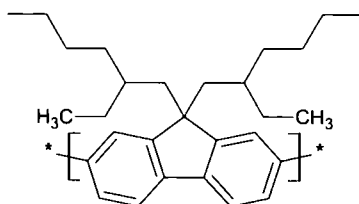


**Figure 5-1** The structure of PF2/6

This chapter aims to quantify the significance of the SSA and STA process as a quenching mechanism for singlet and triplet states and to provide clarification of the processes which lead to charge generation in thin films of the conjugated polymer poly-9,9-diethylhexylfluorene (PF2/6). The structure of the polymer is given above. The polymer is investigated with excitation density dependant measurements to investigate the intrinsic properties of the polymer and those at high excitation density. The majority of the work has been done using ultrafast pump-probe spectroscopy, which has been described in the experimental chapter. In addition, for the STA measurements a background level of triplets was generated by a 50mW 3.06eV diode laser, focussed to a 0.5cm<sup>2</sup> spot. At low temperature, the long lifetime of triplets in comparison to singlets allows a high background triplet population to be built up during continuous excitation by the diode laser. Because of the fact that the singlets are comparatively mobile with respect to the triplet population, the triplets should appear as static quenching sites for the singlets, the exact triplet population has been dealt with further on in this chapter. Ultrafast pump probe decays were then measured with the background triplet population to understand its effect on the singlet decay.



## 5.3 Singlet – Singlet Annihilation and Charge Generation in PF2/6

### 5.3.1 Results

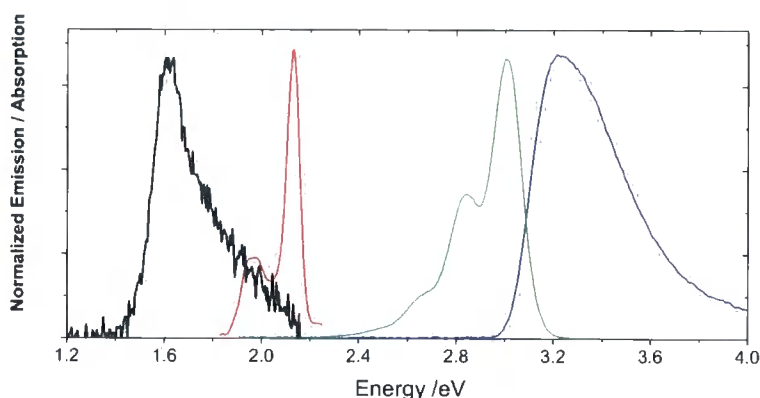


**Figure 5-2 (from right), Absorption, fluorescence, phosphorescence and transient triplet absorption for the polymer Pf2/6.**

Figure 5.2 shows a compendium of spectra for the polymer PF2/6, including absorption, fluorescence, transient triplet absorption and phosphorescence, the spectra are in accordance with what is expected from the features of similar polyfluorenes. The room temperature pump-probe spectra at different excitation density are shown in figure 5.3. The spectra were acquired with the two different detection systems, the diode array spectrometer was used for the high excitation density set, which has  $dT/T$  peaking at  $\sim 0.03$  whereas at lower excitation density, where  $dT/T \sim 0.0002$ , the lockin detection system is used. It should be noted however, that the same spectral shapes are observed with the two different detection systems, it is the only the level of noise that is affected. There is an immediate difference between the trends at the two different excitation densities; figure 5.3a shows similar features to other published high spectra for conjugated polymers, including polyfluorenes<sup>9, 26</sup>. Within the energy range of my experiment, three features are observed, the sharp absorption at around 1.6eV labelled PA1, the broad absorption which grows in at 2.4eV (PA2) and a small amount of stimulated emission in the region of the PF2/6 fluorescence at high energy. At low

excitation density in figure 5.3b, the spectrum only shows one strong feature, the PA1 absorption at  $\sim 1.6\text{eV}$ .

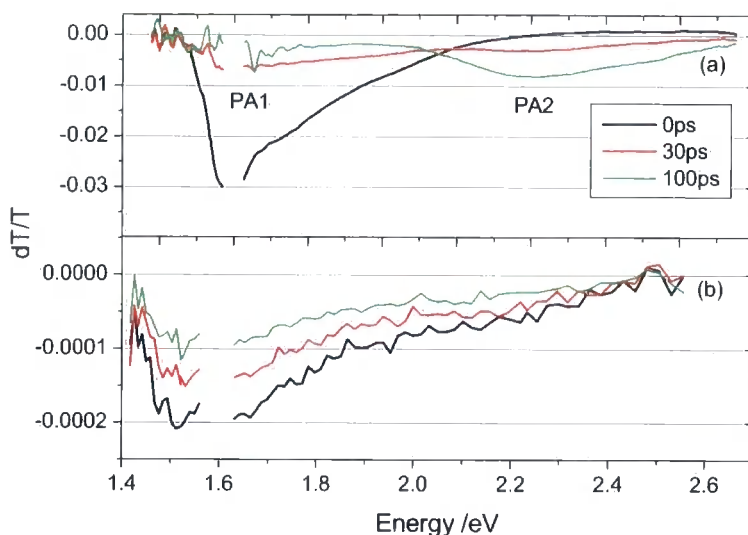


**Figure 5-3** Room temperature excited state absorption spectra of PF2/6 films at high excitation density ( $25\mu\text{Jcm}^{-2}$ ) (a) and low excitation density ( $0.35\mu\text{Jcm}^{-2}$ ) (b) for different times after excitation.

Many previous studies of conjugated polymers have characterised the features in the transient absorption spectrum, assigning the PA1 peak unambiguously to the singlet exciton  $S_1-S_n$  transition, this has usually been done by favourably comparing its behaviour with the stimulated emission<sup>11, 26, 27</sup>. The high energy PA2 peak in polyfluorene has been investigated previously by field assisted pump-probe spectroscopy; these experiments allow the feature to be assigned to a polyfluorene charged state<sup>14</sup>. In the field assisted pump probe experiment, free carriers are generated by an electric field and which is accompanied by a concomitant increase in the PA2 peak. Also, pulse radiolysis experiments and doping induced absorption provide strong evidence that this peak is the absorption of the polyfluorene radical cation<sup>28</sup>. In the high excitation dose spectra, figure 5.3a, there is a clear isobestic point at 2.15eV between the build up of the charges and the decay of the singlets. This is strong evidence that the charges form as a direct result of decay of the singlet states; they are therefore the product of the quenching of the singlet excitons. The lack of absorption in the region of PA2 immediately after photo-excitation is a direct proof

that for pristine films of PF2/6 charges do not form directly by optical absorption as the PA2 absorption only appear after the laser pulse. In the low excitation dose spectra of figure 5.3b, there is no rapid quenching of the singlets and no formation of charges; this conformation that formation of charges in polyfluorene is not an intrinsic process, but one that is only prevalent at high excitation doses.

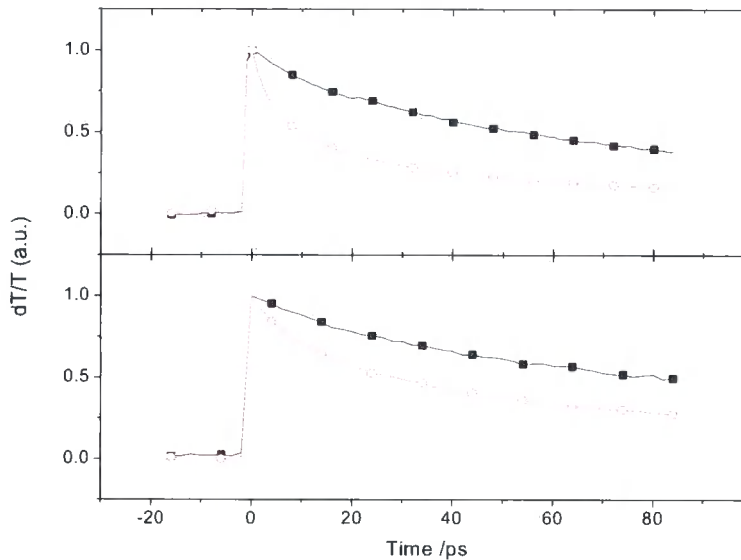


**Figure 5-4 Decay of PA1, the singlet excited state absorption for high excitation dose (○) ( $7\mu\text{Jcm}^{-2}$ ) and low excitation dose (■) ( $0.35\mu\text{Jcm}^{-2}$ ) at 300K (top) and 10K (lower)**

The decay of the singlet exciton's excited state absorption (PA1) is shown in figure 5.4, at high excitation ( $7\mu\text{Jcm}^{-2}$ ) and low ( $0.35\mu\text{Jcm}^{-2}$ ) excitation dose for 300K and 10K. At low excitation dose the unquenched decay is similar to the  $\sim 200\text{ps}$  fluorescence lifetime measured by time correlated single photon counting, the lifetime being slightly longer at low temperature. At high excitation density, an additional fast component begins to dominate the decay at both temperatures; this is the effect of the high excitation density quenching the singlet states. It is possible to quantify the change of decay rate with excitation density by comparing the intensity of the PA1 peak at 100ps to the initial intensity of the absorption, this is shown in figure 5.5, along with the change in intensity of the signal in the region of PA2 (2.4eV) after 100ps. It is immediately clear that the initial intensity of PA1 varies linearly with the excitation density, this is important as it is proof that the results were performed at excitation densities a long way from saturation of the ground state absorption;

something which has been a problem in previous studies of this nature. At low excitation density ( $<1\mu\text{Jcm}^{-2}$ ), the intensity of the singlet state induced absorption, and hence the population of the singlet states after 100ps is linear and parallel to the initial intensity. This is confirmation that at low excitation density, the excitation density dependant decay does not compete with the natural lifetime of the exciton during the first 100ps of the decay. Above  $\sim 1\mu\text{Jcm}^{-2}$  (which corresponds to an excitation density of  $1.5 \times 10^{17} \text{ cm}^{-3}$ ), a deviation from the linear relationship is observed; in a double logarithmic presentation the relationship turns over to a slope of  $\sim 0.5$ . At a similar threshold, the intensity of the PA signal at PA2, which is the charge absorption (and a small part of the tail of the underlying singlet signal), develops additional increase in intensity.

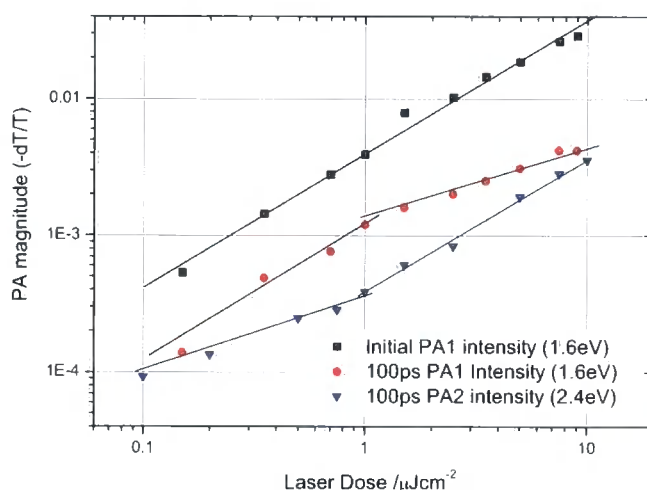


**Figure 5-5 Laser dose dependence of the intensity PA1 and PA2 excited state absorptions for Pf2/6 films at room temperature. The intensity initially and after 100ps are shown. Straight lines of gradient 0.5 and 1 are drawn as a guide to the eye.**

The turn over of the singlet excitation density dependence after 100ps to a slope of  $\sim 0.5$  at high excitation densities is a clear indicator of a bimolecular quenching process beginning to dominate the decay of the singlets at high excitation densities. It is possible to rule out all multiphoton processes such as two photon absorption or sequential absorption of pump photons, as increasing the intensity of PA2, because the spectra in figure 5.3 show that the rise of PA2 is a consequence of the decay of the singlet. In addition, the sub linear dependence of the decay of the singlet clearly does not occur within the pump pulse, as the initial intensity of the PA1

signal is linear with excitation density. The only feasible scenario for a bimolecular quenching process in a pristine film of a conjugated polymer is singlet-singlet annihilation (SSA). The charges that are formed by the annihilation reaction (equation 5.1) are the origin of the characteristic charge absorption (PA2) in the photoinduced absorption spectra at excitation densities above  $\sim 1 \mu\text{Jcm}^{-2}$  ( $2 \times 10^{12}$  photons  $\text{cm}^{-2}$ ). The threshold fluence for SSA dominating the decay of the singlet, which is lower than some previously reported values for conjugated polymers is measured directly without the need to fit data to complex models of exciton dynamics which are often necessary when data is only available at higher excitation densities<sup>11, 23, 29, 30</sup>. This could in part explain the apparent confusion over the mechanism of charge generation in ultrafast experiments on conjugated polymers. The bimolecular annihilation reaction leads to the generalised rate equation for the singlets ( $N_s$ ) and the charges ( $N_{\pm}$ ):

$$\frac{dN_s}{dt} = G(t) - \frac{N_s}{\tau} - \gamma(t)N_s^2 \quad \text{Equation 5-2}$$

$$\frac{dN_{\pm}}{dt} = -\frac{N_{\pm}}{\tau_{\pm}} + \gamma(t)N_s^2 \quad \text{Equation 5-3}$$

where,  $G(t)$  represents the exciton generation function,  $N$ , the exciton/charge population,  $\tau$  the exciton/charge lifetime and  $\gamma(t)$  annihilation parameter which can in some cases have a time dependence.

The bimolecular annihilation reaction is simply an energy transfer from one excited singlet to another; it can therefore proceed by two mechanisms, the long range Förster process of resonant energy transfer or the shorter range Dexter process. The rate limiting step also has two possibilities, either the energy transfer itself, or the diffusion of two excitons to within the active range of the energy transfer process. If the energy transfer processes were very efficient then one would expect the former to be the most likely mechanism. However, for inefficient Förster energy transfer or the short range Dexter process, the excitation must diffuse to within the sphere of interaction of the accepting singlet, the size of which is determined by the Förster radius for Förster transfer or the spatial extent of the excited states for Dexter transfer.

The condition for energy transfer by the long-range Förster interaction is that there must be overlap of the fluorescence of the donor and the absorption of the acceptor, which is the excited singlet state. By Förster's equation (equation 2.7) it is possible to calculate the range of the interaction, the Förster radius, which characterises the distance at which the energy transfer competes equally with the radiative decay of the state. The efficiency of the energy transfer is inversely proportional to the distance between the donor and acceptor to the sixth power. Thus if the distance between the species is greater than the Förster distance by any significant amount then the energy transfer is very inefficient. For PF2/6 there is only a small overlap between the fluorescence and the excited state absorption of the singlet, the calculation of the Förster radius for SSA gives  $R_{SSA}=11\pm 5\text{Å}$ , which is of similar magnitude to the separation of chains in the film<sup>31</sup>. This is significantly smaller than the calculated excited state separation of  $\sim 214\text{Å}$  at the threshold for SSA to begin to dominate the decay. Therefore SSA cannot be driven purely by static quenching by the long range Förster process. Returning once again to figure 5.4, the difference between the efficiency of the quenching due to SSA is considerably less at low temperature. The difference between the effect of SSA at room and low temperatures provides the clue to the higher than expected rate of singlet annihilation: exciton diffusion. The excitons are able to move around the film, therefore when an exciton approaches another close enough, the annihilation reaction can take place. Previous studies of the effect of temperature on the rate of exciton diffusion to dye molecules have shown that as the temperature is reduced, then so does the rate of exciton diffusion<sup>32</sup>, data for polyfluorene shows a reduction in the diffusion constant from  $1.44\text{nm}^2\text{ps}^{-1}$  at 300K to  $0.43\text{nm}^2\text{ps}^{-1}$  at 10K. When this is extended to SSA it is clear that as the excitons are able to move faster at room temperature so the effect of the bimolecular quenching is greater. The spatial extent of the exciton itself could also have an influence on the rate of SSA, some studies report that the exciton is highly delocalised over  $\sim 5\text{nm}$ . Thus limiting the usefulness of the point dipole approximation in calculating the rate of energy transfer and could potentially increase the distance over which resonant energy transfer can operate; this would not however show the observed temperature dependence<sup>33</sup>.

The very short Förster radius calculated from the spectral overlap factors, suggest that for Förster transfer to take place the excitons would have to be either on

the same chain or most likely on neighbouring chains. Energy transfer at length scales comparable to the spatial extent of the excited state would normally be expected to proceed by Dexter type exchange energy transfer as there will be significant orbital overlap between the donor and accepting state allowing efficient tunnelling of electrons between the states<sup>34</sup>.

The possibility of a time dependant annihilation rate mentioned above originates from the measurements made on molecular crystals<sup>21</sup>. In some systems when the rate of diffusion is low compared to the spatial distribution of the states a time dependence appears in the energy transfer rate. This originates from the localised depletion of the excited states causing the rate of energy transfer to slow. To fully understand this and to calculate the annihilation parameter  $\gamma(t)$  the decay of the singlet states must be fitted to the integrated form of the rate equation (equation 5.2), this is made difficult by the time dependant nature of the annihilation parameter. One approach to finding this time dependence relies on replotting the data with a new variable  $y(t)$ <sup>10</sup>:

$$y(t) = e^{-t/\tau} / N(t) \quad \text{Equation 5-4}$$

where  $N(t)$  is the singlet population when SSA is active and  $\tau$  is the lifetime of the singlet when there is no annihilation. It then follows that the rate equation becomes,

$$\frac{dy}{dt} = \gamma(t)e^{-t/\tau} \quad \text{Equation 5-5}$$

It is therefore easy to retrieve the annihilation parameter with full time dependence from the derivative of the function  $y(t)$ . Previously, this method has been used by Dogariu at al. to derive the time dependence of the annihilation rate. Due to the noise on their data it was necessary to derive an integral form of  $\gamma(t)$ . However, in our case the data is fitted with a multiexponential function to accurately describe the data, from this a smooth derivative can be calculated and  $\gamma(t)$  directly plotted for the data at 10K (figure 5.6). The initial annihilation parameter is  $\gamma(0)=2.5*10^{-8}\text{cm}^3\text{s}^{-1}$  at 10K and

$\gamma(0)=9.5 \cdot 10^{-8} \text{ cm}^3 \text{ s}^{-1}$  at 300K. The ratio of these initial annihilation parameters is  $\sim 3.8x$  which is similar to the  $\sim 3.3x$  change reported in the diffusion constant going from 10K to 300K.

The theoretical understanding of the localised depletion of the states which leads to the time dependence of the annihilation parameter in molecular glasses leads to the parameter having the form<sup>10,35</sup>:

$$\gamma(t) = 4\pi DR \left( 1 + \frac{R}{\sqrt{\pi Dt}} \right) \quad \text{Equation 5-6}$$

where D is the diffusion constant and R the Förster radius of the energy transfer reaction. Figure 5.6 shows that there is an appreciable time dependence to  $\gamma(t)$  however, after the first few picoseconds the system is in the high diffusion regime, i.e.  $D > R^2/\pi t$  so the equation can be simplified, giving  $\gamma=4\pi DR$ , which no longer contains any intrinsic time dependence. In simple terms, this means that because the diffusion constant is high compared to the separation of the states, the excitons are always able to rearrange themselves so that the exciton density is homogenous and there is no localised depletion of the states. Also in figure 5.6 is the calculated annihilation parameter from equation 5.6 including the diffusion constant and Förster radius for the interaction from above. It is clear that for the theoretical curve, as predicted, the time dependence is quickly lost after a few ps and the annihilation parameter becomes constant. For the experimental curve, the annihilation parameter is higher for longer than is expected by the model, then after about 25ps, the annihilation parameter has decayed to the correct constant value given by the theoretical prediction of equation 5.6 in the long time limit.



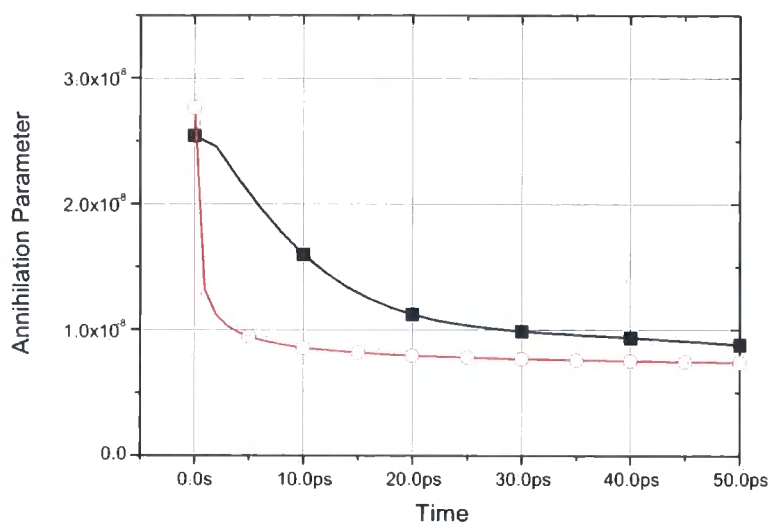


**Figure 5-6** Time dependence of the singlet-singlet annihilation parameter,  $\gamma$ , at 10k. The curves are calculated from the transient absorption data ( $\blacksquare$ ) and a theoretical plot of the expected annihilation parameter from equation 5.6, using the values of R and D given in the text ( $\circ$ ).

One possibility for the origin of the higher annihilation rate in the intermediate time is due to the nature of the diffusion in conjugated polymers. The large inhomogeneous broadening of the states leads to a time dependence of the diffusion constant. In the early time there are excitons high up in the distribution of states which can rapidly migrate downhill to the lower tail states. Once the excitons are thermalized, slower diffusion takes over and the excitons are only able to move amongst the lower states<sup>36-38</sup>. This process is known as dispersive exciton migration<sup>39, 40</sup>. At long times when the dispersive migration is over, the annihilation rate tends to the theoretical value. At low temperature, after the dispersive process is over the number of states that are accessible for diffusion is very low because the energy transfer amongst the states can only overcome an energy barrier of  $\sim 1\text{meV}$  at 10K compared to 26meV at 300K, hence the reduction in the diffusion constant, and consequently the annihilation parameter, at low temperature.

To consider the singlet-singlet annihilation as a phenomenon that switches on and off at a certain excitation density threshold is to over simplify the issue. At low excitation densities there will still be some singlet annihilation, but the probability is so low that it does not dominate the decay. The switch between the two regimes of

the decay being dominated by SSA rather than the natural lifetime of the state is surprisingly sudden; this is demonstrated by the sharpness of the switch of the gradient from 1 to 0.5 of the data in figure 5.4. In order to understand this phenomenon one can consider the rate of the quenching of the singlets due to annihilation for decays of all intensity. It is not so trivial to calculate the rate of quenching of the singlets by other singlets, because the annihilation reaction is bimolecular and the rate of annihilation is time dependant. A simplified way of quantifying the singlet decays is to extract from the data the time for the PA1 signal to decay to  $1/e$  of the initial intensity for the decays at each excitation density. From each of these times an idealised decay rate can be calculated. If one assumes the simple case that at the lowest excitation dose used there is no interaction between the excitons at all, then the difference between the idealised decay rate at the different powers ( $k_n$ ) and the decay rate at the lowest powers ( $k_0$ ) can be calculated. From the excitation dose, if one assumes homogenous excitation it is a simple step to calculate the mean distance between excitons ( $r$ ), thus a plot of  $(k_n - k_0)$  vs  $r$  can be constructed to give an idea of the variation of the quenching rate due to singlet-singlet annihilation with the separation of the excitons (figure 5.7).

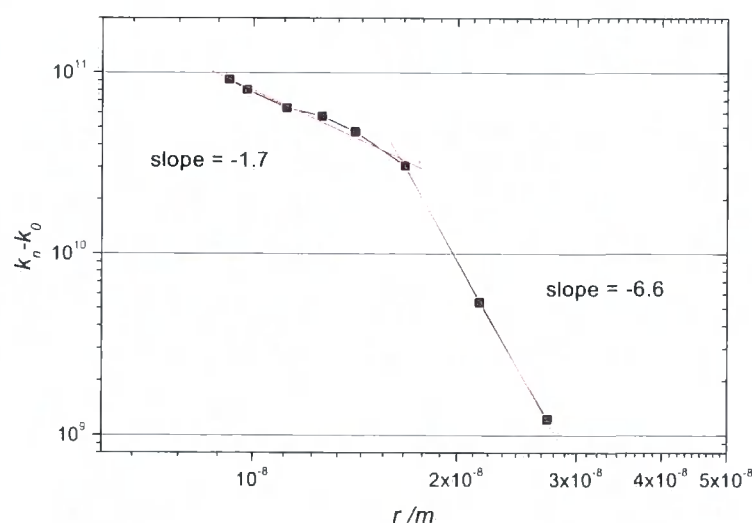


**Figure 5-7 Double logarithmic plot of the variation of the quenching rate due to SSA with the separation of the excitons.**

In figure 5.7, there are clearly two regimes for the variation of the quenching rate. At low excitation density ( $r > 16\text{nm}$ ) where the decay of the states is not dominated by SSA there is still some quenching due to SSA, but the rate is low and the variation in the rate is steeply rising towards the regime where the decay is dominated by SSA. The slope of the steep part of the curve is -6.6. For purely Förster energy transfer between static excited states, the rate of energy transfer is proportional to  $1/r^6$ , which in a double logarithmic presentation would lead to a slope of -6. The observed slope of -6.6 is close to this theoretical value. Therefore, it is most likely that at low concentration the exciton mobility is not sufficient to allow the excitons to interact by a collisional mechanism so the only interaction between the singlet states is by long range Förster transfer which is very weak due to the short Förster radius of the interaction. To understand the theoretical slope of the graph at high excitation density, where the separation of the states is less than 16nm, one must consider the theories of diffusion.

In a random walk, the simplest theories predict that the mean square of the distance travelled from the start point will be proportional to the time taken, this is known as the diffusion displacement and is the formal definition of the diffusion constant (D):

$$\langle r^2 \rangle = Dt \quad \text{Equation 5-7}$$

Form this equation one can simply rearrange to form an equation for the rate of approach of a particle to a particular point:

$$k = \frac{1}{t} = \frac{D}{\langle r^2 \rangle} \quad \text{Equation 5-8}$$

Thus for a diffusion controlled process the rate should be proportional to  $1/r^2$  and therefore show a slope of -2 in a double logarithmic graph, which is similar to the observed slope of -1.7 in figure 5.7. This is confirmation that at high excitation density exciton diffusion controls the singlet-singlet annihilation.

In summary the main conclusion of the data are threefold, firstly that there is no intrinsic optical generation of charges in polyfluorene; singlet-singlet annihilation is the principal source of charge generation at moderate excitation density and finally that SSA is made very efficient due to the high mobility of the excitons.

#### 5.4 Singlet-Triplet Annihilation in PF2/6

Similar to the bimolecular annihilation of singlets, singlets can interact with triplets, in this case two different species are interacting, and the process is as follows:



This process does not result in a highly excited singlet and therefore there is no possibility for the generation of charges. It is possible that the highly excited triplet can dissociate into free carriers but there is little evidence for this. The reaction would proceed with the following rate equations:

$$\begin{aligned} \frac{dN_s}{dt} &= G(t) - \frac{N_s}{\tau_s} - k_{isc} N_s - \gamma_{ST} N_s N_T \\ \frac{dN_T}{dt} &= k_{isc} N_s - \frac{N_T}{\tau_T} + \gamma_{ST} N_s N_T \end{aligned} \quad \text{Equation 5-10}$$

Measuring the STA in the same way as for SSA is not possible, the intersystem crossing yield is low, therefore the number of triplets created under pulsed excitation is very low compared to the number of singlets and any attempted measurements of the STA rate would be swamped by the highly efficient SSA. Instead it is necessary to measure the effect of quenching of the singlets with a high background of triplets present. This can be done by exploiting the long lifetime of the triplets at low temperature, as the decay of triplets is generally dominated by the diffusion controlled bimolecular annihilation of triplets, at low temperature the

lifetime of the triplets can be increased by many orders of magnitude into the millisecond time scale. Because of this, at low temperatures it is possible to build up a large background of triplet states which are able to interact with the singlets. This is done in this thesis by using a 3.06eV cw diode laser (excitation density 100mW cm<sup>-2</sup>) to excite the same area of the film simultaneously to the pump-probe experiment that will measure the lifetime of the singlet states.

In order to evaluate the effect of the background triplet population on the singlet decay it is necessary to have knowledge of the triplet population in the film, this is not trivial because even at low temperatures there is bimolecular annihilation of the triplets<sup>41, 42</sup>. In addition there is debate over the number of triplets generated by intersystem crossing and the rate of annihilation of the triplets. The rate equation for the triplet population gives:

$$\frac{dN_T}{dt} = A - \gamma_{TT} N_T^2 - k_i N_T \quad \text{Equation 5-11}$$

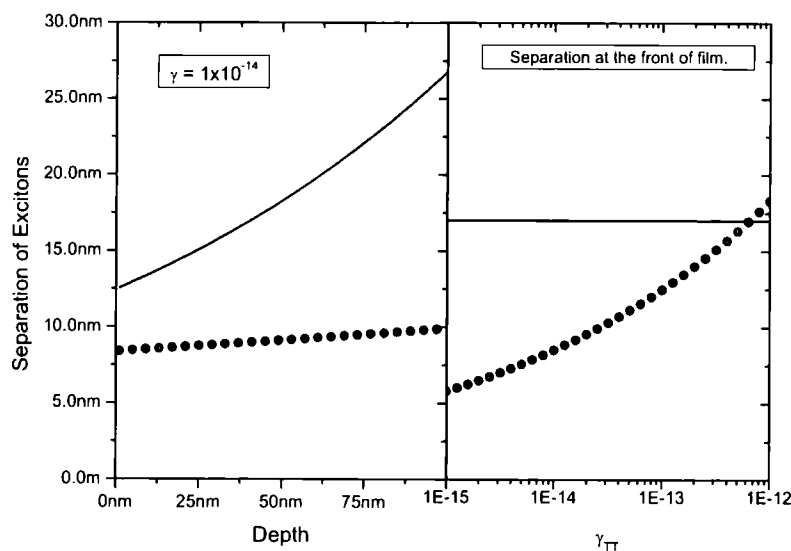


**Figure 5-8** variation of the separation of singlet excitons at the point where SSA dominates the decay of the singlet excitons (solid), Singlet – Triplet separation when a background of triplets are created with cw excitation (dots). Variation with depth into the sample (left) and triplet-triplet annihilation rate (right).

The solution of this equation is complex and has been dealt with in the work of Rothe et al<sup>41</sup>. However, once the phosphorescence term is removed, which is possible because the radiative decay of the triplets is insignificant compared to the triplet annihilation term, the overall effect is that the triplet population is proportional to  $\sqrt{A/\gamma_{TT}}$  (where A is the rate of triplet formation and  $\gamma_{TT}$  is the TTA parameter)<sup>41</sup>. A number of groups including ourselves have measured  $\gamma_{TT}$  for a number of polyfluorenes and polyfluorene derivatives. A large spread of values has been reported for conjugated polymers at low temperatures, with values of the triplet-triplet annihilation parameter between  $10^{-15} \text{ s}^{-1}$  and  $10^{-13} \text{ s}^{-1}$  reported<sup>38, 41</sup>. From the calculation of the cw triplet excitation density and the singlet population created by the pump pulse it is possible to work back to the separation of singlets and triplets in the film. This calculation is complicated by the fact that there are more excited states created at the front of the film. Based on the assumption that the maximum separation of singlets and triplets occurs when one singlet is exactly between two triplets, the variation of S - T separation with  $\gamma_{TT}$  is shown on the right hand panel of figure 5.8. Also shown for comparison is the mean separation of singlets at the threshold for SSA. For the triplet separation to become greater than the separation at the threshold for SSA, the TTA rate would have to be approximately 10 times the highest reported values. The left panel of figure 5.8 shows the variation of singlet separation and the variation of S-T separation with sample depth, calculated using the Beer-Lambert law for the singlet distribution and the Beer-Lambert law in combination with the above equation for the S-T distance. Both the calculations in figure 5.8 show that the S-T distance during cw photoexcitation is always less than the singlet separation required for SSA. The number of triplets created by the fs pump beam can be effectively ignored as the cw power of the fs beam during the experiments was less than  $1 \text{ mWcm}^{-2}$ , negligible compared to the cw excitation beam used to generate a background of triplets. In order to prevent the confusing effect of observing both SSA and STA, the fs excitation beam was kept below the threshold for SSA during the experiment.

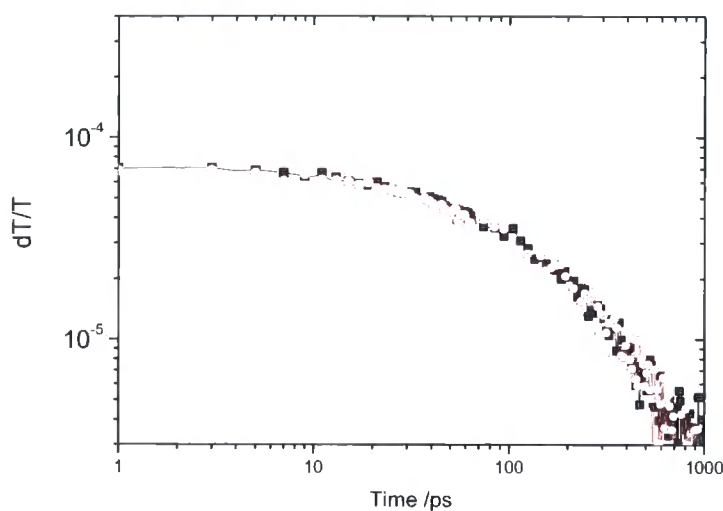


**Figure 5-9** Decay of the singlet exciton excited state absorption PA1 both with (○) and without (■) a background of triplet population, for cw excitation ( $100\text{mWcm}^{-2}$ ).

The measurement of the singlet lifetime with a background triplet population at low temperature has no noticeable effect on the singlet lifetime. Figure 5.9 shows the decay of the singlet states, measured by the decay of PA1, with and without a background of triplets present in the film. An easy comparison shows that the two decays are almost identical; the decay remains unchanged throughout the whole of the triplet population. Although this seems unexpected given the ease of singlet-singlet annihilation, our previous measurements on devices have shown that the emission observed under electrical and photoexcitation are additive. When a device is simultaneously excited electrically and optically, the emission intensity is the sum of the emission when the device is excited independently by light or electrical current<sup>43</sup>. In devices under electrical excitation there are a large number of triplets present, it would seem that here also the large number of triplets present does not affect the lifetime of the singlet. The implication of these findings is very promising for potential for the potential maximum efficiency of high brightness polymer OLEDs.

As with singlet-singlet annihilation by Förster transfer it is possible to calculate the Förster radius for the singlet triplet interaction can be calculated from the overlap of the singlet fluorescence and the widely reported triplet excited state absorption for polyfluorene<sup>44</sup> (figure 5.1). This is larger than that for the singlet-singlet interaction;  $R_{\text{STA}}=21\pm 5\text{Å}$ . For the simplest case of Forster transfer it should be

comparatively easier for the singlets to annihilate with triplets than with other singlets. However, this Förster radius is still smaller than the mean separation of the singlets and triplets, so for the simple case of annihilation by Förster transfer one would not expect STA at typical excitation densities used in the experiment. What is surprising though is that the SSA process is very efficient for similar separation of singlet states and similar Förster radius. This is due to the high mobility of the singlets, the STA process does not seem to be diffusion activated in the same way which is confusing considering that the mobility of the singlet states should be the same in both cases. To understand the process that causes this one must return to the earlier observation on the mechanism of the energy transfer that at the short distances that are involved in SSA, Dexter transfer dominates the annihilation process. Assuming that both the SSA and STA proceed via a Dexter, electron exchange mechanism, one of the requirements for Dexter transfer is the overlap of electronic orbitals of the donor and acceptor. Understanding fully such processes there are a number of observations one can make about the spatial nature of the singlet and triplet state.

#### **5.4.1 The Delocalisation of the Singlet and Triplet state**

Both the singlet and triplet state are localised on the main backbone of the polymer and as such they modify the electron density in part of the chain. Investigation of the spatial extent of the states has previously been carried out by investigating the photophysical properties of oligomeric analogues of conjugated polymers. The progression of the transition energies of absorption, fluorescence, phosphorescence and transient absorption with the length of the oligomers can be used to determine the spatial extent of the state, i.e. the length of the chain that is affected by the modification of the electron density. The oligomers length at which saturation of the state's excitation energy is found generally gives an idea of the maximum length of the state's delocalisation, up to saturation, the relationship is expected to be linear between the transition energy and the inverse of the oligomers length; as the state becomes less confined the transition energy drops. In most conjugated polymers it has been observed that the singlet states occupy a large part of the chain, there being a pretty much linear relationship between the absorption and



fluorescence transition energies and the inverse oligomers length<sup>45-47</sup>. In long chain polymers the transition energy does at some point saturate, however, this is not due to any intrinsic localisation of the singlet but due to the presence of defects on the polymer chain, which limit the effective conjugation length that the state occupies.

The triplet state, unlike the singlet shows saturation of the phosphorescence and transient triplet absorption, transition energies after a few repeat units of the polymer, from this it is concluded that the triplet only occupies as many as three repeat units of the polymer<sup>48-50</sup>; this could be due to two potential causes. Either the triplet is more sensitive to defects such as slight twists in the chain or conformational disorder than the singlets, so the triplet sees a shorter effective conjugation length. Or the triplet is only delocalised over a few phenyl rings, the former possibility is unlikely as the same progression of triplet energy with oligomers length is seen with many different polymers, some fully planar and some with a high degree of intra ring twisting. Therefore, it seems that the triplet is only delocalised over a few phenyl rings rather than the high degree of delocalization of the singlet. This conclusion has also been confirmed by quantum chemical calculations and investigations into the localisation of the triplet state in copolymers<sup>48, 51</sup>.

The fact that the triplet only occupies a short segment of the effective conjugation length becomes important for the Dexter transfer process. The Dexter process requires overlap of the electronic orbitals that the state occupies for the energy transfer to take place. If the triplet state only sits on a small part of the effective conjugation there could be a large buffer between itself and a state next to it on the same chain, this buffer region of the chain could be preventing the energy transfer from proceeding.

## 5.4.2 The Orientation of the Singlet and Triplet States

When considering the nature and delocalisation of the singlet and triplet states with regard to the possibilities for orbital overlap between the two, one must also consider their position and orientation relative to the polymer backbone. One way to investigate their orientation is to use polarised spectroscopy; the polarisation of the

light that a transition absorbs or emits is polarised along the axis of the transition dipole moment. This phenomenon can be exploited to understand many different processes, for example the ultrafast depolarisation of fluorescence or transient absorption can be used to follow the fast diffusion of excited states between randomly oriented chains in an amorphous film<sup>52-54</sup>. The use of films where the polymer chains are oriented in a macroscopic way can be used to create polymer OLEDs with polarised emission, they also facilitate the investigation of the transition dipole moments in conjugated polymers through bulk measurements rather than resorting to single molecule methods<sup>55</sup>. One method of creating macroscopic order in conjugated polymer films is to stretch films of conjugated polymers in an inert host; this method has been used to great effect to investigate the orientation of the transitions in a number of conjugated polymers, including the polyfluorene PF2/6<sup>55-59</sup>.

The orientation of absorption, fluorescence, transient absorption and phosphorescence transitions have been investigated by polarised spectroscopy. For the singlet transitions, absorption and fluorescence, the spectra measured parallel and perpendicular to the stretch direction are shown in figure 5.9. In both cases the polarisation of the emission / absorption parallel to the stretch direction is considerably greater than the perpendicular orientation, with a dichroic ratio of approximately 10 times for absorption and 20 times for the fluorescence. This high dichroic ratio shows not only that the transition is strongly polarised along the stretch direction, but the film is very well ordered with the chains predominantly along the stretch direction. This confirms that the absorption and fluorescence transition dipole moments are oriented along the polymer backbone which is what is generally observed in conjugated polymers.

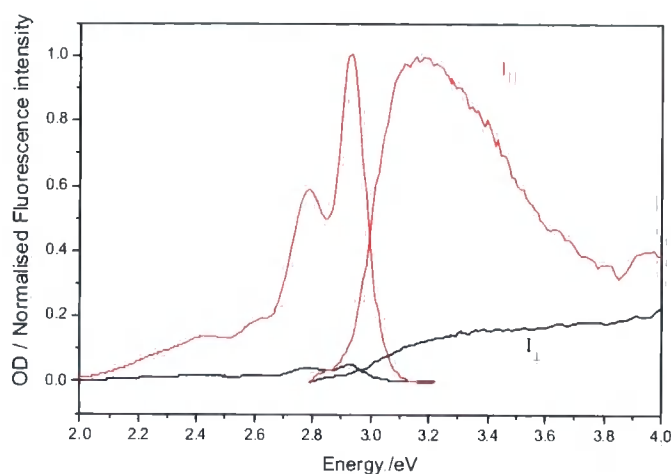


**Figure 5-10 Absorption and fluorescence of an aligned film of PF2/6. The absorption spectra are measured with the polarisation parallel (red) and perpendicular (black) to the film orientation. In the case of the fluorescence spectra, the excitation is made parallel to the film orientation and the analyser polarisor oriented parallel and perpendicular to the film orientation, as appropriate.**

Figure 5.10 shows the intensity of the phosphorescence measured with the analyser polariser parallel and perpendicular to the film orientation. The spectral shape is as expected, unchanged from the unpolarised phosphorescence spectra measured previously. The spectra were measured with the gated integrated CCD system described in chapter 3, with a gate time 40ms and integration time 90ms.

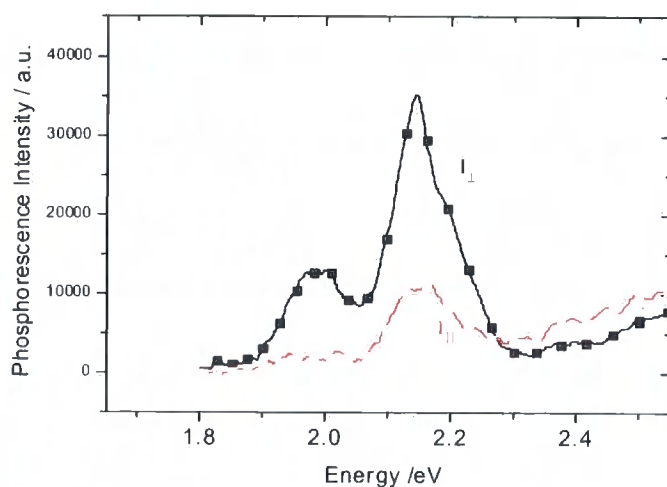


**Figure 5-11 Polarised phosphorescence spectra measured parallel (red - □) and perpendicular (black - ■) to the chain alignment.**

At variance to all the other transitions measured, the phosphorescence has a strong, dominant component perpendicular to the orientation of the polymer chains. Exciting the film perpendicular to the direction of alignment gives only a small amount of fluorescence and no phosphorescence emission, concomitant with the very low perpendicular absorption in figure 5.8 and the very low intersystem crossing rate in conjugated polymers resulting in few overall triplets<sup>60, 61</sup>. Similar observations have previously been made in platinum containing conjugated polymers where phosphorescence is the principal emission from the polymer<sup>62</sup> as well as in experiments on the fluorene monomer and other planar polyacenes<sup>55, 63-65</sup>.

From the dichroic ratio one can see that the transition dipole moment is clearly not strongly oriented along the polymer chain. Therefore, consideration must be made for the three dimensional nature of the molecule. There are two directions that are orthogonal to the polymer chain, the short axis of the molecule and the out of plane axis. As the chains are only aligned in one dimension and the polymer backbone can adopt a helical structure<sup>66</sup> it is not possible to differentiate between the two orientations orthogonal to the backbone. Thus while the phosphorescence transition dipole moment has a dominant component orthogonal to the chain backbone, without alignment of the polymer in two dimensions it is difficult to accurately predict the precise direction of the dipole moment.

In order to understand the significance of the transition dipole moment, one must make recourse to the formal definition of the transition dipole moment<sup>67</sup> '*...the integral taken over the product of the wavefunctions of the initial and final states of a spectral transition and the dipole moment operator of the electromagnetic radiation. Its direction in the molecular framework defines the direction of transition polarization.*' Thus the transition dipole moment gives the difference in the electron distribution between the ground state and the excited state, it is a measure of the rearrangement of the electrons in the molecule when it is excited or when the excitation decays. For the singlet state there is a wealth of theoretical information about the excited states, not only have there been numerous experimental investigations, but also many theoretical formulations and computational models have been developed relating to the extent of the singlet state and its transition dipole moment and oscillator strength<sup>68-70</sup>. All indications confirm that the singlet is highly

delocalised along the chain and in common with many conjugated molecules the state and its associated transition dipole moment is oriented along the long axis of the molecule.

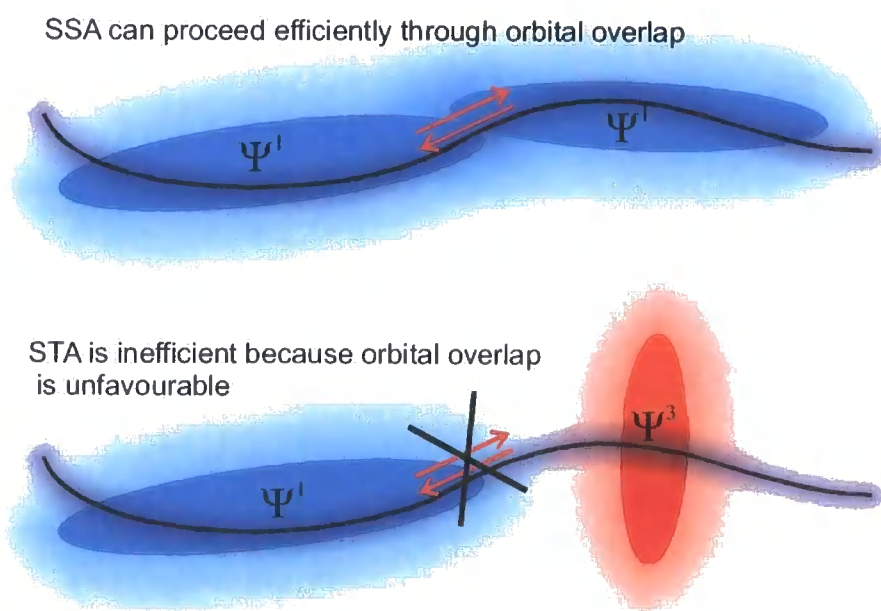
Triplet states in conjugated polymers have been mainly investigated experimentally, with only a few theoretical calculations made and as a result little information is available about the symmetry and electron distribution of the triplet excited state<sup>71</sup>. However, as discussed above a number of experiments have been made both on oligomeric systems and copolymers which show that the spatial extent of the triplet excited state is more localised than the singlet, being confined to as few as four phenyl rings<sup>48, 72, 73</sup>. The polarisation measurements presented here show that the transition dipole moment for the phosphorescence has a dominant component perpendicular to the chain. This suggests that the electron distribution of the triplet excited state is oriented orthogonal to the chain.

The orthogonal nature of the triplet exciton in conjugated molecules can take two forms; either the state can be oriented across the short axis of the molecule or through the plane of the molecule. In small aromatics these two can be differentiated between by calculating the 2-dimensional alignment of the molecule, this is not possible in polyfluorene as there is no way of controlling the torsional angles between the neighbouring units. However, all indications from the literature on small aromatics, including the fluorene monomer suggests that the phosphorescence is polarised out of the plane of the molecule<sup>63, 64</sup>, it is possible to carry this forward to the polymer and suggest that the triplet in polyfluorene is also oriented out of the plane of the molecule.

To understand the nature of the out of plane and in plane components of the phosphorescence one must briefly examine the quantum mechanical nature of the phosphorescence. Decay from a purely triplet excited state to a purely singlet ground state is spin forbidden. Thus, for phosphorescence emission to be observed from the triplet state there must be some admixture of the triplet state with some states of singlet character in order for the transition to become allowed. As discussed earlier, this mixing is caused by spin orbit coupling, rationalising the spin orbit effect with the polarisation of the transition is easy and has been performed previously for the planar

aromatics, including the fluorene monomer<sup>64, 65</sup>. The predominantly out of plane polarisation of the state is expected because direct spin-orbit coupling between (predominantly in plane)  $\pi$ -type levels is ineffective compared to  $\sigma\pi$ -mixing, thus the in-plane contribution is weak and for the predominantly out of plane spin orbit interaction dominates both the formation of the triplet through intersystem crossing and its phosphorescent decay<sup>64</sup>. The implications of this for intersystem crossing in planar and twisted molecules are discussed further on in this thesis.

The implications for Dexter transfer of the out of plane nature of the triplet and the in plane nature of the singlet are as follows. For an interaction such as Dexter transfer which require high levels of overlap between the states, this will be difficult because of the very different orientation of the states therefore the interaction between singlets and triplets will be less than the interaction of singlets with singlets. This is a possible reason for the lack of STA observed in the presence of highly efficient SSA. In addition the difficulty triplets may have, approaching the singlets due to the small localisation of the triplets within the chain segments may reduce the efficiency of STA further. Below is an illustration of the potential reasons outlined above why the STA is ineffective whereas SSA is highly efficient. This theory corresponds well with the lack of observation of STA in single molecule studies, suggesting that where STA has been observed in previous studies at high excitation density it is interchain in nature<sup>74</sup>.



## 5.5 Conclusions

Singlet-singlet annihilation has been observed to become the dominant decay mechanism for singlets even for a low pump threshold of  $\sim 1 \mu\text{Jcm}^{-2}$ , corresponding to an excitation density of  $1.5 \cdot 10^{17} \text{ cm}^{-3}$ . The process is diffusion controlled and as such, there exist two regimes, below the threshold for the SSA making a significant contribution to the decay of the singlet some SSA can proceed very inefficiently by long range Förster interaction. However, when the singlet separation is low enough that the states are able to diffuse sufficiently close within their lifetime to interact efficiently by Dexter transfer the SSA process becomes entirely diffusion controlled. The low pump fluence required for SSA highlights the importance of using low excitation densities in ultrafast studies of conjugated polymers and could be the cause of some of the confusion over the nature of charge generation by photoexcitation. It was that there is no intrinsic mechanism of charge generation by photoexcitation, the dominant mechanism of charge generation being SSA, which proceeds after photoexcitation.

Additionally there is no evidence of singlet–triplet annihilation when there is a background triplet density comparable to the singlet density required for SSA, this is attributed to the differing shape and spatial extent of the triplet states compared to the singlet hampering the energy transfer process.

## 5.6 References

- 1 S. A. Jenekhe and J. A. Osaheni, *Science* **265**, 765 (1994).
- 2 E. M. Conwell, *Synthetic Metals* **85**, 995 (1997).
- 3 M. Gaal, E. J. W. List, and U. Scherf, *Macromolecules* **36**, 4236 (2003).
- 4 M. Yan, L. J. Rothberg, F. Papadimitrakopoulos, et al., *Physical Review Letters* **73**, 744 (1994).
- 5 V. I. Arkhipov, E. V. Emelianova, and H. Bassler, *Physical Review B* **70**, 205205 (2004).
- 6 M. N. Shkunov, R. Osterbacka, A. Fujii, et al., *Applied Physics Letters* **74**, 1648 (1999).
- 7 N. Tessler, N. T. Harrison, and R. H. Friend, *Advanced Materials* **10**, 64 (1998).
- 8 N. Tessler, G. J. Denton, and R. H. Friend, *Nature* **382**, 695 (1996).
- 9 G. Lanzani, G. Cerullo, D. Polli, et al., *Physica Status Solidi a-Applied Research* **201**, 1116 (2004).
- 10 A. Dogariu, D. Vacar, and A. J. Heeger, *Physical Review B* **58**, 10218 (1998).
- 11 E. S. Maniloff, V. I. Klimov, and D. W. McBranch, *Physical Review B* **56**, 1876 (1997).
- 12 I. B. Martini, A. D. Smith, and B. J. Schwartz, *Physical Review B* **69**, 035204 (2004).
- 13 C. Silva, A. S. Dhoot, D. M. Russell, et al., *Physical Review B* **64**, 125211 (2001).
- 14 C. Gadermaier, G. Cerullo, G. Sansone, et al., *Physical Review Letters* **89**, 117402 (2002).
- 15 V. I. Arkhipov, E. V. Emelianova, and H. Bassler, *Chemical Physics Letters* **340**, 517 (2001).
- 16 R. Kersting, U. Lemmer, M. Deussen, et al., *Physical Review Letters* **73**, 1440 (1994).
- 17 E. Frankevich, H. Ishii, Y. Hamanaka, et al., *Physical Review B* **62**, 2505 (2000).
- 18 B. Kraabel and D. W. McBranch, *Chemical Physics Letters* **330**, 403 (2000).
- 19 C. Daniel, L. M. Herz, C. Silva, et al., *Physical Review B* **68**, 235212 (2003).



- 20 J. B. Birks, *Organic molecular photophysics* (J. Wiley, London, New York,,  
1973).
- 21 M. Pope and C. E. Swenberg, *Electronic Processes in Organic Crystals and  
Polymers* (Oxford University Press, Oxford, 1999).
- 22 T. Virgili, D. Marinotto, C. Manzoni, et al., *Physical Review Letters* **94**  
(2005).
- 23 Q. H. Xu, D. Moses, and A. J. Heeger, *Physical Review B* **68**, 174303 (2003).
- 24 E. J. W. List, U. Scherf, K. Mullen, et al., *Physical Review B* **66** (2002).
- 25 Y. Zaushitsyn, K. G. Jespersen, L. Valkunas, et al., *Physical Review B* **75**  
(2007).
- 26 B. Kraabel, V. I. Klimov, R. Kohlman, et al., *Physical Review B* **61**, 8501  
(2000).
- 27 D. W. McBranch, B. Kraabel, S. Xu, et al., *Synthetic Metals* **101**, 291 (1999).
- 28 H. D. Burrows, J. S. de Melo, M. Forster, et al., *Chemical Physics Letters* **385**,  
105 (2004).
- 29 C. Silva, M. A. Stevens, D. M. Russell, et al., *Synthetic Metals* **116**, 9 (2001).
- 30 C. Silva, D. M. Russell, M. A. Stevens, et al., *Chemical Physics Letters* **319**,  
494 (2000).
- 31 M. Knaapila, K. Kisko, B. P. Lyons, et al., *Journal of Physical Chemistry B*  
**108**, 10711 (2004).
- 32 B. P. Lyons and A. P. Monkman, *Physical Review B* **71**, 235201 (2005).
- 33 H. Wiesenhofer, D. Beljonne, G. D. Scholes, et al., *Advanced Functional  
Materials* **15**, 155 (2005).
- 34 J. R. Lakowicz, *Principals of Fluorescence Spectroscopy* (Kluwer Academic,  
New York, 1999).
- 35 R. C. Powell and Z. G. Soos, *Journal of Luminescence* **11**, 1 (1975).
- 36 S. C. J. Meskers, J. Hubner, M. Oestreich, et al., *Journal of Physical  
Chemistry B* **105**, 9139 (2001).
- 37 K. Brunner, J. van Haare, B. M. W. Langeveld-Voss, et al., *Journal of  
Physical Chemistry B* **106**, 6834 (2002).
- 38 M. Westerling, C. Vijila, R. Osterbacka, et al., *Physical Review B* **69** (2004).
- 39 B. Movaghar, B. Ries, and M. Grunewald, *Physical Review B* **34**, 5574  
(1986).
- 40 B. Ries, H. Bassler, M. Grunewald, et al., *Physical Review B* **37**, 5508 (1988).

- 41 C. Rothe, H. A. Al Attar, and A. P. Monkman, *Physical Review B* **72** (2005).
- 42 C. Rothe and A. P. Monkman, *Physical Review B* **68**, 075208 (2003).
- 43 C. Rothe, S. M. King, and A. P. Monkman, *Physical Review Letters* **97**  
(2006).
- 44 C. Rothe, S. M. King, F. Dias, et al., *Physical Review B* **70** (2004).
- 45 H. Meier, U. Stalmach, and H. Kolshorn, *Acta Polymerica* **48**, 379 (1997).
- 46 K. Mullen and G. Wegner, *Electronic Materials: The Oligomer Approach*  
(Wiley-VCH, Weinheim, 1998).
- 47 J. Rissler, *Chemical Physics Letters* **395**, 92 (2004).
- 48 A. van Dijken, J. Bastiaansen, N. M. M. Kiggen, et al., *Journal of the*  
*American Chemical Society* **126**, 7718 (2004).
- 49 L. S. Swansson, J. Shinar, and K. Yoshino, *Physical Review Letters* **65**, 781  
(1990).
- 50 E. J. W. List, J. Partee, J. Shinar, et al., *Physical Review B* **61**, 10807 (2000).
- 51 C. Rothe, K. Brunner, I. Bach, et al., *Journal of Chemical Physics* **122** (2005).
- 52 H. L. Vaughan, F. M. B. Dias, and A. P. Monkman, *Journal of Chemical*  
*Physics* **122**, 0141902 (2005).
- 53 A. Ruseckas, P. Wood, I. D. W. Samuel, et al., *Physical Review B* **72**, 115214  
(2005).
- 54 M. M. L. Grage, Y. Zaushitsyn, A. Yartsev, et al., *Physical Review B* **67**,  
205207 (2003).
- 55 J. Michl and E. W. Thulstrup, *Spectroscopy With Polarized Light* (VCH,  
1995).
- 56 W. Klopffer, *Introduction to Polymer Spectroscopy* (Springer-Verlag, Berlin,  
1984).
- 57 T. W. Hagler, K. Pakbaz, K. F. Voss, et al., *Physical Review B* **44**, 8652  
(1991).
- 58 L.-O. Pålsson, H. L. Vaughan, and A. P. Monkman, *J. Chem Phys* (awaiting  
publication).
- 59 S. M. King, H. L. Vaughan, and A. P. Monkman, *Chemical Physics Letters*  
**440**, 98 (2007).
- 60 H. D. Burrows, J. S. de Melo, C. Serpa, et al., *Journal of Chemical Physics*  
**115**, 9601 (2001).

- 61 S. M. King, C. Rothe, D. Dai, et al., *Journal of Chemical Physics* **124**, 234903  
(2006).
- 62 J. S. Wilson, R. J. Wilson, R. H. Friend, et al., *Physical Review B* **67**, 125206  
(2003).
- 63 J. J. Dekkers, G. P. Hoornweg, K. J. Terpstra, et al., *Chemical Physics* **34**, 253  
(1978).
- 64 S. P. McGlynn, T. Azumi, and M. Kinoshita, *Molecular Spectroscopy of The  
Triplet State* (Prentice Hall, Englewood Cliffs, New Jersey, 1969).
- 65 J. J. Dekkers, G. P. Hoornweg, W. P. Cofino, et al., *Chemical Physics Letters*  
**67**, 24 (1979).
- 66 M. Knaapila, R. Stepanyan, B. P. Lyons, et al., *Advanced Functional Materials*  
**16**, 599 (2006).
- 67 *IUPAC Compendium of Chemical Terminology*, (1997).
- 68 J. Cornil, I. Gueli, A. Dkhissi, et al., *Journal of Chemical Physics* **118**, 6615  
(2003).
- 69 J. Cornil, D. Beljonne, R. H. Friend, et al., *Chemical Physics Letters* **223**, 82  
(1994).
- 70 J. L. Bredas, *Advanced Materials* **7**, 263 (1995).
- 71 D. Beljonne, J. Cornil, R. H. Friend, et al., *Journal of the American Chemical  
Society* **118**, 6453 (1996).
- 72 D. Wasserberg, S. P. Dudek, S. C. J. Meskers, et al., *Chemical Physics Letters*  
**411**, 273 (2005).
- 73 C. Y. Chi, C. Im, and G. Wegner, *Journal of Chemical Physics* **124**, 024907  
(2006).
- 74 J. M. Lupton, 2005).

## **5.7 Publications Arising From This Chapter**

S.M. King, D. Dai, C. Rothe, and A.P. Monkman, *Exciton annihilation in a polyfluorene: Low threshold for singlet-singlet annihilation and the absence of singlet-triplet annihilation*. Physical Review B, 2007. **76**(8).

S.M. King, H.L. Vaughan, and A.P. Monkman, *Orientation of triplet and singlet transition dipole moments in polyfluorene, studied by polarised spectroscopies*. Chemical Physics Letters, 2007. **440**(4-6): p. 98-102.

## 6 Spiroconjugation Enhanced Intramolecular Charge-Transfer state Formation in a Conjugated Polymer

One of the materials with the most promise for efficient blue emitting devices is the conjugated polymer polyspirobifluorene (PSBF). The polymer, developed by Covion Organic Semiconductor GmbH (Merck OLED) has proven successful for the production of efficient, stable blue PLEDs. Based on the prototypical polyfluorene backbone the polymer has been functionalised by the addition of an additional fluorene unit as the side group, the two fluorene units bonded in a spiro configuration at their 9 positions. The structure of the polymer and the prototypical poly-9,9-diethylhexylfluorene (PF2/6) are shown in figure 6.1.

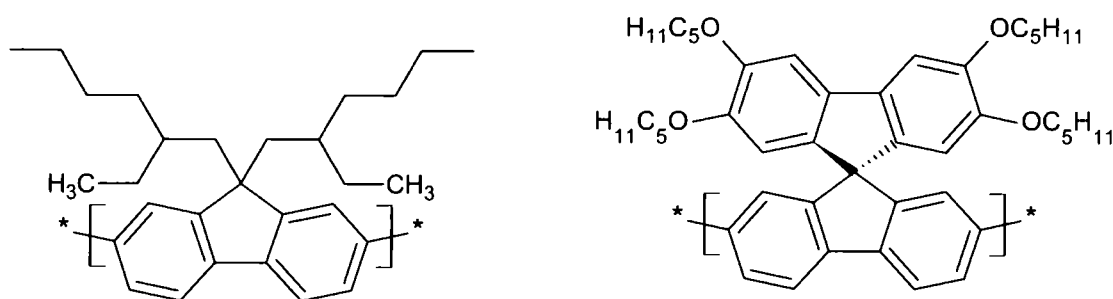


Figure 6-1 The polymers poly-9,9-diethylhexylfluorene (PF2/6) and polyspirobifluorene (PSBF)

Previously, conjugated polymers have been functionalised by copolymerisation or the addition of end groups; these methods have been used to great success to improve the charge transport, emission efficiency or to tune the emission colour<sup>1-5</sup>. However, making significant changes to the conjugated polymer structure can often have undesired effects, for example, the addition of moieties to improve charge transport can induce changes in the emission chromophore or the stability of the polymer. The general consequence of developing highly sophisticated functionalised polymers is to greatly increase the complexity of their photophysics.<sup>6-8</sup> Increasing the understanding of the photophysics and in some cases, the undesirable photochemistry, allows material scientists to further tailor the polymers to maximize device performance.

The polymer PSBF aims to rectify three of the biggest challenges faced by the standard polymer polyfluorene; the formation of keto defect groups<sup>9, 10</sup>; the microcrystalline nature of some derivative of polyfluorene<sup>11, 12</sup>; and the poor hole injection and transport of polyfluorene homopolymers<sup>13-15</sup>. This must of course be done whilst maintaining its strongest feature, which is the blue emission colour and high PLQY. The success in all of these areas has been remarkable; oxidation of the 9 position of the fluorene is made impossible by the linking of the side group fluorene in the spiro configuration. In common with other spiro configured molecules, the possibility of photo-oxidation is removed by the need to break both bonds simultaneously and the consequential difficulty in forming the intermediate alcohol. This is verified by the removal of the green-white emission, which originates from the formation of such keto species<sup>16-20</sup>. Both hole transport and solubility of the polymer have been improved by the addition of the electron donating ethylhexyloxy groups to the spiro fluorene side group<sup>21, 22</sup>. A lowering of the HOMO of such alkoxy substituted spirofluorenes has been previously reported, thus facilitating better hole injection<sup>16</sup>. Increased hole transport has been verified by the good device performance compared to conventional polyfluorene homopolymers, device efficiencies of up to 1.6Cd/A have been measured for PSBF compared to 0.25Cd/A for the prototypical PFO. In fact the efficiency of hole transport can be further improved in PSBF by copolymerisation with the hole transporting unit triaralenediamine (TAD) further increasing device efficiency up to 3.8Cd/A<sup>22, 23</sup>. The problem of microcrystalline ordering in some polyfluorenes has been well characterised, the work of Salbeck et al has developed the use of spiro centers as a way of stabilising the amorphous nature of conjugated materials. The spiro carbon forces the sidegroup orthogonal to the main chain creating a large amount of steric hindrance preventing any kind of ordering of the polymer. An increase in the glass transition temperature has been observed in both small molecules and conjugated polymers containing spiro centers, this morphological stability improves both the processability and device performance of polyfluorene materials<sup>19, 24</sup>.

In terms of photophysics, the PSBF derivative studied in this chapter has been poorly characterised, the only data available is very basic information about the fluorescence and device electroluminescence. However, small molecules containing spiro centers have been characterised well, in symmetric spirobifluorene molecules

the work of Milota et al. has concluded that the spiro linkage does not play a significant part in the photophysics in solution. Single exponential decays are observed for fluorescence and the conclusion was drawn that there is little interaction between the two parts of the molecule<sup>25</sup>, only morphological advantages were gained from having the spiro centre in the molecule. Conversely, in non symmetric spiro molecules containing an electron donor and acceptor coupled by a spirobifluorene bridge ultrafast electron transfer was observed from one side of the molecule to the other followed by a slow relaxation of the solvent molecules as they stabilise the excited state<sup>26</sup>. The extensive work of the Salbeck group on symmetrical and asymmetrical spiro compounds with a focus on their use in optoelectronic devices has developed an understanding of the phenomenon of spiroconjugation which allows a strong interaction of the two halves of a spiro bridged molecule through the overlap of the electronic orbitals of the two halves. The stabilisation of broad charge transfer emission bands has been observed in some solvent mixtures attributed to the formation of a charge transfer state between the two halves of the molecule, the effect of such a donor acceptor system is enhanced by the presence of the spiro centre<sup>27-29</sup>.

In relation to conjugated polymers containing spiro centres it has been observed that the addition of heteroatoms to the spirofluorene unit induces a red shift in the absorption and fluorescence spectra of the molecule<sup>30</sup>. This observation of that a side group can be used to donate electrons to the main chain chromophore represents a step change in the approach to the photophysics of polyfluorene derivatives. Conventionally the side groups are only believed to control the interaction between the polymer and its surroundings, for example, solubility, aggregate formation and the morphology in the bulk. The donation of electron density through the 9 position of the fluorene is especially surprising because one would not normally consider the conjugation of the molecule to extend through the 9-carbon. The reasons are twofold, not only is it not part of a series of alternating single and double bonds, but also because the  $\pi$ -orbital of the side group fluorene is forced orthogonal to the that of the backbone fluorene.

The first step in any investigation of photophysical properties of a new material is usually done in dilute solutions, understanding the behaviour of isolated

molecules is fundamentally important. There is one caveat to this, it is often found that the nature and dynamics of excited states in conjugated polymers alter dramatically in the solid state compared with dilute solution<sup>11, 31</sup>. This is to be expected when it is considered that interactions between polymer chains are possible when in close proximity to one another. These effects can generally be categorized into two groups; the effect of the interaction on the unexcited polymer and the excited state effects. The ideal conjugated polymer is totally amorphous and the relationships between neighbouring chains are entirely random. All indications from previous work on spiro bridged polymers suggest this is a fairly accurate description for PSBF; the effect of the amorphous nature is that the interactions between one chromophore and its neighbours is not necessarily the same for different chromophores in a film. As each chromophore feels slightly different surroundings there is a distribution of chromophore energies, which, when the chromophores are considered as an ensemble, gives rise to strong inhomogeneous broadening of the electronic transitions.

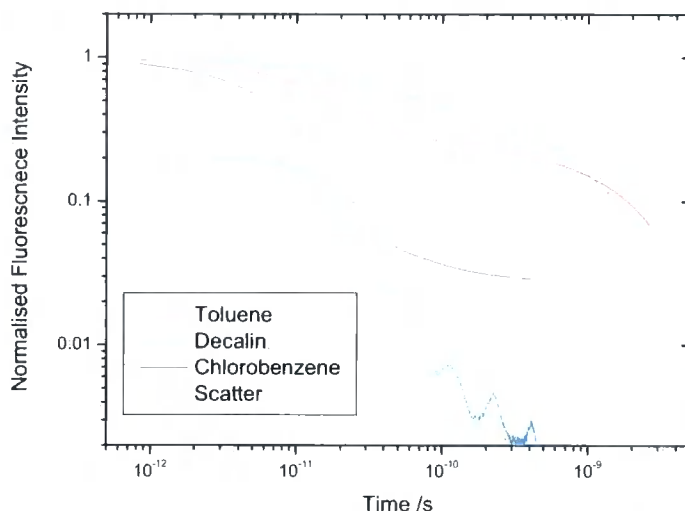
In addition to the ground state interactions, the close proximity of the polymer chains has a great effect on the excited states, the excitons generally become much more mobile as they are now able to hop between neighbouring chains easily. This dramatically increases the way defect or trap states affect the excitation dynamics and emission quantum yield of the polymer as excitons are able to very quickly reach quenching or dopant sites<sup>32-34</sup>.

## **6.1 Previous Work - Time Resolved Fluorescence & DFT Calculations**

The previous work on PSBF carried out in our group by Hintschich et al. focussed on the kinetics of the spectrally integrated fluorescence measured with a streak camera. In figure 6.2a the fluorescence decay is shown in a variety of different solvents; the three solvents shown were chosen to display a change of either viscosity or polarity between solvent pairs. Decalin and toluene have similar polarity whereas toluene and chlorobenzene have similar viscosity. Table 6.2b shows some of the solvent parameters and characteristics of the decay. At first glance all three decays show two components, the weighting of the amplitudes varies according to the solvent. The conclusion can be drawn that the fast component in the decay becomes



more significant in more polar, less viscous solutions; as mentioned earlier, this fast component represents the quenching of the singlets, which appears to be dependent on the polarity and viscosity of the solvent. This is in fact reproduced in the photoluminescence quantum yields of the three solutions, the lowest PLQY is observed for the more polar, less viscous solvent, chlorobenzene.



	Viscosity [cP]	Polarity ( $\Delta f$ )	Decay Kinetics [ps]	PLQY
<b>Decalin</b>	3.55	0.011	$t_{1/2} \sim 100$	$0.85 \pm 0.04$
<b>Toluene</b>	0.60	0.017	(0.7) $\sim 20$ ; (0.3) 2300	$0.80 \pm 0.04$
<b>Chlorobenzene</b>	0.8	0.14	(0.96) $\sim 20$ ; (0.04) 3000	$0.44 \pm 0.04$

**Figure 6-2** Decays and the decay parameters and PLQYs for PSBF in different solvents, the data is reproduced with the kind permission of S.I.Hintschich.

The work of Hintschich et al<sup>35</sup> also includes density functional theory calculations on the HOMO, LUMO and excited state of derivatives of the polymer. The electron configuration of two analogues was calculated; a PSBF trimer with no alkoxy substitutions on the sidegroup and a trimer of PSBF with methoxygroups attached to the side group fluorene the results are shown below. The former, with no substitutions (a) shows the HOMO and LUMO entirely confined to the fluorene

backbone, analogous to previous results for the more standard polyfluorenes like PF2/6. The alkoxy substituted PSBF (b) has a LUMO which is similar to the previous but a HOMO which extends into the side fluorene. The result is that the excited state (c) is shared over the backbone and the side group, confirming that the suggestion carried over from the small spiro molecules that the excited state extends over both sides of the spiro bridge.

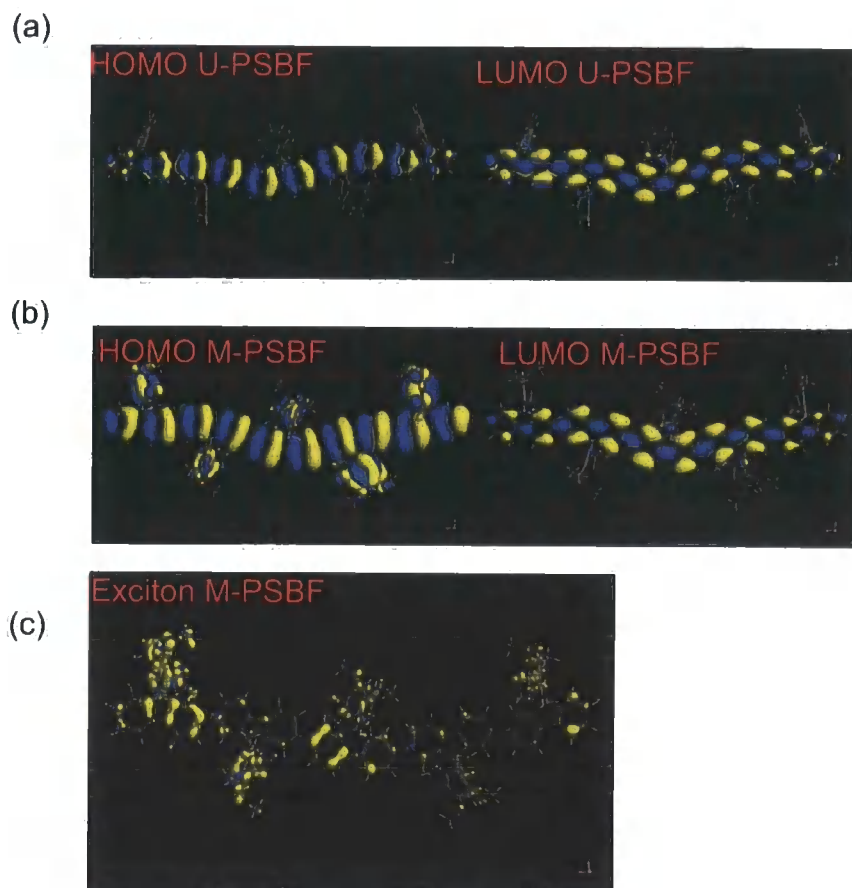


**Figure 6-3 Results of Density functional theory calculations for an unsubstituted PSBF (a) and an alkoxy substituted PSBF (b &c) similar to the polymer studied.**

## 6.2 Results

### 6.2.1 Absorption and Fluorescence

Absorption and photoluminescence of PSBF in dilute Toluene solution and thin films are shown in figure 6.4. In thin film the spectra are compared with PF2/6, the ground state absorption is red shifted by  $\sim 180\text{meV}$  and the fluorescence by  $\sim 100\text{meV}$  with respect to PF2/6. There is also an additional high energy band in the absorption; selective excitation throughout the whole of the ground state absorption results in no significant change in the cw fluorescence spectrum shape, therefore the excitation energy for all experiments is kept at  $3.2\text{eV}$ , the second harmonic of the Ti:Sapphire laser. In common with other conjugated polymers the first mode of the fluorescence is reduced in intensity compared to the dilute solution due to reabsorption in the optically thick film ( $\text{OD} \sim 1$ ); the greater Stokes shift in the solid state is also commonly observed. The photoluminescence quantum yield for the solutions were measured previously using 9,10-diphenylanthracene as a reference, and  $\phi_F = 0.80 \pm 0.04$  for PSBF. PLQY of films of both PSBF and PF2/6 was measured with the integrating sphere method<sup>36</sup> of *Palsson et al.* yielding  $\phi_F = 0.25 \pm 0.1$  and  $\phi_F = 0.35 \pm 0.1$  respectively.

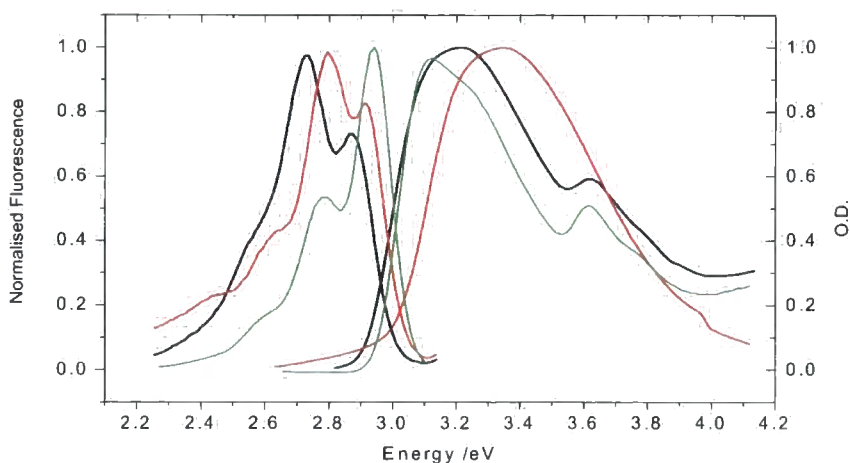


Figure 6-4 Absorption and photoluminescence of the polyfluorene derivatives Pf2/6 films (red) and PSBF in solution (green) and PSBF films (black).

## 6.2.2 Ultrafast Excited state Absorption and Ground State Recovery

The pump-probe spectrum of thin films of PSBF is compared to PF2/6 and the toluene solution in figure 6.5. An absorption band at  $\sim 1.6\text{eV}$  (780nm) labelled PA1 is present in all three spectra. In the literature, for polyfluorenes this feature is generally assigned to the induced absorption of the singlet exciton<sup>37-39</sup> ( $S_1-S_n$ ) transition. There is a strong correlation of the kinetics of the PA1 feature with the fluorescence decay in both solution and solid state (figures 6.6 and 6.7). The behaviour of the PA1 feature is also similar to the small amount of stimulated emission observed at very high energies. On this basis, one can unambiguously assign the PA1 feature to the singlet exciton, thus far the singlet excited state behaviour seems similar to PF2/6. However, as with the toluene solution and the solid state the PSBF pump – probe spectra show an additional broad high energy feature centred at  $2.13\text{eV}$  (580nm) which is not present in the PF2/6 spectrum when measured under the same experimental conditions.

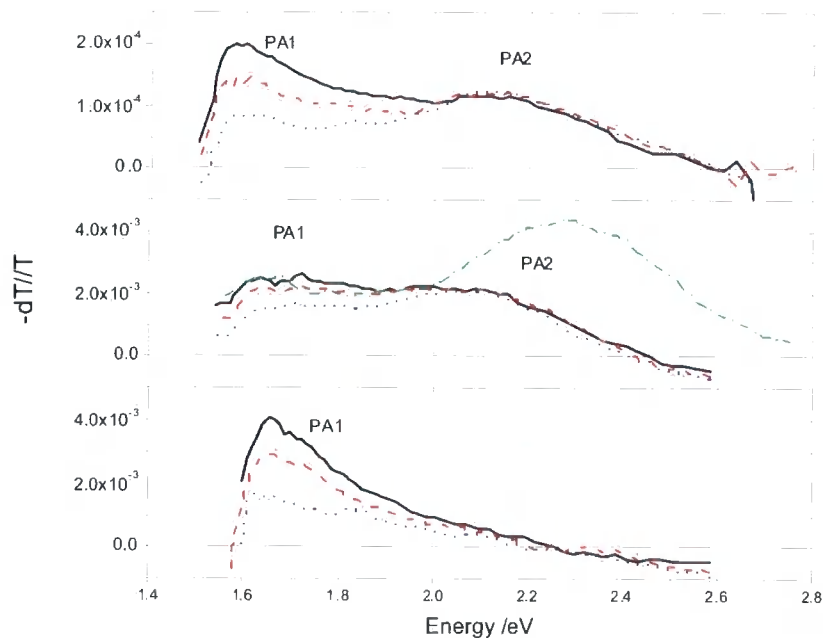
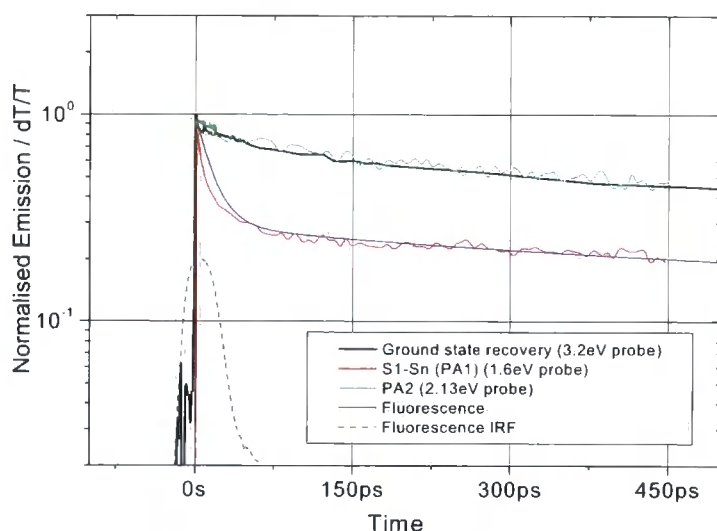


Figure 6-5 Compendium of time resolved pump probe spectra, Pf2/6 300K (lower), PSBF film (middle) and PSBF toluene solution (top) measured at different delay times after excitation (solid – 10ps, dash – 20ps, dot – 50ps, dot/dash – 0ps 10K), (pump excitation density  $\sim 1\mu\text{Jcm}^{-2}$ ).

The decay dynamics of the two features in solution for PSBF and thin film for the two polymers are shown in figure 6.6 and 6.7, they are compared to the ground state recovery measured at the pump energy 3.2eV (390nm).



**Figure 6-6 Pump-probe kinetics for PSBF in solution, compared with the ground state recovery and fluorescence decay.**

Once again the difference between the two polymers is stark. Considering PF2/6 only the dynamics of the singlet exciton (PA1) and the ground state recovery are broadly in agreement; the ground state recovery shows the decay of all the excited states so the similarity between the GSR and the singlet excited state absorption dynamics confirms that, as expected the singlet exciton is the dominant excited state. It is therefore responsible for most of the total number of excited state decays. The long tail in the ground state recovery for the PF2/6 is due to long lived triplets and trap states such as the aforementioned keto defect<sup>40</sup>. However, for PSBF, as with the solution kinetics there is a large difference between the ground state recovery and the singlet exciton throughout the whole decay. Whilst the singlet excited state absorption (PA1) decays rapidly (along with the fluorescence), the recovery of the ground state is much slower, with a lifetime similar to PA2. This suggests that there is another species other than the singlet exciton created in PSBF, which represents the significant proportion of excitations in the solid state. The decay of the PA2 band has

a long lifetime similar to the recovery of the ground state, thus most of the excitations created decay with the same lifetime as **PA2**. This would suggest that the state responsible of the excited state absorption **PA2** represents a significant number of excited states.

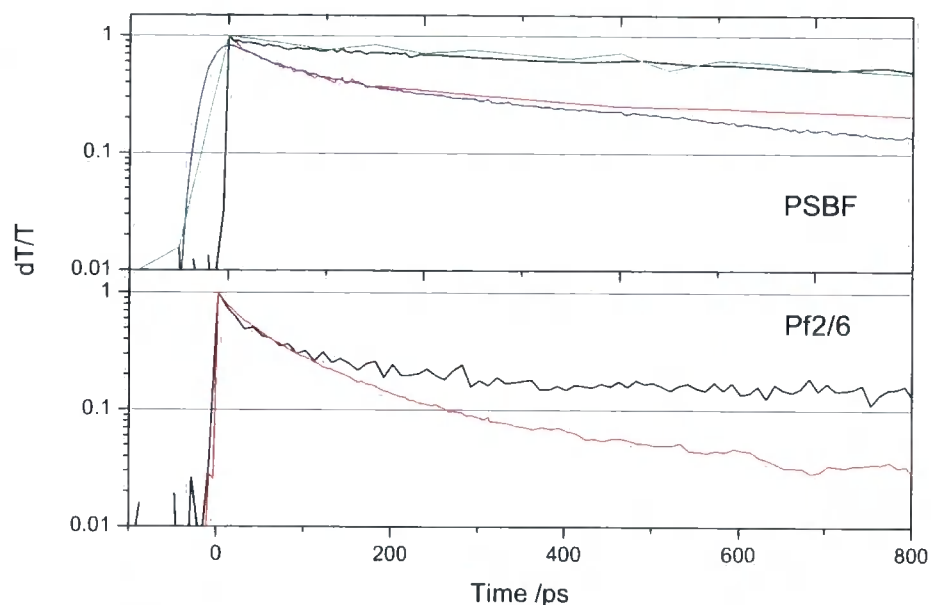


**Figure 6-7 Dynamics of the excited state features in films of the two polymers, Black – ground state recovery, Red – PA1, Green – PA2, Blue – Fluorescence.**

The dependence of the magnitude of both PA1 and PA2 on the excitation dose has been measured, shown in figure 6.8. The peak intensity of both features is approximately linear with excitation dose. In addition, in order to assess whether the decay of the PA1 feature is excitation density dependant, the intensity of the PA1 absorption after 50ps is also shown, the independence of the decay to excitation density is proven by the parallel nature of the initial intensity to the intensity after 50ps.

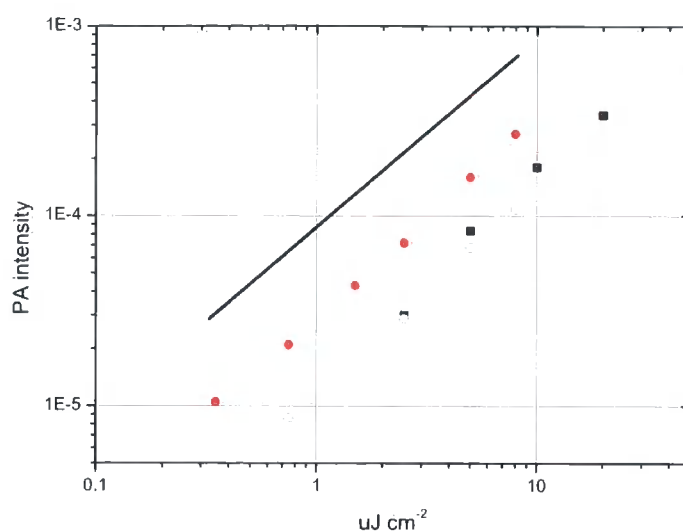


**Figure 6-8** Excitation dose dependence of the intensity of the pump-probe spectral features PA1 initially (●), PA1 after 50ps (○) and PA2 (■). The solid line shows a linear relationship between the pump dose and the intensity of the PA signal.

### 6.2.3 Device Measurements: Field Assisted Pump-Probe and Charge Induced Absorption

Figure 6.9 shows the spectra of the charge induced absorption and the field assisted pump-probe for PSBF devices. The charge induced absorption is a broad feature peaking at 2.1eV (590nm) this is in a similar position to the PA2 band in the zero field pump-probe spectra. The time resolved field assisted pump probe spectra also show two distinct features, which approximately correspond to the PA1 and PA2 features described earlier. The feature at **PA1**, the singlet exciton, shows a negative peak which corresponds to a reduction in the induced absorption signal, and hence a reduction in the population when the electric field is applied. **PA2** shows a positive signal, indicative of an increase in the population of the state. At high energies, ~2.5eV where the small amount of stimulated emission is in the zero field spectrum the field induced signal is positive, indicating a reduction in the stimulated emission intensity as the field is applied. It is notable that there is no stable isobestic point in the time resolved spectra, the zero crossing point of the superposition of the two states appears to move to lower energy with time; this provides a hint that the two features are not related by a simple donor acceptor relationship.

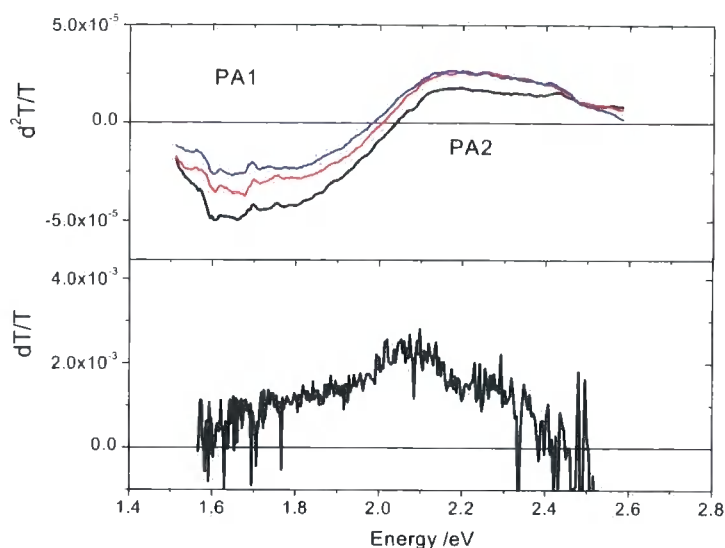


**Figure 6-9** Top panel: Field assisted pump-probe spectra at various delay times after excitation (Black - 10ps, Red - 20ps, Blue - 30ps). Lower panel: Charge induced absorption spectrum for a PSBF device.

### 6.3 Discussion

The apparent quenching of the singlet excitons along with the presence of the additional **PA2** induced absorption feature in PSBF compared with PF2/6 for both the Toluene solution and the thin films confirms that as suspected the excited state behaviour is much more complex for PSBF compared with more conventional polyfluorenes. Previous photoinduced absorption studies on conjugated polymers have found similar broad absorptions at high energy which have been attributed variously to charge carriers, charge-transfer excitations and interchain excitations. In the PPV type polymers the presence of interchain excitations in the solid state has led to similar absorptions as **PA2**<sup>41, 42</sup>. This can be immediately discounted for PSBF as the strong **PA2** absorption is present in the solution state photoinduced absorption spectrum where the possibility of a strong interchain interaction is negligible. This is especially true for PSBF given the significant amount of steric hindrance to aggregate formation caused by the very bulky orthogonal side group fluorene.



Charge state pulse radiolysis experiments carried out by Burrows et al have shown clear absorption features of charged species, both cationic and anionic, for polyfluorene in chloroform solution which peak at 570nm.<sup>43</sup> However these species are generally sharp, with a low energy tail, rather than the broad, symmetrical, species observed in PA2. In addition such charged species originate from an electron transfer reaction with the solvent, caused by charging the solvent directly during the pulse radiolysis experiment. Such electron transfer reactions would generally not be expected to occur for optical excitation apart from the in the special case of a strongly electron withdrawing solvent, in which case the polyfluorene chain can be oxidised and the solvent reduced. This has been observed by Burrows et al and is particularly problematic in highly chlorinated solvents like dichloromethane or chloroform<sup>44</sup>.

Given the presence of **PA2** and the strong quenching effect on the singlet exciton in dilute solutions, the most likely possibility for the additional absorption has to be an intrachain charged state. The quasi-cw current induced absorption (CIA) spectrum, which shows a strong absorption in the region of **PA2** corroborates this idea, the charge induced absorption experiment excites the polymer electrically thus charges and charged states are generated in a far higher proportion than in experiments with optical excitation. The charges observed in the CIA could either be free carriers, which would be the polymer cations or anions that transport the current through the device prior to formation of an emissive exciton. Alternatively, the charges can be trapped at a site with a preferential affinity for one charge or another; this process results in the formation of a charge transfer (CT) state.

In an optical excitation experiment a CT state can be populated by a number of mechanisms, direct optical absorption of the pump photons, energy transfer from the excited singlets to the CT state or an excited state reaction which results in the exciton dissociating and the charges becoming trapped. The work of Gadermaier et al has shown that polyfluorenes with a large number of keto defect groups show a low energy band in the pump probe spectrum which is attributed to the excited state absorption of the charge transfer state of the fluorenone<sup>45</sup>. As previously discussed, PSBF is resistant to keto formation, so the origin of the low energy band cannot come

from excitation of the CT state of the fluorenone, especially given its absence in the ‘standard’ PF2/6 when measured under the same excitation and sample handling conditions.

As shown in chapter 5, singlet-singlet annihilation can result in the formation of charge carriers which are then observed in the pump probe spectrum either as free carriers or CT states<sup>46</sup>. This bimolecular mechanism of charge generation results in an intensity dependant decay of the singlet state and a quadratic dependence of the charge state induced absorption on the excitation density. One would also expect the charge state absorption to show a build in during the accelerated decay of the singlet excitons. Neither of these indications are observed for the absorption **PA2** in PSBF. The **PA2** signal rises within the instrument response and both the decay of **PA1** and the magnitude of the **PA2** state shows a linear relationship with pump intensity (figure 6.8), thus it is extremely unlikely that the state is formed by exciton annihilation or any other two photon or bimolecular process. The spectra and excitation dependency of the features shown in figures 5.3 and 5.5 can be compared with these results for PSBF and the difference is clear. It is in fact interesting to note that while singlet-singlet annihilation is very efficient in PF2/6 due to the high mobility of the singlets, for PSBF at comparable excitation energies there is no SSA observed. In fact previous work that I have carried out into triplet-triplet annihilation in PSBF has shown that there can be intrachain triplet-triplet annihilation without any SSA, this is very surprising as it indicates that the singlet mobility, at least along the chain, is lower than the triplet mobility<sup>47</sup>.

The intrinsic presence of an additional intramolecular charge transfer excited state in PSBF seems the most likely origin of the **PA2** band. There remains two possibilities for the population of this second state, firstly direct optical excitation of the state; the similarity between the ground state absorption spectrum of PSBF and PF2/6 at low energies, particularly at the 3.2eV excitation energy, makes this unlikely. The remaining possibility for population of the state is efficient energy or electron transfer from an on chain exciton state to the CT state. As no build in is observed, this must be faster than the time resolution of the pump-probe experiment. For this to be the case, the acceptors in the energy transfer process would have to be in very close proximity

to the excited states, which is perfectly feasible for an intramolecular process where there is an electron transfer between the polymer backbone and the sidegroup.

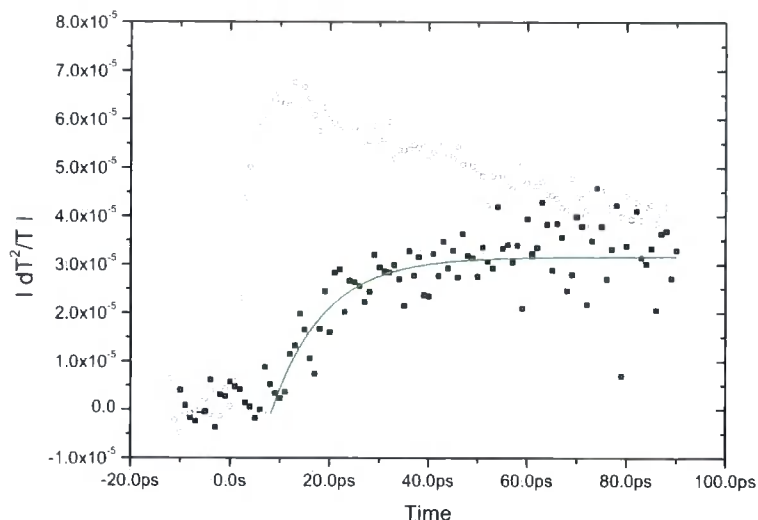


**Figure 6-10 Build up of the field induced pump probe signal at PA1 (o) and PA2, the solid line in the PA2 trace is the fit to a single exponential rise with lifetime rise time 10.5ps.**

As an additional check, to confirm that the observed second excited state is a localised CT state rather than free carriers, one must return to the field assisted photoinduced absorption spectrum. Figure 6.10 shows a reduction in the singlet photoinduced absorption peak **PA1** when the field is applied and an increase in the CT state absorption **PA2**. The kinetics of the field induced change in the spectra are shown in figure 5.8, the difference in the build up times of the features provides a clue to the nature of the **PA2** state. It seems that when the field is applied, the singlets are rapidly dissociated, ( $\sim 3$ ps) whereas it takes significantly longer for the increase in population of the CT state to occur ( $\sim 10.5$ ps). Considering this, one can suggest that the 10ps build up time for the increase in the absorption of **PA2** is the time it takes for the polarons that are rapidly created by the field-induced dissociation of the singlets to become trapped as a CT state. If the **PA2** absorption were from truly free carriers then the absorption should occur at the same time as the dissociation of the singlet excitons. In the work of Cabanillas-Gonzalez et al. on a fluorene trimer similar experiments have been performed and a theory of two step generation of free carriers via a polaron pair has been suggested<sup>48</sup>. However, in the fluorene trimer, there is no

evidence of intrinsic CT state formation as there is for PSBF so the charges, once formed, are able to recombine directly as singlet and triplet excitons. Whether in PSBF the CT state is populated directly by free charges, the polaron pairs or a two-step process involving both scenarios is not possible to tell from these experiments. However, this is not important, as the population of an intrinsic CT state in PSBF by the field-induced dissociation of singlet excitons is confirmed.

Having rationalised the presence of an additional state of CT character in the polymer film its relationship with the singlet exciton can be examined. In the solid state an intrinsic state on a polymer chain such as this can be populated rapidly by energy or electron transfer hence the lack of build in observed in the **PA2** band. The rapid quenching of a significant proportion of the singlets by a CT state would be expected to have a significant effect on the solid-state fluorescence quantum yield of the polymer. However, the PLQY is only reduced from 0.35 in PF2/6 to 0.25 in PSBF and yet from the ground state recovery kinetics it appears that a high proportion of the excited states decay via the longer lifetime of the CT state. The clue to this anomaly is confirmed by the surprising effect of temperature on the lifetime of the singlet. As the temperature is reduced the lifetime of **PA1** becomes shorter (figure 6.11), this is the opposite to the normally observed trend of increasing lifetime with decreasing temperature. However, in a two level system with both forward and reverse energy transfer an apparent reduction in the lifetime at low temperature becomes possible. At high temperature the thermal background energy (approximately 26meV at 300K) provides sufficient energy for the back transfer from the lower state to the upper, but at low temperature there is insufficient energy for the back transfer to take place. Thus from the variation of the back transfer rate with temperature one can estimate the energetic separation of the states, this is of course a well established theory governed by the Arrhenius equation.

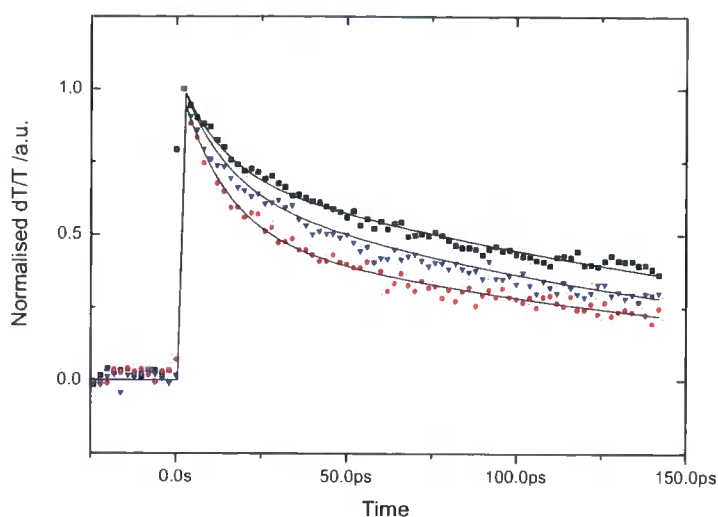


**Figure 6-11** The effect of the temperature on the decay of the singlet induced absorption signal at PA1.

Modelling the decays of the singlet exciton photoinduced absorption peak **PA1** to include the energy back transfer is based on the logical assumption that at low temperature the energy transfer rate is zero. Thus the decays at different temperatures were fitted with the same kinetics as the low temperature (20K) data with an additional free component (a build in) for the back transfer rate. This method yields good fits to all the decays, three examples are shown in figure 6.11 and the table of values is provided in table 6.1. From the Arrhenius plot for the back transfer rate in figure 6.12 the energy difference between the states can be calculated from the slope of the straight line, the calculation gives an energy barrier of approximately 14meV. It is worth noting that the broad distribution of conformations that the polymer chains adopt in the solid state means that there should be a similarly broad distribution of energy states to act as donors in the energy transfer. Thus, the Arrhenius plot only shows the mean energy separation of the distributions rather than the distributions themselves. Because of the broad distribution of states in conjugated polymers, there may be some states that are available for energy transfer at all temperatures. However, if this were a significant number then the temperature dependence of the excited state lifetime would not be observed. The polymer remains emissive because at room temperature the thermal background energy puts the states in quasi equilibrium, so the short radiative lifetime of the singlet exciton compared to the longer lifetime CT state allows an appreciable fraction of the excitations to decay radiatively. The difference

in the effect of the energy back transfer between 10K and 300K is clearly illustrated by measuring the low temperature pump-probe spectrum. The middle panel of figure 6.5 shows a comparison between the room and low temperature spectra.

	$k_{ET} (10^{10} \text{ s}^{-1})$
20K	0
120K	1.33
160K	1.37
200K	1.72
240K	1.96
260K	2.85
300K	$2.94 \pm 0.5$

**Table 6-1 Rates for energy transfer from the spiro CT state to the emissive singlet state.**

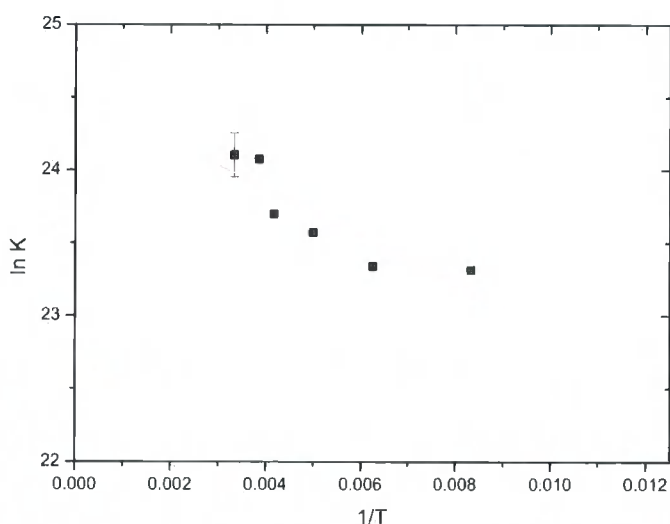


**Figure 6-12 Arrhenius plot for the energy transfer between charged state and singlet exciton. The values are taken from table 5.10.**

In solution, the fluorescence lifetime data presented in figure 6.2 supports the hypothesis of a two state model with reversible energy transfer between the states. In the unpolar, viscous solvent, decalin the fluorescence decay has a long lifetime, on going to toluene and chlorobenzene the decay is split into two clear lifetimes. The

more polar solvent decays more by the shorter lifetime. The origin of this is clear, the polar solvent stabilises the intramolecular CT state just like in the TICT forming molecules in chapter 4, thus lowering its energy and reducing the energy transfer back from the CT state to the emissive singlet state. As a result, there is less emission with the long lifetime of the CT state observed. In decalin and toluene, where the CT state is less stabilised, the energy transfer back to the singlet is efficient thus, the PLQY remains high and the emission decay contains a large proportion of the CT lifetime.

### 6.3.1 The Kinetic Scheme

The kinetic scheme of a reversible two state model can be solved from the rate equations for the singlet exciton and CT state. In this scheme the effect of triplet formation by intersystem crossing is neglected, this is valid both because of the generally low rate of intersystem crossing in conjugated polymers and also the similarity between the singlet and triplet excited state absorptions means that it is difficult to follow the population of the triplets during the singlet lifetime.

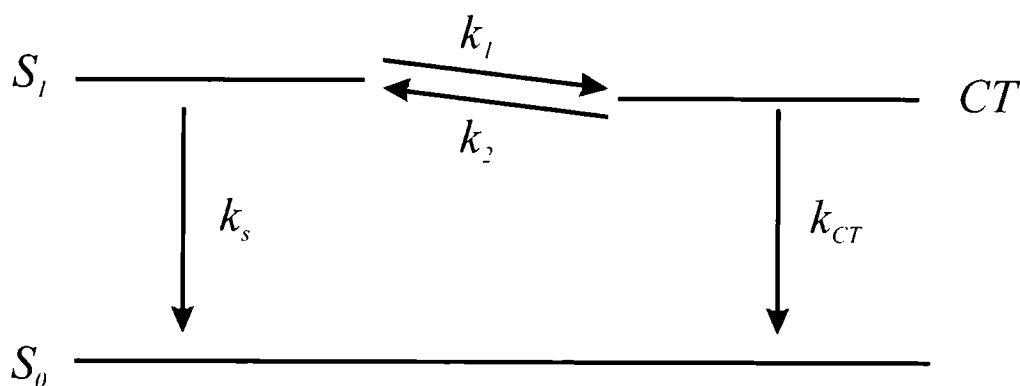


Figure 6-13 Reversible two state kinetic model as applied to PSBF.

Singlet rate equation,

$$\frac{dN_s}{dt} = -(k_s + k_1)N_s + k_2N_{CT} + G(t) \quad \text{Equation 6-1}$$

CT state rate equation,

$$\frac{dN_{CT}}{dt} = -(k_{CT} + k_2)N_{CT} + k_1N_s \quad \text{Equation 6-2}$$

If it is assumed that the singlet excitation profile  $G(t)$  can be considered as a  $\delta$ -pulse.

The solution of equations 5.1 and 5.2 gives

$$N_s = \alpha_1 \exp(-\gamma_1 t) + \alpha_2 \exp(-\gamma_2 t) \quad \text{Equation 6-3}$$

$$N_{CT} = \beta_1 \exp(-\gamma_1 t) - \beta_2 \exp(-\gamma_2 t) \quad \text{Equation 6-4}$$

Where  $\gamma_{1,2}$  are the observed lifetimes of the two states, and  $\alpha$  &  $\beta$  are the observed coefficients of the lifetimes in the decays.

The ground state recovery after photobleaching gives the overall effect of the decay of all the states (N) :

$$N = N_s + N_{CT} \quad \text{Equation 6-5}$$

$$N = (\alpha_1 + \beta_1) \exp(-\gamma_1 t) + (\alpha_2 - \beta_2) \exp(-\gamma_2 t) \quad \text{Equation 6-6}$$

The observed lifetimes are given by:

$$\gamma_1 = \frac{1}{2} \left[ (k_s + k_1 + k_{CT} + k_2) + \sqrt{((k_{CT} + k_2) - (k_s + k_1))^2 + 4k_1 k_2} \right] \quad \text{Equation 6-7}$$

$$\gamma_2 = \frac{1}{2} \left[ (k_s + k_1 + k_{CT} + k_2) - \sqrt{((k_{CT} + k_2) - (k_s + k_1))^2 + 4k_1 k_2} \right]$$

The most significant result of the solution of the rate equations is that the lifetimes found in the decay of the two states are the same ( $\gamma_1$  and  $\gamma_2$ ). This is exactly the same as observed in the pump-probe and fluorescence decays of figures 5.3 and 5.5. Thus the presence of a long lifetime in the tail of the fluorescence emission and singlet excited state absorption are indicators that the emissive state is being fed by



another longer lifetime non emissive state. It is the equilibrium between the natural lifetimes of the states and the rates of back and forward energy transfer that not only determines the observed decay rates; but also the proportion of states that decay radiatively through the singlet and hence the fluorescence quantum yield.

In the pump-probe spectra, there is a large overlap between the spectra of the singlet exciton and the CT state, comparison with the PF2/6 spectra shows that there is a significant proportion of the singlet absorption underlying the CT state. As the singlet decays, the CT state builds in, this explains the apparent small change of the intensity of the CT absorption as the underlying singlet clearly decays.

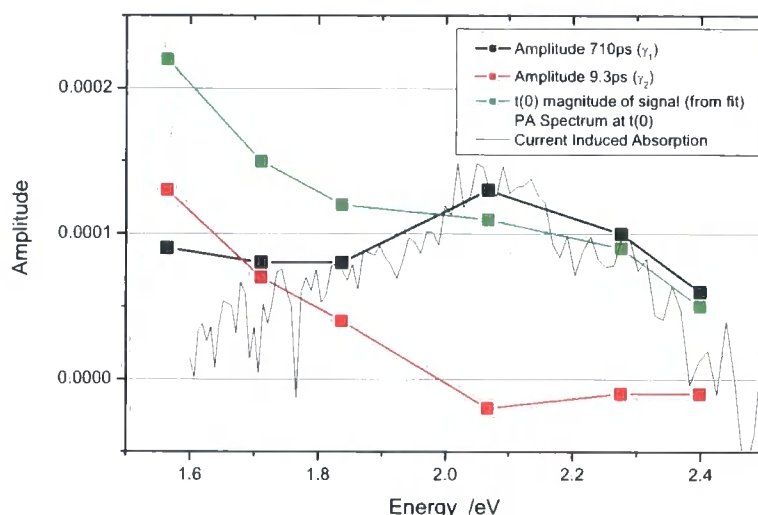


**Figure 6-14 Amplitudes of the components of fitting the pump - probe decays of PSBF in Toluene solution at the different wavelengths to equation 5.6, Also shown is the amplitude calculated from the fits at  $t(0)$ ; the amplitudes are compared to the pump-probe spectra at  $t(0)$ , and the charge induced absorption spectrum (scaled appropriately).**

The technique of global analysis can be used to analyse the decay of the pump-probe features and plot the decay-analysed spectra. In global analysis, all the spectra at different wavelengths are analysed together to calculate the two (or more) lifetimes that describe the temporal decay of the whole spectrum. This is very useful for the analysis of spectra that overlap, especially given that the both spectra should show the same lifetimes with differing amplitudes. This has been done for the pump-probe decays of PSBF in toluene solution and the decay-analysed spectra (DAS),

which show the amplitudes of the two components at different wavelengths (figure 6.14). One component has a short lifetime (9.3ps) which is  $\gamma_2$  in the kinetic scheme and the other has a long lifetime, represented by  $\gamma_1$ . In the blue-green region of the spectra the  $\gamma_1$  compares well with the charge induced absorption spectrum; as predicted the amplitude of the short component ( $\gamma_2$ ) is negative in this region, indicating the tail of the energy transfer to the CT state. In the red region, there is still a significant proportion of the states decaying with the long lifetime ( $\gamma_1$ ), this is the result of the lengthening of the singlet decay by the energy transfer back from the CT state to the singlet. It is important to note the presence of the long tail in the fluorescence decay as this confirms that long lifetime observed in the singlet feature of the pump-probe (PA1) is not just from the overlap of the spectra of the CT state and singlet exciton and therefore the kinetic system for a two state system is appropriate.

### 6.3.2 Spiroconjugation

The formation of a charge transfer state is always associated with the localisation of the electron and hole on different parts of the molecule. For example, in PSBF where the side group is electron deficient due to the ethylhexyloxy-substitutions one would expect the electron to reside on the side group fluorene and the hole to reside on the main polymer backbone. However, it seems unusual that the formation of a charge transfer state would be possible for a system with only a small difference in the electron affinity of the two halves of the molecule. The alkoxy substitutions are weakly electron withdrawing, but when attached to other conjugated polymers such as in MEH-PPV, no charge transfer formation is observed.

The reason for the formation of the CT state is that the donor acceptor effect between the backbone and the sidegroup is enhanced by the structure of the polymer through the phenomenon of spiroconjugation. Firstly, as there is no conjugated link between the side group fluorene and the main chain fluorene, there can be no delocalisation of the main chain  $\pi$ -electrons into the side group which would dilute the effect of the electron withdrawing groups on the side group. In addition, the

spiroconjugation interaction allows the HOMO and LUMO orbitals on the sidegroup to interact with those on the polymer backbone. The effect of this is that when there is spiroconjugation between an electron acceptor and an electron donor as is the case here, the energy of the resulting CT state is no longer simply dependant on the donor's HOMO and the acceptor's LUMO level as would be the case in an unspiroconjugated molecule. In a symmetrical spiroconjugated molecule the spiroconjugation increases the energy of the transition by decreasing the HOMO increasing the LUMO of the transition. This phenomenon is only possible if the states on the donor and acceptor are of the correct symmetry, if so, the HOMOs of the donor and acceptor interact to form a HOMO, which spans the whole molecule, and the LUMOs interact to form a single LUMO. In an unsymmetrical spiro- configured molecule an electron donor and acceptor, separated by the spiro bridge, can form the HOMO and LUMO states in the transition. It can be possible given the correct orbital symmetry, for the LUMO of the acceptor to interact with the HOMO of the donor. This leads to two spiroconjugated frontier orbitals with a larger energy gap than the unspiroconjugated case with a resulting intramolecular charge transfer<sup>24, 49, 50</sup>. This phenomenon has previously been used to create charge transfer relays between perpendicular  $\pi$ -systems, which would not normally be expected to interact. A schematic of the spiroconjugation interaction and its effect on the orbitals is shown below in figure 6.15.

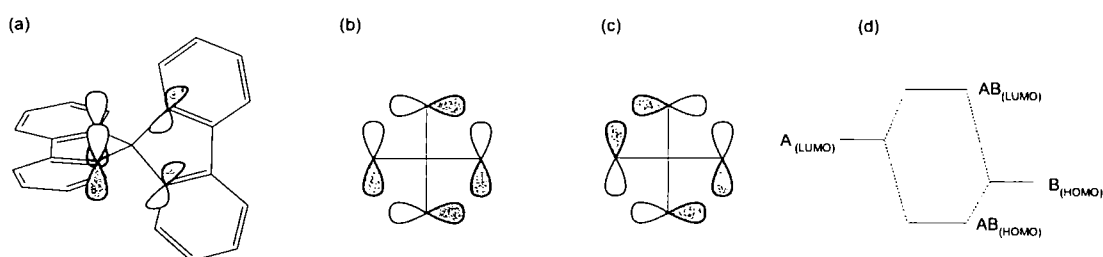


**Figure 6-15** The orbital overlap required for spiroconjugation and the effect on the energy levels of the HOMO and LUMO. (a) shows the p-orbitals involved in the interaction, (b) is a Fischer projection of the orbitals where the symmetry is not appropriate for spiroconjugation, (c) shows the correct orbital symmetry for spiroconjugation. (d) shows the effect of the spiroconjugation interaction on the LUMO on one half of the molecule and the HOMO on the other half forming the spiroconjugated frontier orbitals.

In dilute solutions the energy transfer between the two states is affected by the stabilisation of the CT state by polar solvent molecules. It is also possible that the

interaction between the polymer and the solvent can affect the orbital overlap between the sidegroup and the backbone through structural relaxations of the chain, most notably, scissor-type motions of the sidegroup.

In the solid state the polymer motions are effectively fixed, in the ground state the polymer adopts a myriad of different conformations due to the amorphous nature of the films and therefore the strains on the sidegroup can be varied. Therefore there is most certainly a broad distribution of energies for the backbone polyfluorene state and no doubt for the spiro-CT state as well. The effect of such a broad DOS is that there are sites where one state or other is favoured. The most likely scenario is that the energy transfer between the singlet states is efficient, until the exciton encounters a site where the formation of the spiro-CT state is favourable at which point it becomes trapped until either it decays non-radiatively or can energy transfer back to the singlet. This is of course most likely at room temperature where intermolecular energy transfer is only halted by the deepest of trap states. Returning to the observation of the lack of singlet-singlet annihilation in PSBF compared to its relative ease in PF2/6 one can suggest that the singlet mobility is low as a large proportion of singlets are trapped in the form of the spiro-CT state, preventing the diffusion controlled SSA seen in PF2/6.

Once the presence of the CT state and its relationship with the singlet is verified, the method of population of the state is trivial; a rapid electron transfer between the backbone and the sidegroup is possible because of the high degree of orbital overlap of the backbone and sidegroup (figure 5.13). This electron transfer is driven by the enhanced donor acceptor effect between the backbone and sidegroups that the spiroconjugation causes.

### **6.3.3 Significance of the CT State in Device Physics**

Previously, the polymer has displayed better device performance and stability of blue emission in polymer OLEDs, compared to the prototypical PF2/6. One can conclude therefore that the presence of equilibrium between a spiro-CT state and an

emissive backbone state in the solid state of PSBF has important implications for the polymer in light emitting devices. It is the view of Karabunarliev et al. that an intramolecular CT state is the initial recombination product for the injected carriers in a device<sup>51</sup>. For a system such as PSBF where the formation of the CT state is facile, one would expect the charge-trapping step to be efficient at the sites where the CT state is favoured. At room temperature, the quasi equilibrium between the emissive state and the CT results in the population of the emissive state by energy or electron transfer back to the backbone. As a result, both the charge trapping and the emission are efficient processes resulting in high device efficiency.

## **6.4 Conclusions**

The work in this chapter has demonstrated the significant differences between the excited state behaviour of PSBF compared to a model polyfluorene. The polymer PSBF has a charge transfer excited state located at energy of approximately 14meV below the singlet exciton. The formation of the CT state is driven by the effect of spiroconjugation enhancing the donor acceptor effect between the backbone and the electron deficient sidegroup; under optical excitation rapid electron transfer between the polymer backbone and the sidegroup forms the spiro-CT state. At room temperature, there is efficient energy transfer between the backbone singlet state and the spiro-CT state in both directions. The characteristics of such a reversible two state model give both states the same long lifetime tail. The two states are therefore in a quasi equilibrium at room temperature, with the CT acting as a reservoir for the emissive backbone singlet. It is suggested that in devices, the CT state is the primary excited state and efficient singlet emission is the result of the efficient energy transfer between the states and the much shorter radiative lifetime of the emissive singlet compared to the long lifetime of the CT state.

## 6.5 References

- <sup>1</sup> I. Perepichka, I. F. Perepichka, M. R. Bryce, et al., *Chemical Communications*, 3397 (2005).
- <sup>2</sup> Y. Z. Lee, X. W. Chen, S. A. Chen, et al., *Journal of the American Chemical Society* **123**, 2296 (2001).
- <sup>3</sup> D. Neher, *Macromolecular Rapid Communications* **22**, 1366 (2001).
- <sup>4</sup> M. Kreyenschmidt, G. Klaerner, T. Fuhrer, et al., *Macromolecules* **31**, 1099 (1998).
- <sup>5</sup> A. Charas, J. Morgado, J. M. G. Martinho, et al., *Synthetic Metals* **127**, 251 (2002).
- <sup>6</sup> F. I. Wu, P. I. Shih, Y. H. Tseng, et al., *Journal of Physical Chemistry B* **109**, 14000 (2005).
- <sup>7</sup> T. van Woudenbergh, J. Wildeman, P. W. M. Blom, et al., *Advanced Functional Materials* **14**, 677 (2004).
- <sup>8</sup> F. B. Dias, S. M. King, R. J. Matherson, et al., in preparation (2007).
- <sup>9</sup> E. J. W. List, R. Guentner, P. S. de Freitas, et al., *Advanced Materials* **14**, 374 (2002).
- <sup>10</sup> S. I. Hintschich, C. Rothe, S. Sinha, et al., *Journal of Chemical Physics* **119**, 12017 (2003).
- <sup>11</sup> A. J. Cadby, P. A. Lane, H. Mellor, et al., *Physical Review B* **62**, 15604 (2000).
- <sup>12</sup> M. Ariu, D. G. Lidzey, M. Lavrentiev, et al., *Synthetic Metals* **116**, 217 (2001).
- <sup>13</sup> J. C. Scott, G. G. Malliaras, W. D. Chen, et al., *Applied Physics Letters* **74**, 1510 (1999).
- <sup>14</sup> M. Bernius, M. Inbasekaran, E. Woo, et al., *Journal of Materials Science-Materials in Electronics* **11**, 111 (2000).
- <sup>15</sup> A. J. Campbell, D. D. C. Bradley, and H. Antoniadis, *Journal of Applied Physics* **89**, 3343 (2001).
- <sup>16</sup> K. S. Lee, Y. H. Kim, Y. Lee, et al., *Journal of Polymer Science Part a-Polymer Chemistry* **43**, 2316 (2005).

- <sup>17</sup> F. I. Wu, R. Dodda, D. S. Reddy, et al., *Journal of Materials Chemistry* **12**, 2893 (2002).
- <sup>18</sup> B. Schartel, T. Damerau, and M. Hennecke, *Physical Chemistry Chemical Physics* **2**, 4690 (2000).
- <sup>19</sup> F. Steuber, J. Staudigel, M. Stossel, et al., *Advanced Materials* **12**, 130 (2000).
- <sup>20</sup> A. Kadashchuk, A. Vakhnin, Y. Skryshevski, et al., (submitted).
- <sup>21</sup> C. C. Wu, W. G. Liu, W. Y. Hung, et al., *Applied Physics Letters* **87** (2005).
- <sup>22</sup> F. Laquai, G. Wegner, C. Im, et al., *Journal of Applied Physics* **99**, 23712 (2006).
- <sup>23</sup> B. Huang, J. Li, L. Q. Chen, et al., *Journal of Polymer Science Part a-Polymer Chemistry* **43**, 4517 (2005).
- <sup>24</sup> P. Maslak, *Advanced Materials* **6**, 405 (1994).
- <sup>25</sup> F. Milota, C. Warmuth, A. Tortschanoff, et al., *Synthetic Metals* **121**, 1497 (2001).
- <sup>26</sup> K. T. Wong, S. Y. Ku, Y. M. Cheng, et al., *Journal of Organic Chemistry* **71**, 456 (2006).
- <sup>27</sup> N. Johansson, D. A. dosSantos, S. Guo, et al., *Journal of Chemical Physics* **107**, 2542 (1997).
- <sup>28</sup> T. P. I. Saragi, T. Spehr, A. Siebert, et al., *Chemical Reviews* **107**, 1011 (2007).
- <sup>29</sup> R. Pudzich, T. Fuhrmann-Lieker, and J. Salbeck, in *Emissive Materials: Nanomaterials*, 2006), Vol. 199, p. 83.
- <sup>30</sup> D. Vak, S. J. Shin, J. H. Yum, et al., *Journal of Luminescence* **115**, 109 (2005).
- <sup>31</sup> J. Teetsov and M. A. Fox, *Journal of Materials Chemistry* **9**, 2117 (1999).
- <sup>32</sup> H. Wiesenhofer, D. Beljonne, G. D. Scholes, et al., *Advanced Functional Materials* **15**, 155 (2005).
- <sup>33</sup> F. B. Dias, M. Knaapila, A. P. Monkman, et al., *Macromolecules* **39**, 1598 (2006).
- <sup>34</sup> B. P. Lyons and A. P. Monkman, *Physical Review B* **71**, 235201 (2005).
- <sup>35</sup> S. Hintschich, S. M. King, S. J. Clarke, et al., in preparation (2006).
- <sup>36</sup> L. O. Palsson and A. P. Monkman, *Advanced Materials* **14**, 757 (2002).
- <sup>37</sup> D. W. McBranch, B. Kraabel, S. Xu, et al., *Synthetic Metals* **101**, 291 (1999).

- 38 T. Virgili, G. Cerullo, L. Luer, et al., *Physical Review Letters* **90**, 247402  
(2003).
- 39 G. Lanzani, G. Cerullo, D. Polli, et al., *Physica Status Solidi a-Applied  
Research* **201**, 1116 (2004).
- 40 C. Rothe, R. Guentner, U. Scherf, et al., *Journal of Chemical Physics* **115**,  
9557 (2001).
- 41 I. B. Martini, A. D. Smith, and B. J. Schwartz, *Physical Review B* **69**, 035204  
(2004).
- 42 V. I. Klimov, D. W. McBranch, N. N. Barashkov, et al., *Chemical Physics  
Letters* **277**, 109 (1997).
- 43 H. D. Burrows, J. S. de Melo, M. Forster, et al., *Chemical Physics Letters* **385**,  
105 (2004).
- 44 H. D. Burrows, S. M. King, J. Pina, et al., in preparation (2007).
- 45 C. Gadermaier, L. Romaner, T. Piok, et al., *Physical Review B* **72**, 045208  
(2005).
- 46 M. A. Stevens, C. Silva, D. M. Russell, et al., *Physical Review B* **63**, 165213  
(2001).
- 47 S. King, C. Rothe, and A. Monkman, *The Journal of Chemical Physics* **121**,  
10803 (2004).
- 48 J. Cabanillas-Gonzalez, M. R. Antognazza, T. Virgili, et al., *Physical Review  
B* **71**, 155207 (2005).
- 49 P. Maslak and A. Chopra, *Journal of the American Chemical Society* **115**,  
9331 (1993).
- 50 P. Maslak, A. Chopra, C. Moylan, et al., *J. Am. Chem. Soc.* **118**, 1471 (1996).
- 51 S. Karabunarliev and E. R. Bittner, *Physical Review Letters* **90**, 057402  
(2003).



## **6.6 Publications Arising From This Chapter**

S.M. King, S.I. Hintschich, C. Rothe, and A.P. Monkman, *Spiroconjugation Enhanced Charge Transfer State Formation in a Polyfluorene Homopolymer*. *Journal of Physical Chemistry C*, 2007. **Accepted For Publication.**

S.I. Hintschich, S.M. King, C. Rothe, and A.P. Monkman, *The Solution State Photophysics of Polyspirobifluorene*. **In Preparation**

## 7 Directly Probing the Distribution of States in Conjugated Polymers: Intrachain Migration in MeLPPP

In conjugated polymers, absorption and emission spectra are usually broad and the expected mirror symmetry between absorption and fluorescence spectra is broken. The reason for this is the inhomogeneous broadening of the electronic transitions caused by the polymer's broad distribution of states (DOS), which affects the spectra even in dilute solutions. Conjugated polymers can be considered as a string of chromophores, each that feel slightly different environments. Consequently, the electronic transitions between the same two electronic states are not always the same for different chromophores on the polymer chain or different polymer molecules. The most common reason for this is structural; most conjugated polymers do not have a rigid structure, so the inhomogeneous broadening is dominated by conformational disorder<sup>1-3</sup>. Twists between neighbouring oligomers on the same chain break the conjugation, giving rise to different conjugation lengths and hence different transition energies. The shorter chromophores are associated with a higher transition energy because the excited state is confined by the length of the chain segment. The conformational changes can be a dynamical process; some authors suggest that following photoexcitation there is a rapid planarisation of the molecule in the region of the excitation, which causes a stabilisation of the excited state energy as the conjugation length increases by a few units<sup>4, 5</sup>. It is also possible that polymers of different chain lengths form during the synthesis, short oligomers will be again associated with higher transition energies.

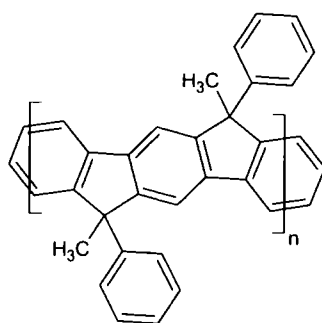


**Figure 7-1 Methyl-Ladder-Polyparaphenylene**

In rigid conjugated polymers such as the ladder type MeLPPP (Methyl-ladder-polyparaphenylene) each oligomer bonds to the next by a pair of bonds, thus there can

be no free rotation between neighbouring oligomers and no conjugation breaks. However, the ensemble fluorescence spectra for MeLPPP are still considerably broader than the homogeneous line width observed in room temperature single chromophore spectroscopy<sup>6</sup>. Therefore there is clearly still a source of inhomogeneous broadening of the excited state transitions.

Previously, the DOS of conjugated polymers was primarily investigated by site selective fluorescence techniques pioneered by the *Bassler* group, both in the steady state and with picosecond time resolution<sup>7-11</sup>. A dynamical shift to the red of the fluorescence spectrum is often observed in the first few picoseconds after excitation. However, this type of study only provides information about the combined effect of the distribution of states for absorption and fluorescence. The DOS is made up of sites of different energy and there can be energy transfer between the sites, as the excitons hop from their excitation position to sites of lower energy. In addition, the chain can relax, changing its conformation to lower the energy of the individual sites themselves. Both these processes contribute to the Stokes' shift and result in a different effective DOS for absorption and emission; different line shapes are observed for the fluorescence compared to absorption and the mirror symmetry of the spectra is broken. These processes are shown in the cartoon in figure 7.2.

Emission techniques do not unambiguously differentiate between the effects of migration within the DOS, to sites of lower energy, or a lowering of the sites in the DOS themselves by conformational relaxation. Both have been used to explain the redshift of the fluorescence spectrum after excitation that is observed both in thin films and dilute solutions. It is generally assumed that in the solid state the energy transfer between chains is very efficient and the solid nature of the material means that conformational relaxation is difficult. Therefore, one would expect energy transfer to dominate in thin films of conjugated polymers<sup>4, 12-14</sup>. Conversely, it is expected that the energy transfer between chains in a polymer in dilute solutions is very weak, due to the large interchain distance. In dilute solutions therefore, the red shift is generally ascribed to the conformational relaxation of the excitations on a free polymer chain<sup>2-4</sup>. However, this is not necessarily the case, as there can be multiple chromophores on one polymer chain; the energy transfer between chromophores on the same chain can still be very efficient even in dilute solutions, therefore migration

cannot be completely ruled out. In addition there have been reports in the literature of ultrafast fluctuations of the conjugation length of the conjugated polymer, and hence the energy of the excited state, occurring on the femtosecond time scale. Such phenomena have been observed with 3 pulse photon-echo spectroscopy<sup>5</sup>, however, the 50fs time scale of the measurement is beyond the time resolution of our system and as such the phenomena are unobservable with the techniques involved in this thesis.

In the previous work of our research group, fluorescence anisotropy and linear dichroism on oriented films of MeLPPP have been used to help understand the photophysics of the polymer. *Vaughan et al.* found that there is a variation in the orientation of the transition dipole moments across the DOS<sup>15</sup>. At the red edge of the absorption spectrum, the transition dipole moments strongly align with the orientation of the films. At higher excitation energies, the transition dipoles become progressively less well aligned with the polymer backbone. In dilute solutions, the steady state fluorescence anisotropy was also measured, there is a change in the fluorescence anisotropy as the excitation energy is changed. For excitation at high energy, the anisotropy of the fluorescence is low, suggesting that the excitations created high up in the DOS have undergone significant changes before emission, due to either migration or conformational relaxation. As the excitation energy is tuned to lower energy the anisotropy of the fluorescence increases until a threshold is reached where the excitons are either trapped in the tail of the DOS or there is not sufficient energy to overcome the activation energy barrier for conformational relaxation.

In this chapter I have used femtosecond pump-probe spectroscopy to directly probe the occupation of the ground state DOS. By concentrating on the ground state photobleaching part of the pump-probe spectrum rather than the excited state absorption region, one can directly follow which sites in the ground state DOS are occupied and thus observe the migration of the excitons from the high-energy segments of the chain to the lower energy tail states.

## **7.1 *Principal of the Experiment***

The ground state DOS forms a histogram of the number of available sites at a given energy, the absorption spectrum is the convolution of the DOS and the vibronic spectrum of the polymer. In most conjugated polymers, the DOS is so broad that in the absorption spectrum the vibronic structure of the polymer is lost. MeLPPP is one of the few polymers with a narrow enough DOS that the vibronics are resolvable in the absorption spectrum. Assuming that only a very low proportion of the available sites are ever excited, the depletion of the ground state (photobleaching) after excitation shows which of the available states are occupied. Therefore, dynamical changes of this ground state photobleaching show the change in the occupation of the sites of different energy. Conformational relaxation does not show up in the photobleaching because the technique only shows the changes to the occupation of the available sites in the ground state absorption spectrum, rather than the changes to energies of the individual sites after photoexcitation. This is explained best by referring to figure 7.2, in (c) the distribution of the unoccupied sites does not change compared to (a), therefore there is no dynamical change in the shape of the absorption spectrum and hence no change in the photobleaching signal. Thus, the transient photobleaching technique can be used investigate energy transfer within the DOS without the potential confusion of simultaneously observing energy transfer and conformational relaxation.

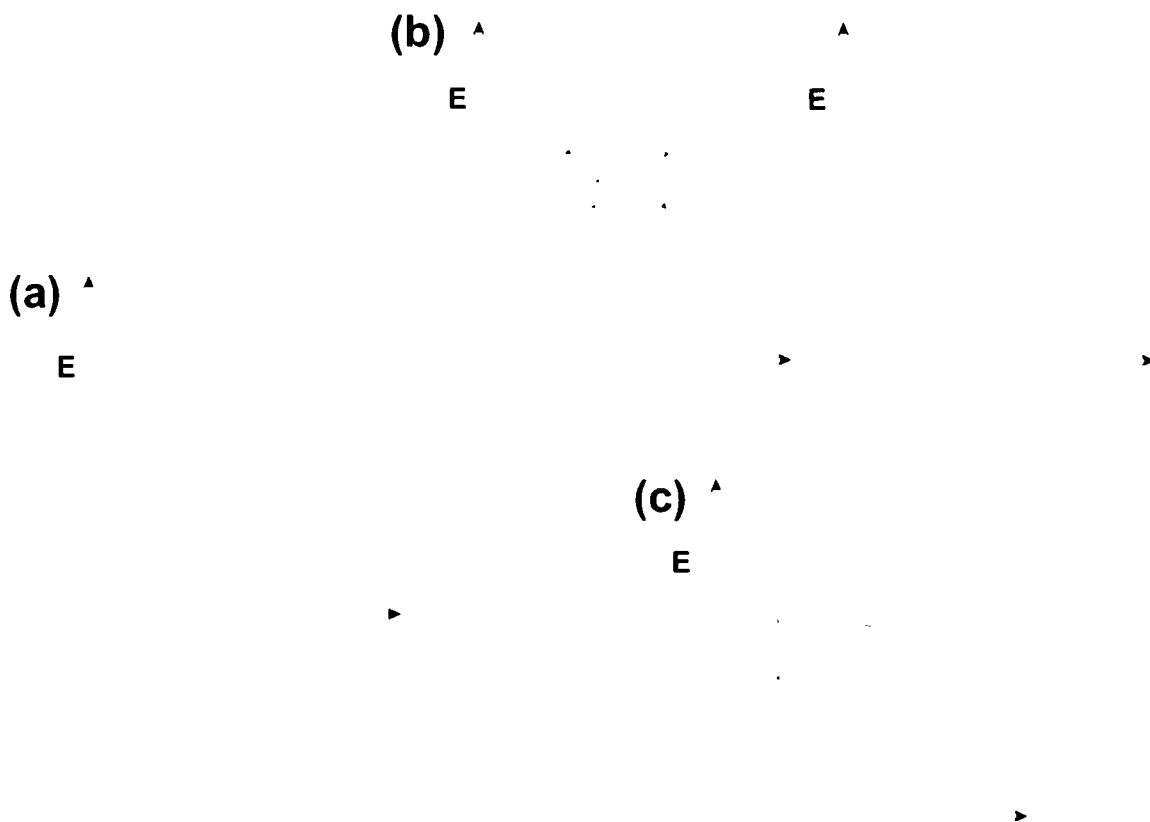


**Figure 7-2.** (a) An exciton distribution is created high up in the DOS. (b) By dispersive migration the excitons can energy transfer to lower sites until trapped in the tail of the DOS. (c) Alternatively, the sites themselves can relax to lower energy, leaving the rest of the DOS unchanged.

The solutions for transient absorption measurements are typically of concentration  $2 \times 10^{-3}$  mg/ml in toluene, although this is high compared to those used in some other techniques, the chain separation is still approximately  $3 \mu\text{m}$ , which is easily sufficient to neglect inter chain interactions and energy transfer between the chains. Thus, any energy transfer from high-energy states to those of low energy must be intrachain in nature.

By performing pump-probe spectroscopy with polarised pump and probe beams it is possible to elucidate not only the occupation of the states in the ground state DOS but the relative orientation of their transition dipole moments. This exploits the technique of polarisation photoselection. When a randomly oriented ensemble of polymer chains is excited by strongly polarised light only those sites in the DOS that are aligned with the polarisation of the excitation beam are excited. In a pump-probe experiment where the probe beam is also highly polarised only those chains whose

excited state transition dipole moments align with the probe beam are probed. The pump-probe anisotropy is defined as:

$$A = \frac{\left[ \frac{dT}{T} \right]_{//} - \left[ \frac{dT}{T} \right]_{\perp}}{\left[ \frac{dT}{T} \right]_{//} + 2 \left[ \frac{dT}{T} \right]_{\perp}} \quad \text{Equation 7-1}$$

where  $dT/T$  is the intensity of the pump-probe signal and  $//$  represents pump and probe beams parallel and  $\perp$  pump and probe beams perpendicular. Initially, at the point of excitation, the pump probe anisotropy should take the theoretical maximum value of 0.4 in an isotropic system. This assumes that the transition dipole moment of the excited state absorption is in the same direction as the ground state absorption, which, as my own work on stretched films of PFO shows, is generally true for the singlet transition in conjugated polymers,<sup>16</sup>.

## 7.2 Results

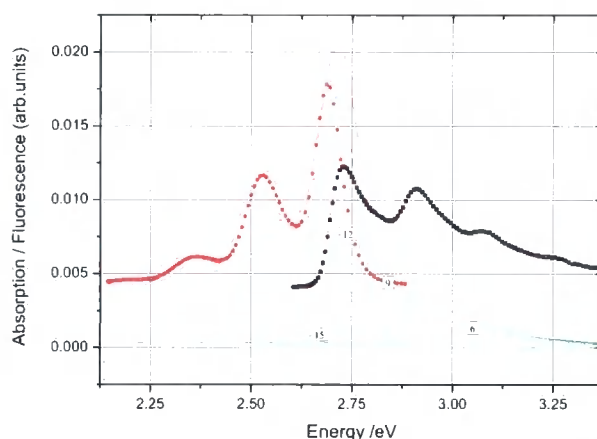


**Figure 7-3 Absorption (■) and Fluorescence (●) spectra for MeLPPP. The red lines are the fits to a series of Gaussians (fluorescence) or the convolution of a Gaussian and an exponential (absorption). The green lines are the individual components. The numbers give an indication of the corresponding oligomer length of various positions in the DOS.**

Absorption and fluorescence spectra for the polymer MeLPPP are shown in figure 7.3, compared to the other conjugated polymers studied in this thesis, the line widths are narrow. This is due to the ladder structure of the polymer preventing inter-oligomer twists, which dominate the inhomogeneous broadening in other polymers

such as polyfluorene. The spectra are overlaid with fits comprised of identical shape but different height peaks repeated with an energetic separation of  $\sim 170\text{meV}$ , the energetic separation between the main peaks corresponds well with other reports of the room temperature vibronic structure of the polymer. In low temperature glasses, the work of *Bassler et al* has shown that each of the main vibronic peaks observed at room temperature can be resolved further into a number of vibrational transitions<sup>7</sup>; however, for this study the overall shape of the spectrum is sufficient. The very small Stokes shift between absorption and emission combined with the relatively high solution concentration required for transient absorption measurements, causes the first mode of the fluorescence spectrum to be weakened considerably by reabsorption from the overlap of the ground state absorption. There is a marked breaking of the symmetry between the absorption and fluorescence spectra. As the outlines show, once reabsorption at the high energy edge is taken into account, the fluorescence spectra fit well with Gaussian peaks of width  $98\text{meV}$  and separation  $170\text{meV}$  for the 0-0 line and its vibronic replicas. However, Gaussian peaks do not fit the absorption spectrum well, if Gaussians are used the line width is overestimated and the fit is poor, this is most problematic in the first mode. Good fitting of the absorption spectrum is best done with a modified Gaussian with an exponential tail (decay  $5.52\text{eV}^{-1}$ ) on one side (the convolution of a Gaussian with an exponential). In both cases the fitting to the spectra is done with all parameters apart from the energy and amplitude fixed, so that each vibronic is fitted as true replicas of one another. The overall effect of this is that there is a high-energy tail to the DOS for absorption, which is not present in the fluorescence spectrum; this is a considerable change in the occupation of the DOS between absorption and emission.



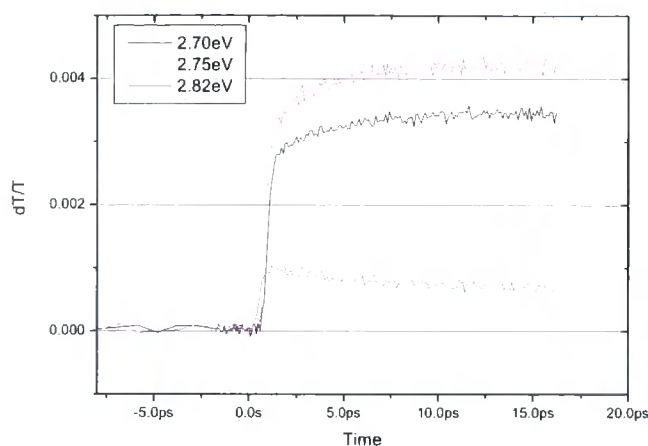


**Figure 7-4 Non-degenerate 3.2eV pump-probe decays for probe energies of 2.72, 2.69 and 2.82eV.**

Time resolved photobleaching decays were measured at a number of probe energies in the first mode of the absorption spectrum for excitation at 3.2eV (figure 7.4). From the decays, it is immediately apparent that for probe energies at the high-energy side of the peak, there is a fast decay and at the low energy side there is a build up. The data is fitted globally to a two exponential model, the two times resolved are 400fs and 6.2ps; the amplitudes of the two components are plotted in figure 7.4 along with the equation for the model. For all energies, the fast component (400fs) is a rise time (negative amplitude decay), which is similar to the time resolution of our system. The second component, with a time of 6.2ps is a rise at low probe energies and decay at high probe energies. As both these times characterise the very fast processes in the excited state behaviour, the  $\sim 200$ ps singlet decay is only included in the fit as an offset ( $y_0$  in figure 7.5). The shape of the amplitudes of the fast component approximates well to the absorption spectrum and the slow component has a similar shape to the first derivative of the absorption spectrum. The observation of decays at the high-energy side of the spectrum and a build in on the low energy side of the absorptions spectrum is characteristic of a redshift of the photobleaching signal. At low energies, the rise has a lower weighting than might be expected. This is most likely because of the overlap of the fluorescence spectrum with the low energy edge of the absorption spectrum, the stimulated emission shows a similar dynamic red shift of the spectrum which intrudes on the photobleaching signal.

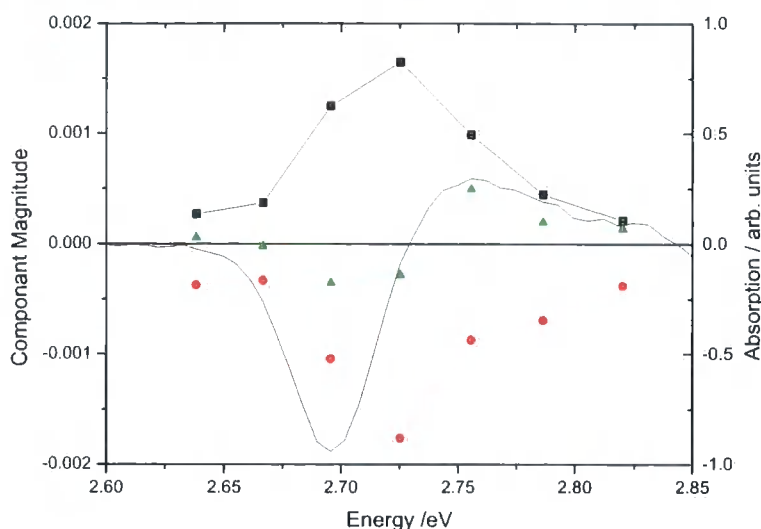


**Figure 7-5 Pre-exponential factors (Decay Analysed Spectra) for the two decay components (400fs -  $\bullet$ ; 4.2ps -  $\blacktriangle$ ;  $y_0$  -  $\blacksquare$ ) for the global analysis of non degenerate photobleaching decays at different energies. These are compared with the (inverted) absorption spectrum (dashed) and its first derivative (solid).**

Degenerate pump-probe decays are shown below in figure 7.6, in this experiment, pump and probe are at the same energy and originate from the same laser beam. The energy of the beam is tuned to different positions in the absorption spectrum and the decay of the pump-probe signal is measured. At low energy, on the red edge of the absorption spectrum (2.69eV, 2.72eV) the decays are similar, there is a low amplitude fast component and then the signal decays with a lifetime of 207ps. At higher energy (2.76eV) the fast component begins to dominate more and at the highest energy (2.78eV) the lifetime is significantly quenched as the fast component takes over the decay. The data have been fitted globally to a two exponential model, yielding lifetimes of 4.2ps and 207ps. The amplitudes of the fast component are shown in figure 7.7 for the different pump/probe energies, up to 2.74eV the fast decay has an approximately constant weighting of  $\sim 0.2$ , at higher energies the weighting increases approximately linearly with pump and probe energy.

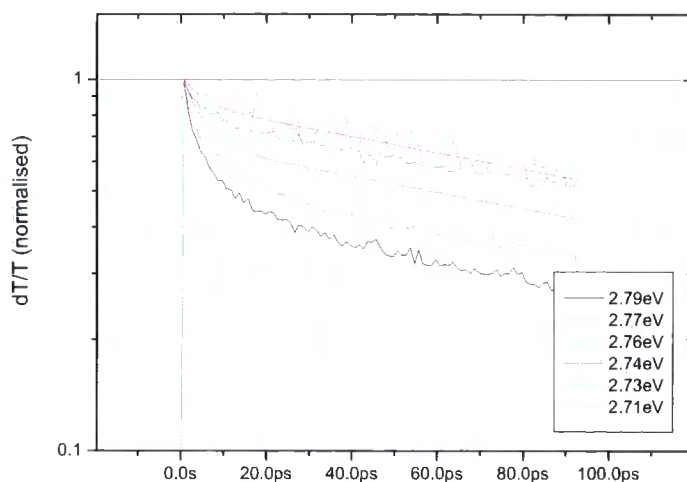


**Figure 7-6 Top: Degenerate pump-probe decays at different pump/probe energies, the red lines are examples of the fits, from which the amplitudes in figure 7.7 originate.**

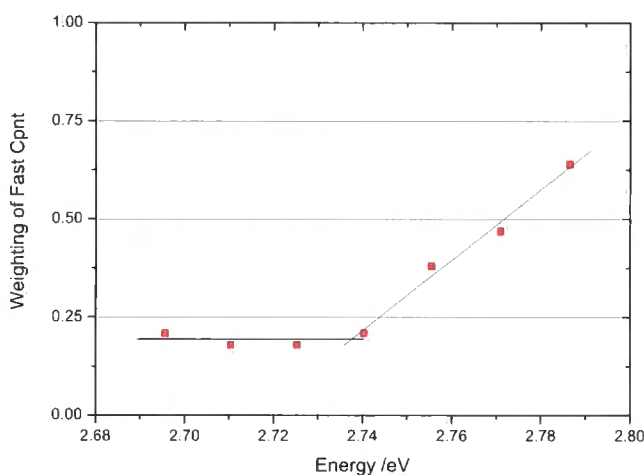


**Figure 7-7 Progression of the proportion of states undergoing a rapid decay, with the excitation energy.**

Using parallel and perpendicular polarisations of the pump and probe, one can calculate the polarisation anisotropy of the ground state recovery. For the non-degenerate pump probe (figure 7.8) with excitation at 3.2eV there is a decay of the anisotropy in the first 10ps after excitation, and then the anisotropy remains flat. At the blue edge (probe 2.78eV) the anisotropy starts close to the theoretical maximum of 0.4 and decays to approximately 0.15, whereas on the red edge of the absorption spectrum, at 2.73eV, the anisotropy starts high and rapidly decays to a stable value of -0.8.

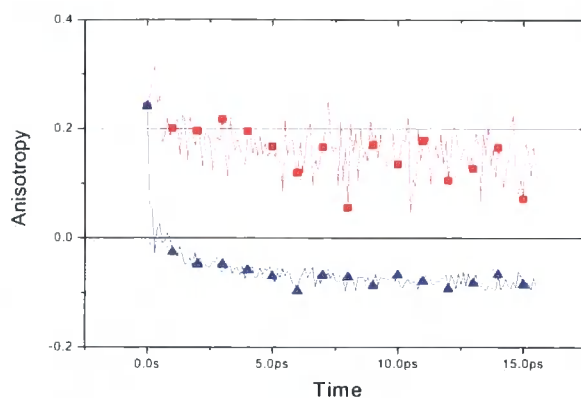


**Figure 7-8 Anisotropy decays for non-degenerate pump probe with the pump beam at 3.2eV and the probe beam at 2.73(▲) and 2.78eV (■) in dilute toluene solution.**

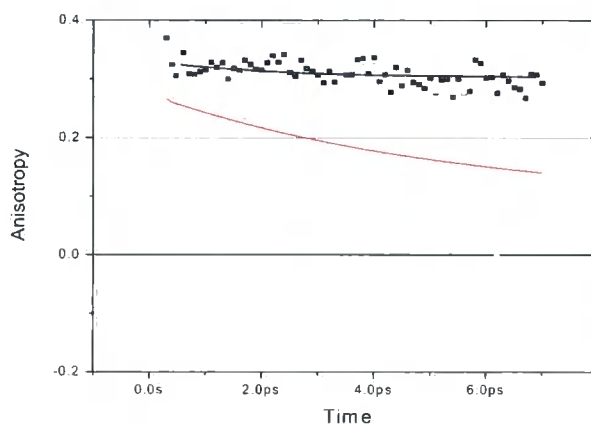


**Figure 7-9 Degenerate anisotropy decays for pump and probe at 2.78eV (○) and 2.69eV (■) in dilute toluene solution.**

The degenerate anisotropy decays in figure 7.9 show that at low energy pump and probe the anisotropy is quite flat with a slight decay in the first few ps, stabilising at about 0.3. At high energy, the anisotropy shows a slightly more rapid decay, with a decay lifetime of 5.5ps.

### 7.3 Discussion

The transient changes in the ground state occupation after excitation show that the excitations are moving from high energy sites to lower energy chain segments. Excitons created on the high energy side of the DOS migrate to the red edge, this is characterised by a decay of the occupation of the ground state at high energy and a

build in at lower energies. This intrachain migration seems to be very efficient; it takes approximately 6.2ps for the excitons to transfer to the lowest states in the DOS. The mechanism of the energy transfer could be either a through bond, Dexter transfer or a Forster type resonant interaction. The mechanism may depend on whether the hopping is a stepwise process, where the excitons hop to successive neighbouring segments of lower and lower energy. Alternatively, a longer-range interaction where the energy transfer takes place between two chromophores on the same chain that are separated by a longer distance may dominate. However, it can be said that at the length scales comparable to the spatial extent of the chromophores, which the stepwise migration would necessitate, one would expect the Dexter mechanism to dominate. The high efficiency of the intrachain energy transfer compared to the emission is the reason for the narrow Gaussian DOS for emission; emission is only observed from the lowest energy segments in the tail of the DOS.

Previous studies of the effect of oligomer length on ladder type parafenylene oligomers allow us to correlate the excitation energy with the oligomer length; the numerals on the fit of the first mode of the absorption spectrum in figure 1 show the approximate oligomer length for the different energies<sup>7, 9</sup>. From the absorption spectrum position and comparison with other studies, one can suggest that the longest conjugated segments are up to about 15 repeat units long<sup>17</sup>. Comparing this with the length of the polymer chain, derived from the molecular weight ( $M_n = 21,500$  g/mol,  $P_d = 1.3$ ), which is approximately 58 units, there is clearly a number of different length conjugated segments in each polymer chain. For the non-degenerate pump probe experiments, excitation is at 3.2eV is nominally in the third vibronic. However, the long tail of the DOS means that excitation at 3.2eV excites a combination of many different energy positions in the DOS. As well as exciting the third and fourth vibronic mode of some long chain sites one excites the first mode of some very short segments. The high overlap of the tails of the DOS for the first three modes at 3.2eV means that almost all parts of the DOS can be excited into the various different vibronics. The vibronic cooling of the states is very rapid compared to the energetic relaxation<sup>10, 18</sup>, so the effect is that at 3.2eV most the DOS is excited, approximately uniformly, especially given the ~10nm bandwidth of the laser. As a result, when the DOS is probed at different energies there is always a component with a rapid rise from the almost instantaneous excitation by the laser and the effect of the

energy transfer only appears on top of this. At very low energies, the rise is almost removed completely and in some cases a small decay component is observed, this is because the signals of photobleaching and stimulated emission are indistinguishable in this region as both are positive signals. However, probing at 2.64eV, which is on the far-red edge of the absorption (and hence photobleaching) is on the blue edge of the emission. Consequently, the move to lower energy of the states in the DOS, is masked by the dual observation of a rise in the signal due to photobleaching and a decay in the stimulated emission signal as both spectra shift to lower energy.

Degenerate pump probe measurements in the first vibronic only excite a narrow band of conjugation lengths, excitation at 2.8eV and 2.7eV excites 10- and 13/14-mers respectively. The 10mers at 2.8eV rapidly energy transfer to longer segments whereas the 13/14mers at 2.7eV do not, this is because they are close to the red edge of the absorption spectrum and as such must be among the longest conjugation lengths found in any significant number on the chain. As the energy of the degenerate pump probe experiment is tuned through the DOS from the high energy side to the low side, the amount of migration to low energy is decreased because there are less available sites of low energy to accept the excitons. Thus, the proportion of the pump probe signal that decays with the fast 3.2ps migration component drops, a plateau is reached where the excitons are on the lowest energy segment for their chain and thus there can be no further migration. This localisation threshold energy is 2.74eV. As the polymer is formed of oligomer units, which due to the two bond linkage between the units, are unable to rotate with respect to one another the conjugation length must be defined by more permanent chemical or structural defects, potentially formed during the synthesis. Figure 5 shows the amplitude of the fast (3.2ps) component in the fit of the degenerate pump probe decays of figure 2, as predicted there is a threshold where the fast component is reduced to a minimum value at 2.74eV, below which there is little change in the weighting. This saturation of the fast component at ~0.15, rather than decaying to zero, is potentially due to there being some other fast decay components, which are not dependant on migration through the DOS, such as internal conversion. The localisation threshold has been estimated previously using steady state fluorescence anisotropy; these results yield a threshold of ~2.73eV, which is in good agreement with the transient photobleaching data<sup>15</sup>.

The polarization anisotropy of the degenerate pump-probe decays shown in figure 7.8 confirms that there is little energy transfer at the red edge. The anisotropy is flat after excitation, only the highly anisotropic segments, which align along the chain, are excited. These are the elongated low energy states and so there is little change in anisotropy as the excitons are trapped in the tail of the DOS. On the blue edge there is anisotropy decay because the excitons are mobile and thus they are able to lose their anisotropy as they migrate along the chain. On the red edge, the excitons are unable to migrate to remain localised where they were excited, thus there is little loss of anisotropy.

The non degenerate polarisation anisotropy becomes more complex, excitation at 3.2eV excites many different chromophores of different energies, and the anisotropy on the blue edge of the absorption spectrum remains high. At first this seems counter intuitive, as the blue excitons are more mobile so should lose their anisotropy. However, when one considers that the blue excitons measured are actually the ones that have not yet migrated to the low energy segments, because they are locally trapped at high energy, it becomes clear that for this experiment their anisotropy should be high as these blue edge excitons remain similar to the initially excited states. At the red edge, the anisotropy decays to a very low value of approximately -0.1. This is a very good indicator that the excitons at the red edge are very different to those that are initially excited as is expected. What seems to be counter intuitive is that the final anisotropy is negative which would suggest that at least some of the transition dipole moments of the red excitons are at a very large angle to the excited excitons. For the simple case of a rigid rod conjugated polymer this would not be expected. In fact one would not expect a large anisotropy loss at all for a rigid rod polymer such as MeLPPP, in dilute solution because the transition dipole moment should always be along the chain axis. The origin of the anisotropy loss most likely comes from the fact that the polymer is not a perfect rigid rod, but a collection of rigid rods joined with the angles between the segments being the angles of the different substitution positions in a phenyl ring,  $\sim 60^\circ$ . This suggestion of a branched pattern to the polymer backbone has been postulated before by *Lupton et al* using polarised single molecule spectroscopy<sup>19</sup>, the evidence to support this claim is

strong, as it is the only really plausible explanation for the loss of anisotropy during intrachain migration.

The rapid rate of intramolecular energy transfer is considerably greater than that measured previously in other polymers such as polyindenofluorene, in MeLPPP we measure 6.2ps for energy transfer to the bottom of the DOS compared with ~ 500ps for intramolecular energy transfer to a low energy perelene endcap in a polyindenofluorene system<sup>20, 21</sup>. The 6.2ps time from the non-degenerate pump-probe for the migration time to the bottom of the DOS seems to be initially at variance to the 4.2ps measured by the degenerate pump-probe experiment for migration away from the excitation position. This discrepancy is in fact easy to account for, as it shows that the excitations take a shorter time to leave their initial site than they take to reach the bottom of the DOS. Therefore at least some of the excitons must move down the DOS in a stepwise process, taking a few steps to reach their final trapped state.

## **7.4 Conclusion**

The technique of transient ground state recovery has been successfully applied to the polymer MeLPPP in order to develop further understanding of the distribution of states. The rapid intrachain migration of the excitons to the lowest energy conjugation segment of each of the polymer chains was observed, thus confirming that there is a distribution of conjugation lengths in a single polymer chain. It takes approximately 6.2ps for the excitons to become thermalised in the lowest energy sites. In addition, the time resolved anisotropy of the ground state recovery has confirmed previous suggestions made in the literature that the structure of the polymer is branched, with the different conjugation segments at an angle to one another.



## 7.5 References

- <sup>1</sup> T. Huser, M. Yan, and L. J. Rothberg, Proceedings of the National Academy of Sciences of the United States of America **97**, 11187 (2000).
- <sup>2</sup> F. B. Dias, A. L. Macanita, J. S. de Melo, et al., Journal of Chemical Physics **118**, 7119 (2003).
- <sup>3</sup> S. I. Hintschich, F. B. Dias, and A. P. Monkman, Physical Review B **74** (2006).
- <sup>4</sup> T. E. Dykstra, V. Kovalevskij, X. J. Yang, et al., Chemical Physics **318**, 21 (2005).
- <sup>5</sup> G. D. Scholes, D. S. Larsen, G. R. Fleming, et al., Physical Review B **61**, 13670 (2000).
- <sup>6</sup> F. Schindler, J. M. Lupton, J. Feldmann, et al., Proceedings of the National Academy of Sciences of the United States of America **101**, 14695 (2004).
- <sup>7</sup> T. Pauck, H. Bassler, J. Grimme, et al., Chemical Physics **210**, 219 (1996).
- <sup>8</sup> S. C. J. Meskers, J. Hubner, M. Oestreich, et al., Chemical Physics Letters **339**, 223 (2001).
- <sup>9</sup> K. Mullen and G. Wegner, *Electronic Materials: The Oligomer Approach* (Wiley-VCH, Weinheim, 1998).
- <sup>10</sup> R. Kersting, U. Lemmer, R. F. Mahrt, et al., Physical Review Letters **70**, 3820 (1993).
- <sup>11</sup> U. Lemmer, R. F. Mahrt, Y. Wada, et al., Chemical Physics Letters **209**, 243 (1993).
- <sup>12</sup> J. Cornil, D. Beljonne, J.P. Calbert, et al., Advanced Materials **13**, 1053 (2001).
- <sup>13</sup> B. Ries, H. Bassler, M. Grunewald, et al., Physical Review B **37**, 5508 (1988).
- <sup>14</sup> R. Hildner, U. Lemmer, U. Scherf, et al., Chemical Physics Letters **429**, 103 (2006).
- <sup>15</sup> H. L. Vaughan and A. P. Monkman, Journal of Chemical Physics **In press** (2007).
- <sup>16</sup> S. M. King, H. L. Vaughan, and A. P. Monkman, Chemical Physics Letters **440**, 98 (2007).

- <sup>17</sup> F. Schindler, J. Jacob, A. C. Grimsdale, et al., *Angewandte Chemie-International Edition* **44**, 1520 (2005).
- <sup>18</sup> M. Pope and C. E. Swenberg, *Electronic Processes in Organic Crystals and Polymers* (Oxford University Press, Oxford, 1999).
- <sup>19</sup> J. G. Muller, J. M. Lupton, J. Feldmann, et al., *Applied Physics Letters* **84**, 1183 (2004).
- <sup>20</sup> D. Beljonne, G. Pourtois, C. Silva, et al., *Proceedings of the National Academy of Sciences of the United States of America* **99**, 10982 (2002).
- <sup>21</sup> E. Hennebicq, G. Pourtois, G. D. Scholes, et al., *Journal of the American Chemical Society* **127**, 4744 (2005).

## 8 General Conclusions

The work presented in this thesis represents three years of investigation into the ultrafast photophysics of conjugated polymers; the process began with the design, construction and development of the femtosecond pump-probe spectrometer, which has been the cornerstone of the investigations presented in the latter chapters. The work carried out successfully proves that by taking the slightly uncommon approach and using a high repetition rate, low pulse energy, laser rather than a standard 1kHz system has allowed superior signal to noise ratios at low pulse energy. This has allowed the study of a number of phenomena not thus far investigated with ultrafast techniques, in particular the use of transient photobleaching and ground state recovery to study the intersystem crossing in conjugated molecules and to investigate directly the intrachain migration in a conjugated polymer. In addition, the low pulse energy measurements are a valuable contribution to the many investigations into the nature of charge generation, and the relationship between charged states, intramolecular charge transfer states and singlet states in conjugated polymers.

As a way of drawing together the body of work in this thesis, there are a number of general conclusions that can be drawn from the various chapters. The first is that the importance of the mobility of the excitons cannot be ignored; it plays a vital role in the annihilation of singlets in conjugated polymers, without the diffusion of excitons the process would not happen at all for moderate exciton densities. In addition, the dispersive migration of the excitons down the distribution of states plays a role in accelerating the process. This dispersive migration to the low energy tail states is even prevalent in a single polymer chain, where there are only a few chromophores present, pump-probe spectroscopy has been used to directly see the migration of singlet excitons from the top of the distribution of states to the low energy tail.

Another area in which the work in this thesis has helped to understand is the relationship between singlets and triplets and the importance that molecular structure and the shape and orientation of the excited states has. In the first chapter of this thesis I have shown that the annihilation of singlets with triplets is very inefficient

because the perpendicular orientation and small spatial extent of the triplet exciton compared to the singlet prevents the states from becoming close enough for the annihilation reaction to take place. The orientation of the states is also very important in understanding the intersystem crossing between the singlet and triplet states, the perpendicular nature of the states impedes the intersystem crossing in planar molecule. It is only when the planarity of the molecule or polymer is broken by either inducing a twist in the molecule or considering a molecule with a large amount of conformational disorder that there are a significant number of triplets created. Using this argument the work in chapter 6 demonstrates that it is possible to increase by 10 times the intersystem crossing rate in an oligomer by inducing a twist in its backbone through the stabilisation of a twisted interconnected charge transfer state.

Finally, the phenomenon of spiroconjugation has been investigated, the incorporation of a spiro bridge into a polyfluorene molecule has shown how an intramolecular charge transfer state can be formed between the polymer backbone and the spiro configured sidegroup. The donor acceptor effect is driven by a slight difference in the electron density between the backbone and the sidegroup, which is vastly enhanced by the spiroconjugation interaction between the  $\pi$  orbitals of the sidegroup and backbone. These states can then act as a reservoir for emissive singlets, or provide a non-radiative decay pathway for the molecule. Once again the phenomenon is heavily dependant on structure and this highlights the way in which a simple structural modification can play an important and unexpected part in the photophysics of a conjugated polymer.

## 9 Publication List

1. S. King, C. Rothe, and A. Monkman, *Triplet build in and decay of isolated polyspirobifluorene chains in dilute solution*. Journal of Chemical Physics, 2004. **121**(21): p. 10803-10808.
2. C. Rothe, S.M. King, F. Dias, and A.P. Monkman, *Triplet exciton state and related phenomena in the beta-phase of poly(9,9-dioctyl)fluorene*. Physical Review B, 2004. **70**(19).
3. C. Rothe, S.M. King, and A.P. Monkman, *Electric-field-induced singlet and triplet exciton quenching in films of the conjugated polymer polyspirobifluorene*. Physical Review B, 2005. **72**(8).
4. M. Tavasli, S. Bettington, M.R. Bryce, H.A. Al Attar, F.B. Dias, S. King, and A.P. Monkman, *Oligo(fluorenyl) pyridine ligands and their tris-cyclometalated iridium(III) complexes: synthesis, photophysical properties and electrophosphorescent devices*. Journal of Materials Chemistry, 2005. **15**(46): p. 4963-4970.
5. S.M. King, H.A. Al-Attar, R.J. Evans, A. Congreve, A. Beeby, and A.P. Monkman, *The use of substituted iridium complexes in doped polymer electrophosphorescent devices: The influence of triplet transfer and other factors on enhancing device performance*. Advanced Functional Materials, 2006. **16**(8): p. 1043-1050.
6. S.M. King, C. Rothe, D. Dai, and A.P. Monkman, *Femtosecond ground state recovery: Measuring the intersystem crossing yield of polyspirobifluorene*. Journal of Chemical Physics, 2006. **124**(23).
7. C. Rothe, S. King, and A. Monkman, *Long-range resonantly enhanced triplet formation in luminescent polymers doped with iridium complexes*. Nature Materials, 2006. **5**(6): p. 463-466.
8. C. Rothe, S. King, and A.P. Monkman, *Systematic study of the dynamics of triplet exciton transfer between conjugated host polymers and phosphorescent iridium (III) guest emitters*. Physical Review B, 2006. **73**(24).
9. C. Rothe, S.M. King, and A.P. Monkman, *Direct measurement of the singlet generation yield in polymer light-emitting diodes*. Physical Review Letters, 2006. **97**(7).
10. S.M. King, D. Dai, C. Rothe, and A.P. Monkman, *Exciton annihilation in a polyfluorene: Low threshold for singlet-singlet annihilation and the absence of singlet-triplet annihilation*. Physical Review B, 2007. **76**(8).

11. S.M. King, S.I. Hintschich, C. Rothe, and A.P. Monkman, *Spiroconjugation Enhanced Charge Transfer State Formation in a Polyfluorene Homopolymer*. *Journal of Physical Chemistry C*, 2007. **In Press**.
12. S.M. King, H.L. Vaughan, and A.P. Monkman, *Orientation of triplet and singlet transition dipole moments in polyfluorene, studied by polarised spectroscopies*. *Chemical Physics Letters*, 2007. **440**(4-6): p. 98-102.
13. M. Westerling, H. Aarnio, R. Osterbacka, H. Stubb, S.M. King, A.P. Monkman, M.R. Andersson, K. Jespersen, T. Kesti, A. Yartsev, and V. Sundstrom, *Photoexcitation dynamics in an alternating polyfluorene copolymer*. *Physical Review B (Condensed Matter and Materials Physics)*, 2007. **75**(22): p. 224306-9.
14. S.M. King, R. Matheson, F.B. Dias, and A.P. Monkman, *Enhanced Triplet Formation by Intramolecular TICT Excited States in Conjugated Oligomers and Polymers*. *Journal of Physical Chemistry B*, 2008(Under Review).

